INTRAOPERATIVE IMAGING, NAVIGATION AND RADIATION MANAGEMENT IN AORTIC AND PERIPHERAL ENDOVASCULAR PROCEDURES

Marloes M Jansen

Intraoperative Imaging, Navigation and Radiation Management in Aortic and Peripheral Endovascular Procedures

Marloes M. Jansen

Intraoperative Imaging, Navigation and Radiation Management in Aortic and Peripheral Endovascular Procedures

Intraoperatieve beeldvorming, navigatie en stralingsbescherming
tijdens endovasculaire ingrepen van de aorta en perifere vaten
(met een samenvatting in het Nederlands)

Proefschrift

ter verkrijging van de graad van doctor aan de
Universiteit Utrecht
op gezag van de
rector magnificus, prof. dr. H.R.B.M. Kummeling,
ingevolge het besluit van het college voor promoties
in het openbaar te verdedigen op

dinsdag 23 januari 2024 des ochtends te 10.15 uur

door

Marloes Marleen Jansen

geboren op 20 augustus 1991
te Deventer

Promotor:

Prof. dr. J.A. van Herwaarden

Copromotor:

Dr. C.E.V.B. Hazenberg

Beoordelingscommissie:

Prof. dr. ir. C.A.T. van den Berg
Prof. dr. P.A.F.M. Doevendans
Prof. dr. D.P.V. de Kleijn
Prof. dr. G.W.H. Schurink
Dr. M. Voskuil

TABLE OF CONTENTS

CHAPTER | 1

General introduction

INTRODUCTION

Endovascular treatment has emerged as an increasingly popular method for managing a wide range of vascular diseases. This thesis focuses specifically on the endovascular treatment of obstructive peripheral artery disease and aneurysmatic aortic disease, and examines the role of image guidance and navigation during these endovascular procedures.

To provide a better understanding of the current status of image guidance and navigation during endovascular procedures, this introduction first provides a basic overview of the current endovascular techniques and imaging methods. We then move on to discuss the two types of vascular diseases and their endovascular treatments, highlighting some of the challenges associated with image guidance, navigation, and radiation exposure.

ENDOVASCULAR TECHNIQUES

Endovascular Devices

The success of endovascular procedures relies heavily on the use of specialized devices such as sheaths, guidewires, and catheters. These devices are inserted through arterial access, typically in the groin, and are advanced through the vascular tree to perform various treatments. There are five main categories of endovascular devices: sheaths, guidewires, catheters, balloons and stents.

- **Sheaths:** These are essential for the safe introduction and exchange of endovascular devices in the arterial system. The preferred access site for most endovascular interventions is the common femoral artery in the groin, although the brachial artery is also a viable alternative. Vascular access is generally achieved via surgical cut-down or ultrasound-guided percutaneous puncture of an arterial access site.
- **Guidewires:** These are used to cannulate vascular segments and facilitate the delivery of catheters, stents and other interventional devices to this segment. There are two main groups of guidewires: floppy guidewires and stiff guidewires. Floppy guidewires are used during navigation and vessel cannulation, whereas stiff guidewires are used during advancement of stents and other treatment devices.
- **Catheters:** These are advanced over-the-wire and provide general steerability, thanks to their tip shape. A wide range of distal tip shapes is available to engage with the various anatomical branch points of the vascular system (Figure 1). The shape of the catheter tip can be straightened by advancing a guidewire in the distal section of the catheter lumen and is retrieved when the guidewire is withdrawn from the catheter tip. This feature enhances the manoeuvrability and steerability of the guidewire-catheter combination as a whole.
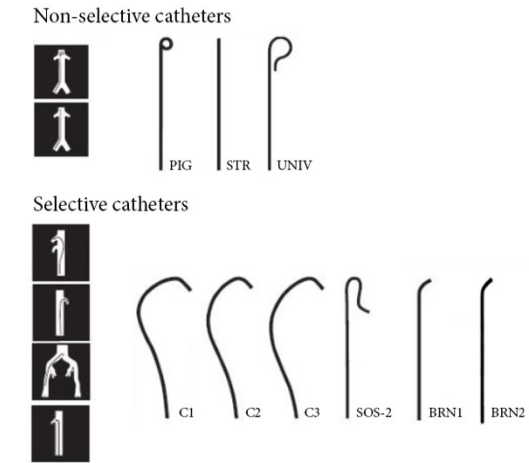
Figure 1. Various non-selective and selective catheter shapes.

- **Balloon catheters:** This subtype of catheter has an inflatable balloon at the distal end used to treat stenotic lesions, connect stent components, or anchor stents to the vascular wall.
- **Stents:** These are used to reinforce weakened or narrowed arteries. The stent consists of a metal, mostly nitinol, wireframe that is covered with synthetic material or left bare. The stent is compressed and retained in a delivery catheter by means of a delivery sheath, which is advanced over a stiff guidewire. The stent is deployed by either retracting the delivery sheath or pushing out the stent (self-expanding stents) or by balloon expansion (balloon-expandable stents). The unconstrained stent is usually oversized, generating radial forces that keep it in position in the vasculature.

Endovascular Image Guidance

To visualize these devices inside the body, we use standard fluoroscopy guidance. Fluoroscopy is a 2D X-ray based imaging modality that is commonly used for this purpose. When the X-ray beam passes through the patient, part of the X-rays will be absorbed or deflected as scatter radiation. Dense tissues such as bone, absorb more X-rays than soft tissues. These differences in tissue interactions create a 'shadow' image where structures with different absorption coefficients are displayed in different tones of grey. Endovascular devices are usually easy to discriminate on a standard fluoroscopy image. Soft tissues such as muscles and vascular structures have similar absorption coefficients and are therefore more difficult to differentiate from each other. Local injection of radiopaque contrast material inside the vasculature is therefore needed to visualize arteries. Often a technique called digital subtraction angiography (DSA) is used, which creates an arterial roadmap that can be projected on top of live fluoroscopy to guide the endovascular devices. DSAs are used for intraoperative diagnosis and
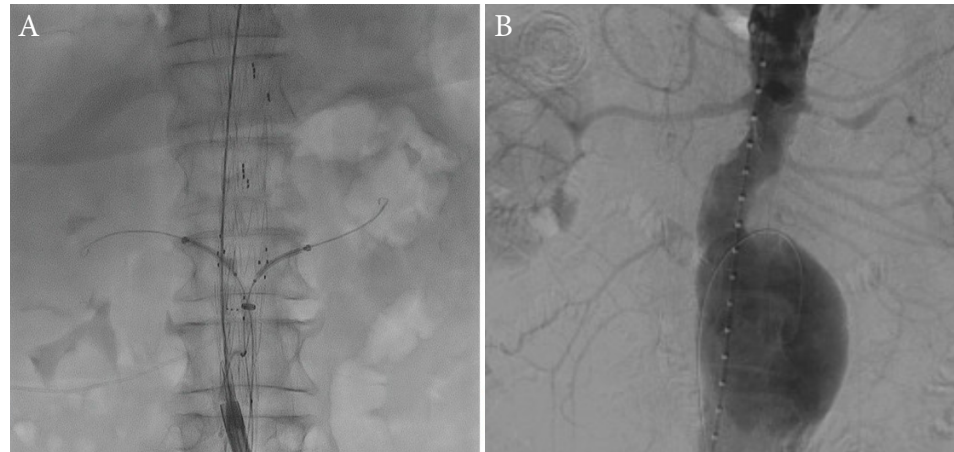
Figure 2: A: Fluoroscopy image with stent and guidewires in-situ. B: Digital Subtraction Angiography of an aneurysmatic abdominal aorta.

treatment verification, but also for the navigational guidance of endovascular devices. *Figure 2* displays examples of a fluoroscopy image and a DSA image.

Fluoroscopy, DSA and roadmaps are all imaging methods based on 2D projections. Meaning that the different anatomical structures are projected on top of each other. This means that the different anatomical structures in the body are overlaid on top of each other, making it challenging to understand their spatial relationships. For example, it can be difficult to understand the bends and twists of vessel structures or the positioning of endovascular devices. As a result, there is a need for more advanced imaging techniques and navigational tools that can provide better visualization and guidance during endovascular procedures. Particularly in complex endovascular procedures, that often require difficult device manoeuvres, precise device placement and careful radiation exposure management. In the next sections, we will explore the standard endovascular treatments for obstructive peripheral artery disease and aneurysmatic aortic disease, as well as more complex procedures and the challenges they present.

OBSTRUCTIVE PERIPHERAL ARTERY DISEASE

Obstructive peripheral arterial disease (PAD) is a steno-occlusive disease of the arteries of the lower extremity. PAD is caused by accumulation of atherosclerotic plaque, resulting in hardening and narrowing of the arterial wall. As the disease progresses and the blood flow in the extremities decreases, symptoms such as intermittent claudication, rest pain, ulceration and tissue loss can arise. In severe cases, the rupturing of an unstable

atherosclerotic lesion can form an acute threat to the affected limb, as this triggers blood clot formation and blocks the arterial flow completely.

Primary treatment for mild to moderate peripheral artery disease involves making lifestyle changes, taking medications to slow down plaque build-up, and participating in guided walking therapy to encourage the growth of new blood vessels (neovascularization). In cases where these measures do not yield the desired results, interventional revascularization may be necessary to restore blood flow through the arteries of the leg. This can be accomplished through either endovascular methods or open surgical techniques.

When compared to open surgical procedures, the endovascular approach is associated with lower periprocedural risks, 30 day mortality and shorter hospital stay according to several studies.[1,2]

Whether treatment is performed via open or endovascular approach depends heavily upon the location and characteristics of the atherosclerotic lesion. The ESVS guidelines recommend endovascular-first strategy in the majority of the lesion types.[3] In line with the guidelines, the EU registry data show that roughly 60-70% of peripheral artery revascularizations are performed via the endovascular or hybrid approach.[4]

It's worth noting that a renewed debate has emerged concerning the most effective treatment strategy of chronic limb-threatening ischemia (CLTI), which represents the most severe manifestation of peripheral artery disease. This debate has been sparked by conflicting outcomes documented in the recent BEST-CLI and BASIL-2 trials that examined optimal treatment strategy (open bypass vs endovascular treatment) for CLTI.[5,6] While ongoing research will shed more light on the best management practices for this critically affected patient subset, the endovascular approach will remain the cornerstone of interventional treatment for other patient groups.

Standard endovascular revascularization of peripheral artery disease
Endovascular treatment of PAD aims to restore adequate blood flow in the affected limb by widening the diameter of the narrowed or blocked artery. The procedure is typically performed under local anaesthesia and involves several steps.

First, the physician gains arterial access in the groin. Guidewires and catheters are then carefully maneuvered through the arterial system until they reach the site of the blockage or narrowing. Next, angiography is performed to visualize the affected vessel and assess the size, location, and severity of the lesion. This helps the physician determine the best treatment approach.

There are several techniques available to treat narrowed lesions, including balloon angioplasty, stenting, and plaque debulking. Balloon angioplasty involves inflating a small balloon within the narrowed area to widen the lumen and improve blood flow. Stenting involves placing a small metal mesh tube within the artery to provide structural support and maintain vessel patency. Plaque debulking uses a specialized device to remove or break up the plaque that is causing the narrowing. Choice of treatment

strategy is primarily based on operator experience and lesion characteristics including the elastic recoil of the plaque, calcification grade and location of the lesion.

Complex endovascular revascularization of peripheral artery disease
Chronic total occlusions are a complex subset of atherosclerotic lesions. These lesions are dense and often contain a fibrous cap, which can be difficult to penetrate with a guidewire. Generally, treatment of chronic total occlusions is associated with longer procedures times, higher radiation exposure and greater use of contrast materials.[5] New endovascular techniques to treat chronic total occlusions include plaque debulking devices and crossing devices. In which the device aids to drill or shave a portal through the true lumen.

These are relatively aggressive techniques, that require a high level of 3D understanding with respect to the anatomy and device orientation, in which standard fluoroscopic imaging does not always suffice.

ANEURYSMATIC AORTIC DISEASE

Aneurysmatic aortic disease is a dilatation or widening of the aorta, caused by a weakening of the artery wall. Aneurysmal dilatations can develop anywhere along the aorta and are classified into thoracic, abdominal and thoraco-abdominal types. Abdominal aneurysms are further subdivided in suprarenal, juxta-renal and infra-renal aneurysms, to indicate involvement of renal and visceral arteries.

Aneurysms are usually asymptomatic and are discovered as an incidental finding during investigation of other pathologies. However, rupture of the aneurysm causes life-threatening internal bleeding.[6] In asymptomatic patients, an aneurysm diameter that exceeds 5.5 cm (or 5.0 cm for women) is considered as indication for elective aneurysm repair, although smaller aneurysms with saccular shape, or rapid growth may be considered earlier [7,8]. These threshold diameters are framed by the balance between the risk of aneurysm rupture and the risk of intraoperative mortality.

The endovascular approach is the most commonly used treatment method for abdominal aneurysm repair due to its lower periprocedural risks, 30-day mortality, and shorter hospital stays when compared to open surgical treatment. This is supported by several randomized controlled trials such as EVAR I[9], DREAM[10], OVER[11] and ACE[12]. However, this early survival benefit is not sustained in the mid-term follow-up. Consequently, the 2019 ESVS guidelines recommend the endovascular approach as the preferred treatment modality for most patients with abdominal aneurysm repair, except for those with a long life expectancy.[7] Currently, more than 70% of standard aneurysm repairs in Western Europe are performed using endovascular techniques[13], demonstrating its effectiveness and popularity.

Standard abdominal endovascular aneurysm repair
Endovascular aneurysm repair (EVAR) ensures that the dilated aneurysm is excluded from circulation with a covered stent, whilst the blood flow towards the relevant arteries is preserved. Aortic stents are composed of a metal wire-frame sealed with synthetics, that reinforces the aorta without pressuring the weakened arterial wall. Fixation and sealing of the stent is provided by anchoring segments in the landing zones. These landing zones are located proximal and distal to the aneurysm and require healthy aortic tissue to provide optimal fixation and sealing. A diverse spectrum of endovascular stents is available, each with its own design and instructions for use.

Most infrarenal aneurysms are suitable for standard EVAR. In general, standard EVAR involves two stent components: the main body and the contralateral limb (*Figure 3*). Vascular access is obtained from both femoral arteries and the thoracic aorta is cannulated with standard guidewires and catheters. The main body of the stentgraft is carefully positioned just below the caudal edge of the renal arteries and partially deployed. This allows for cannulation of the contralateral gate, followed by advancement of the contralateral limb. Both the main body and contralateral limb are fully deployed, with sufficient overlap between the two components, and balloon inflation is used to expand the grafts to the arterial wall in healthy landing zones to provide optimal fixation and sealing.
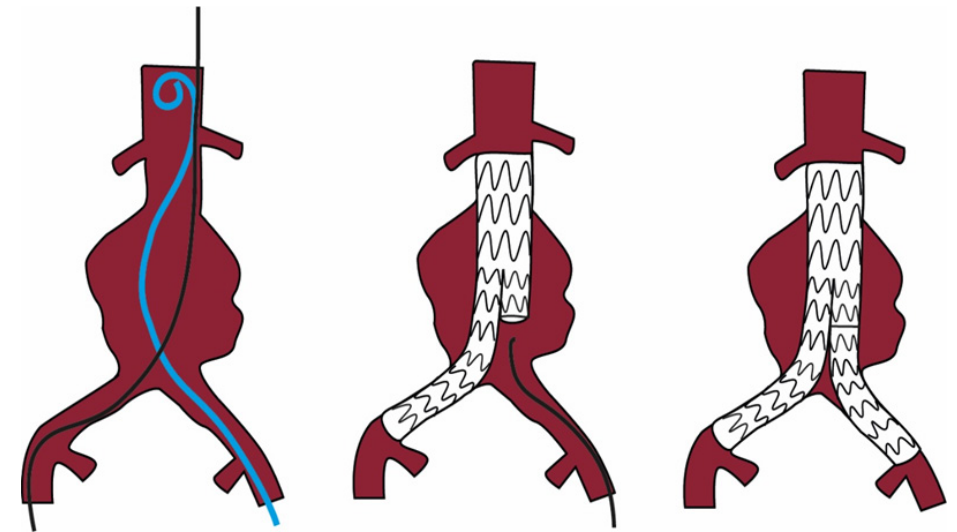
*Figure 3. Standard endovascular aortic repair (EVAR). A) An infrarenal aneurysm, cannulated with a stiff guidewire (black) and a pigtail catheter for contrast injection (blue). **B)** Status after main body deployment. The main body is positioned just below the renal arteries, with the ipsilateral limb extending into the common iliac artery and the contralateral gate located in the aneurysm. The contralateral gate is cannulated using a floppy guidewire. **C)** Status after contralateral limb deployment. Adequate sealing is achieved in the proximal and distal landing zones.*

Complex abdominal endovascular aneurysm repair

Within the domain of endovascular aneurysm treatment, we see an expansion towards more advanced stenting techniques for juxtarenal and suprarenal aneurysms. In both cases, renal and/or visceral arteries will need to be incorporated in the stent to enable a suitable proximal landing zone in the healthy suprarenal segment of the aorta. Two of the main approaches to achieve this are fenestrated and branched EVAR (*Figure 4*). In fenestrated EVAR (FEVAR), the main body contains custom-made holes (fenestrations) that correspond to the position of ostia of the visceral and renal arteries. After deployment of the fenestrated graft, each artery needs to be cannulated and stented with a covered graft. These covered grafts protrude slightly into the aortic lumen, and are flared with a balloon to seal the stent as a whole. Branched EVAR (BrEVAR) is an endovascular technique, in which branches are woven onto the fabric of the main body graft, instead of fenestrations. These branches are extended into the renal and/or visceral arteries by means of covered stents.
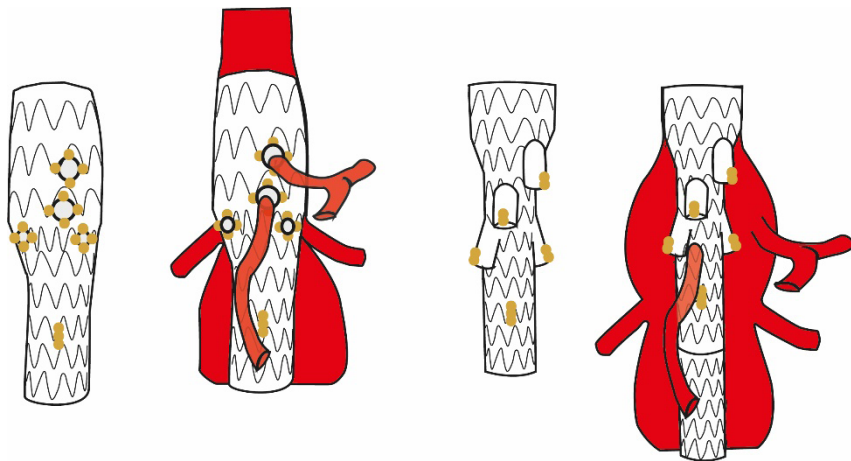
Figure 4. Fenestrated and branched endovascular repair (FEVAR and BrEVAR). A) *A fenestrated main body, and its placement in a juxtarenal aneurysm.* **B)** *A branched main body and its placement within a suprarenal aneurysm with wide arterial lumen. The branches will need to be connected to the target vessels with small stentgrafts.*

Cannulation of the visceral and renal arteries forms the major challenge in both FEVAR and BrEVAR procedures, especially when dealing with tortuous or stenotic arteries within a large aneurysm sac. This phase of the procedure often takes the longest time and requires the highest dose of radiation exposure and contrast. A range of different catheter shapes and sizes may be needed to acquire and maintain 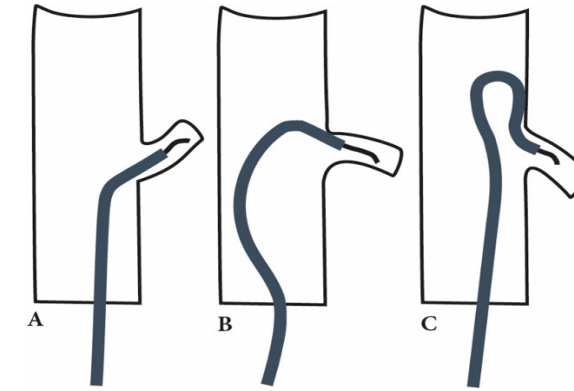a stable guidewire position in the target vessel (*Figure 5*). Reliable and effective image guidance is essential to facilitate this task.

Figure 5. *Cannulation of the renal arteries with different geometry using different selective catheters. A) Berenstein, B) Cobra-2, C) SOS-omni*

CHALLENGES OF COMPLEX ENDOVASCULAR PROCEDURES

Performing complex endovascular procedures present various challenges, as touched upon in the paragraphs above. The majority of the challenges leads back to an inability to gain complete 3D understanding of the orientation of the endovascular devices in relation to the patient's anatomy. Simply because the standard imaging methods such as fluoroscopy and DSA imaging are 2D, which makes it difficult to fully understand the volumetric information of the anatomy and the endovascular devices.

Rotation and angulation of the fluoroscopy images can improve the understanding of the arterial structures and their geometry, by providing projections from different perspectives. While the change of perspective is helpful to improve 3D understanding, it generally leads to higher procedure times, radiation exposure and iodinated contrast material, especially when lateral projection angles are being used. [14,15] In some cases, the desired projection angles are not even achievable due to restrictions of the table and C-arm suspensions.

Excessive radiation exposure poses risks for both patients and physicians. For patients, the stochastic carcinogenic risks associated with radiation are outweighed by the benefits of endovascular treatment itself. Nonetheless, their exposure should be minimized where possible, as the patient is likely to be exposed to additional radiation during follow-up and possible re-interventions.

Physicians are generally exposed to indirect scatter radiation rather dan direct irradiation of the primary beam. Although their exposure levels are significantly lower than those of patients, physicians do accumulate a significant amount of radiation throughout their lifelong careers in endovascular surgery. In fact, the yearly occupational

dose of interventional radiologists and vascular surgeons is amongst the highest observed in employees in medicine.[16] For physicians, intensive use of radiation may cause deterministic injury such as cataract or an increased risk of stochastic carcinogenic effects.

Instead of the 2D projections, physicians should ideally have access to 3D imaging of the entire vascular system and relevant endovascular devices. Real-time 3D feedback of the vascular system would aid morphological assessment, sizing, and spatial guidance of the endovascular devices. Additionally, 3D feedback would improve device steerability by providing cues on tension, curvature and the direction of the distal tip.

In recent years, modern fluoroscopy systems have made progress towards achieving this goal through multimodal image fusion and intraoperative cone-beam computed tomography (CBCT), which allow for 3D acquisition and visualization of the vascular anatomy in combination with real-time fluoroscopy. While these technologies have greatly enhanced the visualisation of the anatomy, there is still significant room for improvement when it comes to the visualization of the endovascular devices itself. Future developments in image guidance and device navigation that can provide real-time 3D feedback and visualization of endovascular devices without the need for radiation or contrast agents would greatly enhance the safety and efficacy of complex endovascular procedures.

AIM OF THIS THESIS

By exploring the latest advancements in imaging technologies, this thesis seeks to identify potential solutions for optimizing imaging and minimizing risks associated with radiation exposure in the endovascular treatment of obstructive peripheral artery disease and aortic disease. This includes the evaluation of benefits and limitations of currently existing techniques, and the development and exploration of new strategies that can improve intraoperative image guidance and device navigation.

Thesis outline
Part I: Radiation and education
The first section is focused on radiation and education and specifically examines the challenges associated with radiation exposure during endovascular procedures. This section evaluates the current techniques available for reducing radiation exposure, and proposes potential solutions for optimizing imaging and minimizing radiation risks.

This section starts off with and introduction in endovascular radiation principles and radiation reduction strategies in **Chapter 2**.

Chapter 3 evaluates the efficacy of a radiation absorbing drape during endovascular treatment of obstructive PAD. These drapes are designed to reduce the radiation exposure of physicians and medical staff during endovascular treatment by absorbing scatter radiation.

Chapter 4 explores the use of fresh frozen human cadavers as an endovascular training and research model. Realistic preclinical models are crucial to facilitate safe and effective training and evaluate new devices and imaging techniques, prior to their introduction in clinical practice.

Part II: Intraoperative image guidance
The second section is focused on intraoperative image guidance and aims to explore new strategies that can improve image guidance and device navigation during endovascular procedures. This section evaluates the benefits and limitations of currently available techniques and investigates the latest advancements in imaging technologies. The goal is to develop new strategies that can improve the safety and efficacy of endovascular procedures while also reducing radiation dosage.

This section starts off with a systematic review of the current state of endovascular image guidance and device navigation techniques in obstructive PAD in **Chapter 5**. In this chapter we aim to provide a broad overview of the latest imaging innovations for both surgeons well acquainted with endovascular imaging techniques and those seeking to become more familiar.

Image fusion guidance is a widely adopted strategy to guide target vessel catheterization during fenestrated and branched EVAR. The accuracy of the image fusion overlay depends strongly on (the lack of) intraoperative changes in anatomy. **Chapter 6** evaluates the intraoperative displacement of target vessels due to stiff guidewire and stent graft introduction, during fenestrated and branched EVAR.

Chapter 7 and **8** provide the first preclinical and clinical experiences with Fiber Optic RealShape (FORS). FORS is a new-to-world endovascular navigation platform by Philips Medical Systems, that provides real-time 3D visualization of FORS-enhanced guidewires and catheters in context to the anatomy.

In **Chapter 9** the main results of this thesis are summarized and future perspectives are discussed.

And **Chapter 10** contains a Dutch summary of this thesis.

REFERENCES

1. Wiseman, J. T. *et al.* Endovascular versus open revascularization for peripheral arterial disease. *Ann Surg* **265**, 424–430 (2017).
2. Tang, Q. H., Chen, J., Hu, C. F. & Zhang, X. L. Comparison Between Endovascular and Open Surgery for the Treatment of Peripheral Artery Diseases: A Meta-Analysis. *Ann Vasc Surg* **62**, 484–495 (2020).
3. Aboyans, V. *et al.* 2017 ESC guidelines on the diagnosis and treatment of peripheral arterial diseases, in collaboration with the european society for vascular surgery (ESVS). *Russian Journal of Cardiology* **23**, 164–221 (2018).
4. Kotov, A. *et al.* The prospective GermanVasc cohort study: Endovascular and open-surgical treatment of symptomatic peripheral artery disease. *Vasa - European Journal of Vascular Medicine* **50**, 446–452 (2021).
5. Bradbury, A. W. *et al.* A vein bypass first versus a best endovascular treatment first revascularisation strategy for patients with chronic limb threatening ischaemia who required an infra-popliteal, with or without an additional more proximal infra-inguinal revascularisation procedure to restore limb perfusion (BASIL-2): an open-label, randomised, multicentre, phase 3 trial. *The Lancet* **401**, 1798–1809 (2023).
6. Farber, A. *et al.* Surgery or Endovascular Therapy for Chronic Limb-Threatening Ischemia. *New England Journal of Medicine* **387**, 2305–2316 (2022).
7. Goldsweig, A. M. *et al.* Patient Radiation Dosage During Lower Extremity Endovascular Intervention. *JACC Cardiovasc Interv* **12**, 473–480 (2019).
8. Reimerink, J. J., Van Der Laan, M. J., Koelemay, M. J., Balm, R. & Legemate, D. A. Systematic review and meta-analysis of population-based mortality from ruptured abdominal aortic aneurysm. *British Journal of Surgery* **100**, 1405–1413 (2013).
9. Wanhainen, A. *et al.* European Society for Vascular Surgery (ESVS) 2019 Clinical Practice Guidelines on the Management of Abdominal Aorto-iliac Artery Aneurysms. *European Journal of Vascular and Endovascular Surgery* **57**, 8–93 (2019).
10. Sweeting, M. J., Thompson, S. G., Brown, L. C. & Powell, J. T. Meta-analysis of individual patient data to examine factors affecting growth and rupture of small abdominal aortic aneurysms. *British Journal of Surgery* **99**, 655–665 (2012).
11. Greenhalgh, R. M., Brown, L. C., Kwong, G. P. S., Powell, J. T. & Thompson., S. G. Comparison of endovascular aneurysm repair with open repair in patients with abdominal aortic aneurysm (EVAR trial 1), 30-day operative mortality results: randomised controlled trial. *J Vasc Surg* **40**, 419–423 (2004).
12. van Schaik, T. G. *et al.* Long-term survival and secondary procedures after open or endovascular repair of abdominal aortic aneurysms. *J Vasc Surg* **66**, 1379–1389 (2017).
13. Lederle, F. A. *et al.* Outcomes following endovascular vs open repair of abdominal aortic aneurysm: A randomized trial. *JAMA - Journal of the American Medical Association* **302**, 1535–1542 (2009).
14. Becquemin, J.-P. *et al.* A randomized controlled trial of endovascular aneurysm repair versus open surgery for abdominal aortic aneurysms in low- to moderate-risk patients. *J Vasc Surg* **53**, 1167-1173.e1 (2011).
15. Lijftogt, N. *et al.* Adjusted Hospital Outcomes of Abdominal Aortic Aneurysm Surgery Reported in the Dutch Surgical Aneurysm Audit. *European Journal of Vascular and Endovascular Surgery* **53**, 520–532 (2017).
16. Gonzalez, L. *et al.* Latest recanalization techniques for complex superficial femoral artery occlusions. *J Cardiovasc Surg (Torino)* **53**, 487–494 (2012).
17. Ruiter, Q. M. B. De, Reitsma, J. B., Moll, F. L. & Herwaarden, J. A. Van. Meta-analysis of Cumulative Radiation Duration and Dose During EVAR Using Mobile , Fixed , or Fixed / 3D Fusion C-Arms. *Journal of endovascular therapy* **23**, 944–956 (2016).
18. Padovani, R. *et al.* International project on individual monitoring and radiation exposure levels in interventional cardiology. *Radiation Protection Dosimetr* **144**, 437–441.

PART I

RADIATION AND EDUCATION

CHAPTER | 2

Reducing Radiation Exposure in Endovascular Procedures – Intraoperative Management

ABSTRACT

Endovascular surgery is a rapidly evolving field of medicine. The growing popularity of endovascular interventions is inextricably linked to an increase in radiation exposure of patients and physicians, due to the intensive use of X-ray imaging. Radiation safety is therefore an integral part of good clinical practice in the endovascular field. This chapter addresses the essentials of radiation physics and provides clinically relevant strategies on radiation reduction to enable physicians to keep the radiation exposure of their patients, their teams and themselves 'as low as reasonably achievable'.

INTRODUCTION

The treatment of vascular patient has shifted from an open surgical approach to an endovascular approach throughout the last decades. Nowadays, more than 70% of the aneurysm repairs in Western Europe are performed using endovascular techniques.[1] This paradigm shift has intensified the use of X-ray imaging.

An average patient undergoing endovascular aortic repair (EVAR) is exposed to an effective radiation dose of 11.7 mSv.[2] The radiation risks associated to this relatively low radiation dose, are outweighed by the benefits of endovascular treatment for these patients. During these procedures, not only the patient, but also the medical staff is exposed to radiation, although their exposure levels are significantly lower than those of patients. Nevertheless, by performing endovascular procedures on a daily or weekly basis, physicians accumulate a significant amount of radiation throughout their careers. In fact, the yearly occupational dose of interventional radiologists and vascular surgeons is amongst the highest observed in employees in medicine.[3] Current trends show an expansion of endovascular workload combined with an increase in procedural complexity and procedure diversity, which suggests a further expansion of the radiation exposure of physicians in the next decade.

Exposure to radiation has been associated to solid cancer, leukaemia and cardiovascular disease. To minimize radiation risks of physicians, an annual occupational dose limit of 20 mSv has been set. However, recent biological studies have shown that DNA damage responses occur in physicians who were exposed to radiation during an endovascular procedure, even if the received dose was well within the defined dose limits.[4] Although further studies are needed to fully understand how these acute biological reactions relate to long term induction of disease, these studies underline the need for cautious use of radiation.

The directives of the International Commission on Radiological Protection (ICRP) instruct that radiation exposure of patients and staff should be kept 'as low as reasonably achievable', often referred to by its acronym ALARA. Despite the broad international adherence of the ALARA principle, a substantial variation in radiation levels is observed in similar endovascular procedures, both in terms of patient dose and physician dose.[5] This variation suggests that radiological protection strategies can be improved in a substantial part of the performed procedures. Physicians play a key role in this optimization process.

In this chapter, the essentials of radiation physics and radiation protection are discussed, as well as strategies to reduce radiation exposure during endovascular procedures, while maintaining sufficient image quality and an ergonomic workflow. These strategies are based on the latest ICRP recommendations and relevant publications on radiation protection.

MATERIALS AND METHODS

Radiation Principles

Fluoroscopy and digital subtraction imaging (DSA) are based on the interaction of X-rays with tissue. Some X-rays pass through the tissue freely, while others are absorbed by the tissue. In which ratio these tissue interactions occur depends upon the tissue density, for example, bones absorb more X-rays than muscle. Differences in tissue density and tissue thickness are reflected in different tones of black and white of the X-ray image. It is also possible that the tissue absorbs only part of the X-ray's energy, in which case the residual energy is scattered into a different direction. Scattered X-rays cause image noise as some of the deflected X-rays hit the detector from an odd angle. This scatter radiation is the main source of radiation exposure for physicians and medical staff.

Stochastic and deterministic effects of radiation

The biological effects of radiation are classified as either deterministic or stochastic. Deterministic effects are tissue reactions such as skin injuries and cataract, which occur after a certain threshold dose is reached. Past this threshold, the severity of the effect increases proportionally with the received dose.

Unlike deterministic effects, stochastic effects occur by chance. Well established stochastic effects include carcinogenesis and hereditary effects, but also cardiovascular and respiratory diseases have been marked recently as a potential stochastic effects.[6,7] Current scientific evidence suggests a linear dose-response relationship between exposure to high-doses of ionizing radiation and the development of stochastic effects (mainly cancer) in humans.[8] This linear correlation is based on the life span study of atomic bomb survivors of Hiroshima and Nagasaki, and was the foundation for the widely used Linear No Threshold (LNT) model. The LNT model suggest that all radiation, even at low dose rates creates an excess risk of cancer. However, the validity of the LNT model in the low-dose spectrum (<100 mSv) is controversial.[9] Epidemiological cohort studies in radiation workers are contradictory and marked by statistic limitations, incomplete dosimetry records and the many confounders involved in carcinogenesis.[10–12] Besides, a more individual approach of risk profiling would be more appropriate, as different individuals are known to have different radiation sensitivities.[4] Despite its controversy, many international commissions use the LNT model to draft guidelines and estimate excess risks caused by low dose radiation exposure, including the ICRP and the committee on Biological Effects of Ionizing Radiation (BEIR).

Dosimetry

Patient dose

Fluoroscopy time (FT) was the first available measure to estimate the patient dose during endovascular interventions. Although the FT is still frequently mentioned in publications, its correlation with radiation dose is generally poor. Dose area product (DAP) and air kerma (AK) have a much stronger correlation to radiation dose.[13] The DAP, expressed in $Gycm^2$ is calculated by multiplying the tissue dose with the irradiated area, the cumulative DAP thereby reflects the total amount of radiation delivered to the patient. The AK, expressed in Gy, is defined as the amount of radiation delivered to the patient entrance reference point, located 15 cm from the system's isocenter. The cumulative AK thereby reflects the peak skin dose of the patient, which can be used to assess the risk of skin injury.

Neither the DAP nor the AK is actively measured inside the patient, but instead computed based on geometry of the X-ray system and measurements performed near the detector. Despite, the fact that these are estimates rather than measurements, the DAP and AK are useful to compare radiation doses amongst interventional procedures, manufacturers and/or institutions. Additionally, high values of DAP (> 500 $Gycm^2$) and AK (>2 Gy) can be used as an indicator for potential skin injury. Whenever these thresholds are exceeded, the patient should be monitored more closely during follow-up to identify tissue reactions in an early stage.

To address the risk of biological damage from radiation exposure the effective dose (ED) is used, expressed in mSv. The concept of ED was developed by ICRP to provide a global risk-adjusted dose quantity that could be used to express all sorts of (medical) radiation. The ED takes into account the type of radiation, the type of irradiated tissue, gender and age of the recipient. For patients, the ED is traditionally based on Monte Carlo simulations in mathematical anthropomorphic phantoms. Alternatively, the ED can be estimated by multiplying the cumulative DAP of the procedure with a procedure-specific or region-specific conversion factor. The conversion factor provided for abdominal endovascular procedures is 0.22 $mSv/Gycm^2$.[14] For women and children this factor is slightly higher due to their susceptibility for radiation.

Physician dose

The radiation exposure of the medical staff is estimated using a dosimeter badge, that is typically worn outside the lead apron at chest level. The dosimeter badges measure the equivalent dose at 10 mm depth (Hp(10)) which can be used as a conservative estimate for the ED, both expressed in mSv. In Europe, the ED limit for medical staff is 20 mSv per year.[15] Additionally, there is a specific dose limit of the eye lens, which has been recently been reduced from 150 mSv per year to 20 mSv, as ophthalmological studies showed an increased incidence of cataract in radiation workers.[16]

Radiation reduction strategies

In general, a reduction of patient dose directly translates to a reduction in dose for the physicians and medical staff. Therefore, radiation reduction strategies will be discussed in general, with specific elaborations on patient or staff dose when applicable.

Radiation safety training of physicians

Most radiation reduction strategies are a trade-off between radiation dose and image quality. The physician holds the ultimate responsibility for the optimization of this balance. However, many physicians have not received formal radiation safety training during their careers.[17] In most countries, radiation safety courses have been added only recently to the mandatory curriculum of vascular surgery. Rather frequently, these courses comprise of general theoretical knowledge, rather than practical implementations in endovascular practice. It is therefore strongly encouraged to attend hands-on training programs on radiation protection or use the training material produced by the International Atomic Energy Agency.[18]

Diagnostic reference levels

Diagnostic reference levels (DRL) were developed as a reference guide on 'acceptable' patient dose during common radiological examinations and procedures. DRLs can be used to determine abnormally high or low patient exposure for a specific procedure and are widely used in diagnostic examinations (e.g. CT scan or X-thorax). For interventional procedures however, the use of DRLs was just recently called into action. The vast majority of the European countries has yet to determine relevant DRLs for common endovascular procedures, by means of surveys and registries. The existing DRLs are summarized in the European Study on Clinical Diagnostic Reference.[19]

Setup of the interventional suite

Radiation safety should be an important consideration during the investment and build of new interventional suites and hybrid operating rooms, as the choice of equipment and setup have large impact on radiation exposure.[20] The operating room should be optimized for its intended procedures, including the choice of X-ray system and the suspension of the ceiling-mounted radiation shields. Large display monitors must be used when possible to reduce the need for image magnification and prevent physicians from leaning over the patient (i.e. radiation source) to get a better view.[21] Facilities that are regularly used by non-sterile nurses and anaesthetists, such as phones and PCs, should be shielded from high radiation zones as much as possible.

Service contracts should include regular maintenance and updates of software and hardware to keep up with the most recent technical innovations on radiation reduction. A past example is the Allura Clarity upgrade on the Philips Allura FD 20 systems (Philips, Best, the Netherlands), which allowed a significant reduction in radiation dose in a variety of procedures, by means of software and hardware adaptions.[22,23]

Imaging protocols

Modern X-ray systems are self-regulatory for the greater part. The kV, mA and filtration of the system are continuously adjusted, based on the dose rate measured near the detector. This feedback-loop is called the automatic exposure control (AEC). The AEC allows the system to generate stable, high image quality even in difficult conditions, such as obese patients or highly angulated projection views. The automatic adjustments are restricted by a maximum dose or dose rate, which is protocol-specific and can differ per manufacturer. Most manufacturers focus on image quality rather than radiation exposure as their primary selling point, and thus, most standard settings are tuned to optimize image quality, even if this is at the expense of radiation dose.

Fortunately, most manufacturers offer customization of their existing imaging protocols on request, including adjusted restriction of maximum dose, added filtration or a reduction in fluoroscopy frame rate. An example of such a customized imaging protocol is the Eco-dose protocol designed by Ruffino et al.[24] which was able to cut the radiation dose in half during standard EVARs.

Cone beam computed tomography

Cone beam computed tomography (CBCT) is an intraprocedural imaging technique that has quickly gained popularity in endovascular surgery. CBCT scans are conventionally used to register the patient's on-table anatomy to a preoperative computed tomography angiography (CTA), but can also be used on their own as a three-dimensional overlay or a verification scan. CBCT thereby provides three-dimension insight in the patient's anatomy.

The acquisition of a CBCT requires a substantial amount of radiation and its use needs to be justified. This means that the use of CBCT should achieve enough navigational or diagnostic benefit to offset its radiation costs. Sailer et al.[25] reported that an average CBCT in the abdominal region accounted for a DAP of 14.7 Gycm² (ED of 4.3 mSv), which corresponded to roughly 7 minutes of fluoroscopy in the same region of interest in terms of DAP, or approximately one third of a standard CTA abdomen in terms of ED. Due to the relatively high radiation exposure of a CBCT, the balance between image quality and radiation dose should be optimized for its intended purpose. In general, a region-specific low-dose CBCT protocol should be selected. Breath-hold should be used to avoid motion artefacts. Modern image reconstruction algorithms should be used when available to reduce image noise and improve image quality. All medical staff, including physicians, should move outside the operating room during the acquisition of the CBCT. When this is not feasible, the distance from the patient should be maximized and additional shielding should be used.[26]

Frame rate

Standard fluoroscopic imaging protocols typically use a frame rate of 15 - 30 fps. Frame rate reductions from 15 fps to 7.5 fps can reduce the radiation dose with 36%, while maintaining diagnostic image quality.[27] Notice that this effect is not strictly linear, due to AEC adaptations that emphasize on image quality of the individual frames when using

lower frame rates. In the cardiology field frame rates of 4 fps have been proven effective when used in combination with frame-interpolation to keep sufficient image fluency and reduce flicker.[28,29]

Collimation

Collimation should be used to reduce the field of view whenever possible without interfering with the task at hand. Collimation decreases the area of irradiation and thereby proportionally decreases the DAP and image noise. Collimation is especially desirable during focussed tasks, such as stent deployment or the cannulation of visceral or renal target vessels during fenestrated or branched EVAR. Figure 1 compares the radiation dose of a non-collimated and a collimated image.
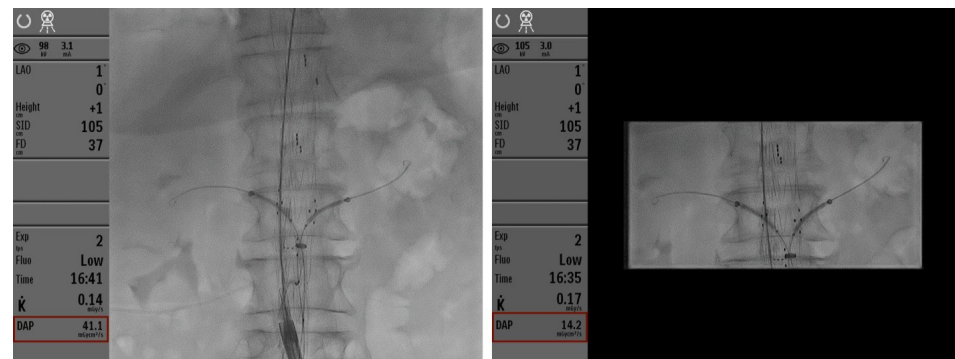
A. Without collimation, full field of view   B. With collimation, selective focus on target vessels

Figure 1. *Field size reduction by means of collimation reduces the dose area product (DAP) significantly (41.1 mGycm²/s vs 14.2 mGycm²/s). Due to automatic exposure control, the kV and mAs are adjusted to optimize the image quality, thereby causing a slight increase in air kerma rate (0.14 vs 0.17 mGy/s).*

Metal objects

Metal has a high attenuation coefficient, which triggers the AEC to increase the dose rate of the X-ray system. Presence of a large metal object within the field of view, such as a clamp or hip prosthesis, should be avoided by either collimation or movement of the field of view.

Magnification

Modern systems with flat panel detectors allow digital magnification by either enlarging the image without true increase of spatial resolution (like a digital photo), or by 'unbinning' grouped pixels into single pixels thereby increasing spatial resolution. While neither of these processes on their own increases the radiation dose, most manufactures have linked magnification to a gradual increase in dose rate, as image noise within these

magnified images is more apparent to the eyes of the observer.[30] Magnification should therefore only be used when clinically necessary. When possible, magnification should be combined with additional collimation to counteract the increase in radiation dose.

Table and detector height

A high table position reduces the peak skin dose of the patient (AK) and increases the field of view without requiring magnification. However, a high table position exposes the legs and pelvis of the physician of higher levels of scatter radiation.[31] Table-mounted and ceiling-mounted shields should be used to shield the operators from this increase in dose (see paragraph on 'radiation shields'). In addition to these radiation considerations, the table position should allow an ergonomic working position for the physician.

Independent of the choice of table position, the airgap between the patient and the detector should always be kept to a minimum. A smaller air gap reduces the patient dose and physician dose and increases image quality.

Projection angle

Irradiation of a patient creates a cloud of scatter radiation, the geometry of this cloud differs per patient and per interventional suite. The scatter profile is also affected by the position and orientation of the C-arm. The highest level of scatter radiation occurs on the side of the X-ray source, adjacent to the skin entry point of the primary beam, as a large portion of X-rays are reflected upon first interaction with tissue. Thus, during an anterior-posterior projection angle the high radiation zone is located at the level of the legs of the physician, while during an 90° LAO projection angle the high radiation zone is located on the right side of the patient, at the level of the abdomen and thorax of the physician.

Angulation of the C-arm does not only alter the geometry of the scatter cloud but also increases the tissue thickness, which is compensated for by an increase in dose rate. Projection angles of 75 – 90° can cause a 4-fold increase of the dose rate compared to an anterior-posterior view.[32] The combination of these high dose rates and the unfavourable geometry of the scatter cloud, has been shown to cause a 15-fold increase of the physician's chest dose.[33]

In general, it is best to use under-table positions of the X-ray source to minimize radiation to the chest and head of the physician. Physicians and sterile nurses should avoid positions on the same side as the X-ray source. Highly angulated views should be used only when absolutely necessary.

Anticipate high radiation exposure

Complex procedures (e.g. fenestrated or branched EVAR) require intensive use of fluoroscopy and are likely to last longer, thereby leading to high patient and physician doses. Obese patients also form a risk factor, as higher doses are needed to pass through the tissue.
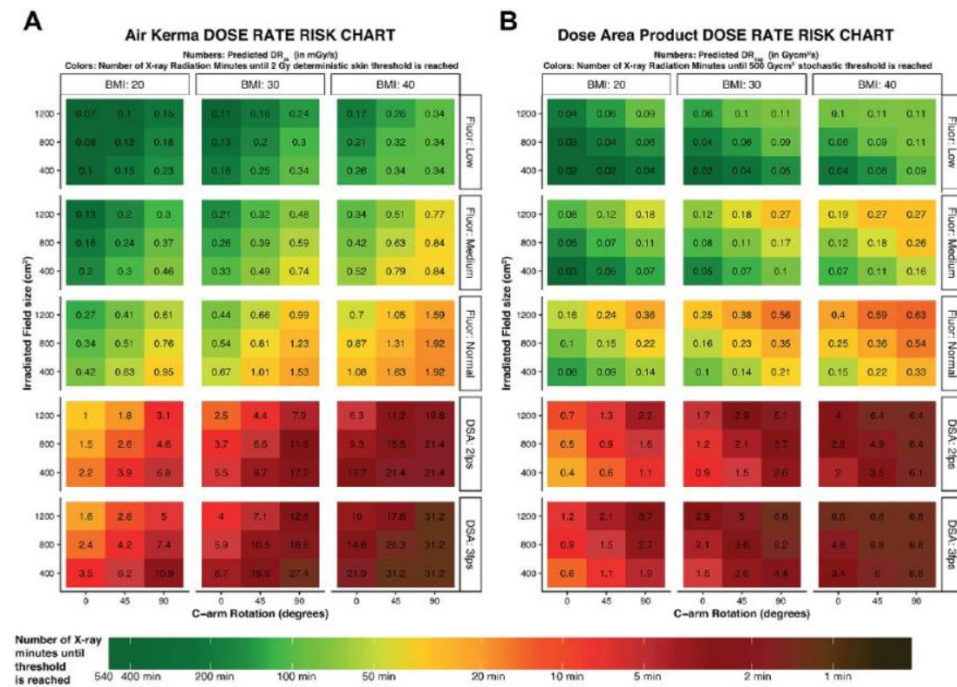
Figure 2. Risk charts for radiation dose rates for (A) air kerma and (B) dose area product for fluoroscopy (Fluor) and digital subtraction angiography (DSA) imaging protocols. The color-coding represents the predicted amount of radiation minutes that can be acquired until the 2-Gy skin threshold for air kerma or the 500-Gycm2 threshold for dose area product is reached. For all predicted outcomes, the C-arm angulation was set at 0°, and the source-to-image distance was set at 100 cm for the DSA charts.

Furthermore, physicians should be aware of the intraprocedural fluctuations in radiation dose. De Ruiter et al.[32] developed a patient risk chart that visualizes the influence of various procedural factors on patient dose (Figure 2). This chart can help the physician to anticipate radiation-demanding steps in the procedure.

Radiation reduction strategies for medical staff

Personal protection
Physicians performing endovascular procedures should always wear a fitted lead apron and thyroid shield. Leaded glass eyewear is desired in aortic, iliac and femoral procedures, to adhere to the reinforced dose limits for the eye lens.[16]

Real-time dosimeters for medical staff
Real-time dosimeter badges display the radiation levels of physicians and medical staff throughout the endovascular procedure. The immediate dosimetric feedback helps to

optimize shielding and standing positions during every step of the procedure. The use of these real-time dosimeters can promote radiation awareness and provide insight in radiation patterns inside the OR. Leading to a higher compliance of radiation protection strategies and a significantly lower radiation dose of all staff members.[34]

Distance
The radiation levels decrease quadratically with increasing distance from the radiation source. All medical staff should therefore aim to maximize distance from the patient when possible.

Radiation shields
When placed properly, radiation shields create a barrier between the source of the scatter radiation (the patient) and the physician or other medical staff.[35,36] The most commonly used radiation shields are table-mounted shields, ceiling-mounted shields, radiation absorbing drapes.

Table-mounted lead shields aim to reduce the radiation dose of the legs and pelvis of the physicians and sterile assistants. The use of a fold-down topshield attached to these shields offers additional protection to the pelvis and abdomen of its users. The shields should be attached to a non-moving table rail, to prevent interference with the C-arm system after table movement.

Ceiling-mounted lead shields aim to reduce the radiation dose to the abdomen, thorax and head of the physicians and sterile assistants. These should be placed directly against the patient to reduce air gaps and maximize the low-radiation 'shadow' casted by the shield. Ideally, the shields should be repositioned with each movement of the C-arm or table, to maintain optimal low-radiation 'shadows' to shield physicians and medical staff. However, in clinical practice this seems rather difficult. The shields are shields are often pushed aside by movements of the X-ray system or the table or moved upwards by the physician to access the femoral sheaths.

Disposable radiation absorbing drapes are designed similar purposes as the ceiling-mounted lead shields, but the drapes require less maintenance in general. The radiation absorbing drapes are placed directly on top of the patient and therefore cast larger shadows and the position of the drapes remains unaffected by table or X-ray movements. However, care should be taken not to place the drape in the primary beam, as this increases the intensity of the beam through automated exposure and creates backscatter within the patient.[37,38] As the absorbing properties of radiation absorbing drapes are generally lower than those of the lead, they should not be used as a replacement for ceiling-mounted shields, but rather as an addition.

Other medical staff members, such as non-sterile nurses and anaesthesiologists, should aim to stand in low-radiation area when possible. Additionally, anaesthesiologists are advised to use moveable leaded wall-shields during complex endovascular procedures

in the thoracic and abdominal region. These wall shields are see-through and can be placed behind the patient's head.

Reduction strategies during DSA

Digital subtraction angiography (DSA) images are based on the subtraction of one fluoroscopy image from another. As both fluoroscopy images contain random image noise, the subtraction process will aggravate the image noise substantially. To counteract this effect, DSA images are acquired at a much higher dose than standard fluoroscopy. DSA runs account for approximately 43% of the DAP, and 50% of the AK during a standard EVAR procedure, while these DSA runs require is less than a minute of fluoroscopy time.[39] Radiation awareness during DSA acquisition has therefore a tremendous impact on cumulative radiation dose of the complete procedure. By adhering to these following steps, derived from previously mentioned radiation reduction strategies, the radiation dose can be reduced significantly:

1. **Projection angle:** When possible, choose a projection angle based on preoperative CTA imaging, to prevent redo's due to over-projection of other vascular structures. Try to avoid high projection angles where possible.
2. **Table and detector height:** Ensure that the table is at adequate height. Minimize the air gap between the patient and detector.
3. **Field of view:** Adjust the field of view to your region of interest. User collimation when possible to reduce the field of view.
4. **Clear the field of view:** Remove metal objects from the field of view.
5. **Optimize the position of radiation shields:** Place the ceiling-mounted lead shields against the patient's body.
6. **Distance:** Increase the distance from the patient by taking a few steps back when possible, aim to stand on the opposite side of the X-ray source. Use a power injector during long DSA runs to allow additional distance from the patient. Make sure that all staff members have moved away before initiating DSA.

FUTURE PERSPECTIVES

Recent developments in robotics and imaging enable partial or complete replacement of X-ray imaging during endovascular procedures. Well known examples are intravascular ultrasound (IVUS) and optical coherence tomography (OCT), which are both already broadly applied in cardiology and gain popularity in peripheral endovascular procedures. Both these catheter-based techniques can be used to guide optimal choice of treatment, deliver endovascular devices and verify stent deployment.[40]

Other innovations focus on the handling and visualization of endovascular devices inside the patient's body. While these technological developments have high future potential, their integration in common clinical practice is likely several years away. These include robotic endovascular systems with steerable catheter tips.[41] Although these robotic systems still require occasional fluoroscopy, the precision and stability of device control can reduce procedure times and radiation exposure to the patient, while the remote control of the robotic system minimizes physician dose.

Other systems have been developed that allow radiation-free, three-dimensional tracking and visualization of endovascular devices by means of either electromagnetic or fibre optic signals.[42] These systems are used in combination with preoperative or intraoperative anatomical roadmaps to navigate endovascular devices to their intended destination.

CONCLUSION

Adequately reduction and protection strategies should be employed to protect physicians and their patients during endovascular procedures. Significant reductions in radiation dose can be achieved by optimizing the X-ray equipment, its settings and its utilization.

REFERENCES

1 Lijftogt N, Vahl AC, Wilschut ED, Elsman BHP, Amodio S, van Zwet EW, et al. Adjusted Hospital Outcomes of Abdominal Aortic Aneurysm Surgery Reported in the Dutch Surgical Aneurysm Audit. Eur J Vasc Endovasc Surg 2017;**53**(4):520–32. Doi: 10.1016/j.ejvs.2016.12.037.

2 Jones C, Badger SA, Boyd CS, Soong C V. The impact of radiation dose exposure during endovascular aneurysm repair on patient safety. J Vasc Surg 2010;**52**(2):298–302. Doi: 10.1016/j.jvs.2010.03.004.

3 Padovani R, Heron J Le, Cruz-Suarez R, Duran A, Lefaure C, Miller DL, et al. International project on individual monitoring and radiation exposure levels in interventional cardiology. Radiat Prot Dosim n.d.;**144**(1–4):437–41.

4 El-Sayed T, Patel AS, Cho JS, Kelly JA, Ludwinski FE, Saha P, et al. Radiation-Induced DNA Damage in Operators Performing Endovascular Aortic Repair. Circulation 2017;**136**(25):2406–16. Doi: 10.1161/CIRCULATIONAHA.117.029550.

5 Hertault A, Rhee R, Antoniou GA, Adam D, Tonda H, Rousseau H, et al. Radiation Dose Reduction During EVAR: Results from a Prospective Multicentre Study (The REVAR Study). Eur J Vasc Endovasc Surg 2018;**56**(3):426–33. Doi: 10.1016/j.ejvs.2018.05.001.

6 Puukila S, Lemon JA, Lees SJ, Tai TC, Boreham DR, Khaper N. Impact of Ionizing Radiation on the Cardiovascular System: A Review. Radiat Res 2017;**188**(4.2):539–46. Doi: 10.1667/rr14864.1.

7 Baselet B, Rombouts C, Benotmane AM, Baatout S, Aerts A. Cardiovascular diseases related to ionizing radiation: The risk of low-dose exposure (Review). Int J Mol Med 2016;**38**(6):1623–41. Doi: 10.3892/ijmm.2016.2777.

8 National Research Council. Health Risks from Exposure to Low Levels of Ionizing Radiation. National Academies Press; 2006.

9 Mossman KL. The LNT debate in radiation protection: Science vs. policy. Dose-Response 2012;**10**(2):190–202. Doi: 10.2203/dose-response.11-017.Mossman.

10 Cardis E, Vrijheid M, Blettner M, Gilbert E, Hakama M, Hill C, et al. Risk of cancer after low doses of ionising radiation - Retrospective cohort study in 15 countries. Br Med J 2005;**331**(7508):77–80. Doi: 10.1136/bmj.38499.599861.E0.

11 Vrijheid M, Cardis E, Blettner M, Gilbert E, Hakama M, Hill C, et al. The 15-Country Collaborative Study of Cancer Risk among Radiation Workers in the Nuclear Industry: Design, Epidemiological Methods and Descriptive Results. Radiat Res 2007;**167**(4):361–79. Doi: 10.1667/rr0554.1.

12 Lee WJ. Lessons from radiation epidemiology. Epidemiol Health 2018;**40**:e2018057. Doi: 10.4178/epih.e2018057.

13 Skripochnik E, Loh SA. Fluoroscopy time is not accurate as a surrogate for radiation exposure. Vascular 2017;**25**(5):466–71. Doi: 10.1177/1708538117698342.

14 Compagnone G, Giampalma E, Domenichelli S, Renzulli M, Golfieri R. Calculation of conversion factors for effective dose for various interventional radiology procedures. Med Phys 2012;**39**(5):2491–8. Doi: 10.1118/1.3702457.

15 DIRECTIVE 2010/63/EU OF THE EUROPEAN PARLIAMENT AND OF THE COUNCIL. Off J Eur Union n.d.

16 Pinak M, Boal TJ. Dose limits to the lens of the eyes: New limit for the lens of the eye - International Basic Safety Standards and related guidance 2013:112–7.

17 Bordoli SJ, Carsten CG, Cull DL, Johnson BL, Taylor SM. Radiation safety education in vascular surgery training. J Vasc Surg 2014;**59**(3):860–864.e1. Doi: 10.1016/j.jvs.2013.10.085.

18 International Atomic Energy Agency - Training Material. https://www.iaea.org/resources/rpop/resources/training-material#1.

19 Damilakis J, Frija G, Hierath M, Jaschke W, Repussard J, Schegerer A, et al. European Study on Clinical Diagnostic Reference Levels for X-ray Medical Imaging Report and review on existing clinical DRLs 2018.

20 Christopoulos G, Christakopoulos GE, Rangan B V., Layne R, Grabarkewitz R, Haagen D, et al. Comparison of radiation dose between different fluoroscopy systems in the modern catheterization laboratory: Results from bench testing using an anthropomorphic phantom. Catheter Cardiovasc Interv 2015;**86**(5):927–32. Doi: 10.1002/ccd.26007.

21 Gailloud P. A large display is a powerful tool to reduce radiation exposure during single-plane fluoroscopically guided procedures. Am J Roentgenol 2015;**204**(4):W483–5. Doi: 10.2214/AJR.14.13246.

22 Stangenberg L, Shuja F, van der Bom IMJ, van Alfen MHG, Hamdan AD, Wyers MC, et al. Modern Fixed Imaging Systems Reduce Radiation Exposure to Patients and Providers. Vasc Endovascular Surg 2018;**52**(1):52–8. Doi: 10.1177/1538574417742211.

23 de Ruiter QM, Moll FL, Gijsberts CM, van Herwaarden JA. AlluraClarity Radiation Dose-Reduction Technology in the Hybrid Operating Room During Endovascular Aneurysm Repair. J Endovasc Ther 2016;**23**(1):130–8. Doi: 10.1177/1526602815622433.

24 Ruffino MA, Fronda M, Discalzi A, Isoardi P, Bergamasco L, Ropolo R, et al. Radiation dose during endovascular aneurysm repair (EVAR): upgrade of an angiographic system from standard to Eco mode. Radiol Medica 2018;**123**(12):966–72. Doi: 10.1007/s11547-018-0924-1.

25 Sailer AM, Schurink GWH, Wildberger JE, de Graaf R, van Zwam WH, de Haan MW, et al. Radiation Exposure of Abdominal Cone Beam Computed Tomography. Cardiovasc Intervent Radiol 2015;**38**(1):112–20. Doi: 10.1007/s00270-014-0900-7.

26 Rehani MM. Radiological protection in computed tomography and cone beam computed tomography. Ann ICRP 2015;**44**:229–35. Doi: 10.1177/0146645315575872.

27 Wilkins B, Simmonds M, Matsis P, Scott B, Gaskin D, Harding S, et al. Effect of Reduced Frame-Rate Protocol on Radiation Dose During Cardiac Catheterisation. Hear Lung Circ 2018;**27**:S491–2. Doi: 10.1016/j.hlc.2018.06.1021.

28 Boudjemline Y. Effects of reducing frame rate from 7.5 to 4 frames per second on radiation exposure in transcatheter atrial septal defect closure. Cardiol Young 2018;**28**(11):1323–8. Doi: 10.1017/S1047951118001257.

29 Hiremath G, Meadows J, Moore P. How Slow Can We Go? 4 Frames Per Second (fps) Versus 7.5 fps Fluoroscopy for Atrial Septal Defects (ASDs) Device Closure. Pediatr Cardiol 2015;**36**(5):1057–61. Doi: 10.1007/s00246-015-1122-8.

30 Nickoloff EL. AAPM/RSNA Physics Tutorial for Residents: Physics of Flat-Panel Fluoroscopy Systems. RadioGraphics 2011;**31**(2):591–602. Doi: 10.1148/rg.312105185.

31 D'Othée BJ, Lin PJP. The influence of angiography table shields and height on patient and angiographer irradiation during interventional radiology procedures. Cardiovasc Intervent Radiol 2007;**30**(3):448–54. Doi: 10.1007/s00270-006-0063-2.

32 De Ruiter QM, Gijsberts CM, Hazenberg CE, Moll FL, Van Herwaarden JA. Radiation Awareness for Endovascular Abdominal Aortic Aneurysm Repair in the Hybrid Operating Room. An Instant Patient Risk Chart for Daily Practice. J Endovasc Ther 2017;**24**(3):425–34. Doi: 10.1177/1526602817697188.

33 Haqqani OP, Agarwal PK, Halin NM, Iafrati MD. Defining the radiation "scatter cloud" in the interventional suite. J Vasc Surg 2013;**58**(5):1339–45. Doi: 10.1016/j.jvs.2013.01.025.

34 Racadio J, Nachabe R, Carelsen B, Racadio J, Hilvert N, Johnson N, et al. Effect of real-time radiation dose feedback on pediatric interventional radiology staff radiation exposure. J Vasc Interv Radiol 2014;**25**(1):119–26. Doi: 10.1016/j.jvir.2013.08.015.

35 Miller DL, Vaño E, Bartal G, Balter S, Dixon R, Padovani R, et al. Occupational Radiation Protection in Interventional Radiology: A Joint Guideline of the Cardiovascular and Interventional Radiology Society of Europe and the Society of Interventional Radiology. Cardiovasc Interv Radiol 2009;**33**:230–9. Doi: 10.1016/j.yrad.2010.12.015.

36 Kloeze C, Klompenhouwer EG, Brands PJM, Van Sambeek MRHM, Cuypers PWM, Teijink JAW. Editor's choice - Use of disposable radiation-absorbing surgical drapes results in significant dose reduction during EVAR procedures. Eur J Vasc Endovasc Surg 2014;**47**(3):268–72. Doi: 10.1016/j.ejvs.2013.12.008.

37 King JN, Champlin AM, Kelsey CA, Tripp DA. Using a sterile disposable protective surgical drape for reduction of radiation exposure to interventionalists. Am J Roentgenol 2002;**178**(1):153–7. Doi: 10.2214/ajr.178.1.1780153.

38 Taharim NK, Yeong CH, Ng KH, Abdullah BJJ. Evaluation of Occupational Dose Reduction in Interventional Radiology Using Lead-Free Protection Drape. 2015. pp. 1–13.

39 de Ruiter QMB, Jansen MM, Moll FL, Hazenberg CEVB, Kahya NN, van Herwaarden JA. Procedure and step-based analysis of the occupational radiation dose during endovascular aneurysm repair in the hybrid operating room. J Vasc Surg 2018;**67**(6):1881–90. Doi: 10.1016/j.jvs.2017.09.043.

40 Spiliopoulos S, Kitrou P, Katsanos K, Karnabatidis D. Expert Review of Medical Devices FD-OCT and IVUS intravascular imaging modalities in peripheral vasculature. Expert Rev Med Devices 2017;**14**(2):127–34. Doi: 10.1080/17434440.2017.1280391.

41 Ghamraoui AK, Ricotta JJ. Current and Future Perspectives in Robotic Endovascular Surgery. Curr Surg Reports 2018;**6**(12):1–7. Doi: 10.1007/s40137-018-0218-5.

42 Tystad Lund K, Tangen GA, Manstad-Hulaas F. Electromagnetic navigation versus fluoroscopy in aortic endovascular procedures: a phantom study. Int J Comput Assist Radiol Surg 2017;**12**(1):51–7. Doi: 10.1007/s11548-016-1466-4.

CHAPTER | 3

Reduction of Occupational
Radiation Exposure of Operators
during Peripheral Endovascular
Procedures by means of
Radiation Absorbing Drapes

ABSTRACT

Objective

Chronic exposure to low dose radiation, as encountered in endovascular procedures, may impact the health of surgeons and radiologists over a timespan of several months to a lifetime. This study evaluates the feasibility and efficacy of a radiation absorbing sterile drape (RADPAD®) to reduce operator exposure during endovascular treatment of obstructive peripheral artery disease (PAD).

Methods

Between February 2016 and September 2017, patients with PAD who received percutaneous transluminal angioplasty, stent placement, remote endarterectomy, or a combination thereof were included in this nonrandomized study. Patients were equally divided over a study cohort (with RADPAD) and a control cohort (without RADPAD). The unshielded body dose (E) of the staff was measured via electronic dosimeters placed at a chest height of the first operator (FO), second operator (SO), and sterile nurse (SN). A virtual maximum operator (MO) dose was constructed, yielding the highest dose per fluoroscopy run for either of the operators. Simultaneously, the dose area product (DAP) and C-arm settings for each fluoroscopy run were extracted. Staff exposures of the study cohort and control cohort were compared in terms of relative exposure (E/DAP). A secondary analysis involved an analysis of the individual fluoroscopy runs using a multivariate generalized linear mixed effect model.

Results

In total, 49 patients were included in this study. The use of RADPAD was technically feasible. Significant reductions of relative exposure were observed when comparing the study cohort with the control cohort. The relative exposure of the FO was reduced with 66.5% (1.82 vs. 0.61 µSv/Gycm2, P < 0.001), the relative exposure of the SO with 68.3% (0.55 vs. 0.17 µSv/Gycm2, P = 0.02), and the relative exposure of the MO with 65.8% (2.06 vs. 0.71 µSv/Gycm2, P < 0.001). Dose levels of SN were too low to draw conclusions under the current sample size. The multivariate generalized linear mixed effect model showed a significant correlation between absolute exposure of the MO and the use of the RADPAD (odds: 0.51, P < 0.001).

Conclusions

Usage of a radiation absorbing drape (RADPAD) during endovascular treatment of PAD results in statistically significant reduction in a relative operator dose while presenting no drawbacks. The use of these drapes is advised in future peripheral endovascular procedures.

INTRODUCTION

The expanding endovascular workload of vascular surgeons and interventional radiologists has raised concerns in terms of occupational exposure to low-dose scatter radiation. Throughout the last decade, technological developments have enabled the treatment of increasingly complex pathologies, which have intensified the use of radiation.[1] A recent multicentre study by Goldsweig et al.[2] reveals that 1 in 14 peripheral endovascular procedures exceed the dose area product (DAP) limit endorsed by the National Council in Radiation Protection (NCRP) of 500 Gycm2. These procedures often involve the treatment of chronic total (femoral and/or below the knee) arterial occlusions, in which long lasting digital subtraction angiography (DSA) runs are required to visualize distal perfusion in the lower extremity via collateral vessels.

For physicians, the intensive use of radiation poses a risk of cataract and malignant disease.[3–5] The risk of malignant disease is commonly estimated using a linear no threshold (LNT) model for purposes of radiological protection.[6] This model assumes that the risk of radiation damage is proportional to the total accumulated dose and delineates that there is no such thing as 'safe' radiation exposure.

Medical staff can prevent unnecessary radiation exposure by using radiation protection devices such as leaded aprons, thyroid collars, and different types of radiation shields. A more recent innovation in radiation shielding is the radiation absorbing drape, such as the RADPAD (Worldwide Innovations & Technologies Inc., Kansas City, KS, USA). These drapes are placed on top of the patient and absorb (part of the) scatter radiation coming from the patient, thereby creating a low-radiation shadow in which the physician can position themselves.

Various studies have reported significant reductions (23–80%) in the operator dose by using radiation absorbing drapes during interventions in the thoracoabdominal region.[7–13] However, data on the efficacy of the drapes during endovascular treatment of peripheral artery disease (PAD) are scarce and fail to take into account the (highly variable) patient exposure.[14] This study aims to provide an analysis of the efficacy of the radiation absorbing drape in the peripheral region.

MATERIALS & METHODS

Patients

This single-center prospective nonrandomized study was conducted between February 2016 and November 2017. Patients undergoing (hybrid) endovascular intervention of the iliac, femoral, popliteal, and crural arterial segment or a combination thereof were

included in this study. Patients were equally divided over a study cohort (with RADPAD) and a control cohort (without RADPAD). Patient allocation was a result of 1) logistics; the RADPADs were not available during the first phase of this study and 2) the aim to have an equal distribution of procedural location between the two groups. Endovascular treatment involved balloon angioplasty (with standard or drug coated balloons), stent placement, remote endarterectomy, or a combined treatment. Because this study does not impose a risk or benefit to the patient, an informed consent was waived by the local ethics committee.

All interventions were conducted in a dedicated hybrid operating room, equipped with the Philips Allura Xper FD20 FlexMove system with ClarityIQ technology (Philips Healthcare Systems, Best, the Netherlands) in combination with a Maquet surgical table with 360° radiolucent tabletop (Maquet GmbH, Rastatt, Germany).

Study protocol

The interventions were performed by at least one staff vascular surgeon (first operator, FO), usually in combination with a surgeon in training (second operator, SO) and a sterile nurse (SN). The FO was responsible for decision making. The FO and SO were both involved in guidewire and catheter manipulation, balloon angioplasty, stent placement, and the use of remote endarterectomy. The working position of the staff members differed between cases based on the type and location of the intervention, the C-arm configuration, and personal preference. Working positions are explained in *Figure 1*.

In both the study and control groups, the principle of 'as low as reasonably achievable' (ALARA) was attained; attention was paid to careful collimation, minimization of source-to-detector distance, and minimization of angulation of the C-arm. Standard radiation shields were used in all procedures, consisting of two table-mounted lead curtains (both sides of the table) and two ceiling-mounted shields of the leaded glass (one on each side of the patient). Restrictions of the ceiling-mounted suspension system inhibited a bilateral use of the ceiling screens in a few procedures.

In the study group, the standard practice was expanded with the RADPAD #5300 radiation absorbing drape (Worldwide Innovations & Technologies Inc., Kansas City, KS, USA). These sterile, lead-free drapes contain bismuth and barium compounds that absorb (scatter) radiation using photoelectric absorption as the main mechanism of interaction. The RADPADs are positioned on top of the patient's hip or leg, such that the operators could position themselves in the low-radiation 'shadow' of the drape. Care was taken not to place the drape in the primary X-ray beam because this increases the radiation intensity of the primary beam and causes backscatter.[9,15] Either one or two RADPADs were used, based on the position of the FO and SO relative to the table; when both operators were positioned on the same side of the table, one RADPAD was used and when the operators were standing on opposite sides of the table, two RADPADs were used (Figure 1).
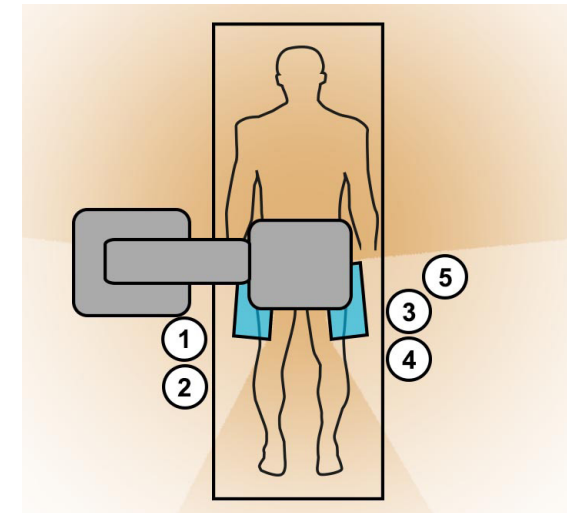
Figure 1: Schematic overview of RADPAD placement and working position of the staff. RADPADs absorb scatter radiation coming from the patient and thereby create a 'radiation shadow' in which the staff can position themselves. The RADPAD is indicated with a blue rectangle and asterisk. Working positions of the staff are indicated by the numbered circles, working positions, and RADPAD placement differs per type of procedure:

- *During right iliac procedures, FO: position 1, SO: position 2, and SN: position 4. RADPADs are used on both sides.*
- *During left iliac procedures, FO: position 3, SO: position 2, and SN: position 4. RADPADs are used on both sides; During both right and left femoral procedures, FO: position 3, SO: position 4, and SN: position 5. A single RADPAD is placed on the left side.*
- *During crossover iliofemoral procedures of the right leg (access left), FO: position 3, SO: position 4, and SN: position 5. A single RADPAD is placed on the left side;*
- *During crossover procedures, iliofemoral procedures of the left leg (access right), FO: position 1, SO: position 2, and the SN: position 2. A single RADPAD is placed on the right side.*

Real-time dosimeters of the DoseAware Xtend system (Philips Healthcare, Best, the Netherlands) were used to provide dosimetry records of the FO, SO, and SN. These dosimeters measure the effective dose over lead (E, in mSv). The dosimeters were attached to the left breast pocket or the left side of the thyroid collar of the FO, SO, and SN. When staff members were substituted by their colleagues during the procedure, the dosimeter was transferred to the substitute.

Relative exposure dose

The operator dose is strongly correlated with the patient dose; the higher the patient exposure, the more scatter radiation will be produced. To compensate for the differences between patient dose, an adjustment for dose area product (DAP, in Gycm2) was used. The DAP is proportional to the dose received by the patient and is calculated by

multiplying the tissue dose with the irradiated area. Throughout this study, the DAP-adjusted relative exposure is used (E/DAP in mSv/Gycm2).

Data collection

Baseline characteristics were extracted from the electronic patient record. Procedural characteristics associated with radiation exposure were collected during the procedure including the lesion location, number of ceiling-mounted shields, and number of RADPADs.

An effective dose of FO, SO, and SN was collected per individual fluoroscopy run. One fluoroscopy run is defined of a single continuous press of the fluoroscopy foot pedal. A virtual maximum operator (MO) dose was constructed, yielding the highest dose per fluoroscopy run for either of the operators. Simultaneously, parameters of C-arm geometry and C-arm dosimetry were collected for each fluoroscopy run, including, but not limited to: fluoroscopy time (FT), dose area product (DAP), tube current (mA), peak tube voltage (kVp), C-arm angulation and rotation, field size, and detector-source distance.

Study objectives

The primary objective of this study was to assess the effect of the RADPAD on relative exposure (E/DAP) of FO, SO, SN, and the virtual MO. Differences in relative exposure of the staff members between the study group and control group were examined using the nonparametric Mann–Whitney U-test. Missing data were excluded in a test-by-test manner, for example, in procedures performed without SO.

As part of the secondary objective, the individual fluoroscopy runs were analyzed to evaluate the correlation between the RADPAD and the relative exposure of the MO in a hierarchical multivariate linear regression model.

Sample size calculation and statistical analysis

A statistical analysis was performed using R (version 3.5.1).[2] A power calculation based on the results of a prior study by Kloeze et al.[12] in the abdominal region revealed a minimum sample size of 20 per group to reach a power of 0.9 with 95% confidence. Baseline characteristics of both groups were compared using the Chi-squared test in combination with either the parametric Student's t-test or the nonparametric Mann–Whitney U-test.

The relationship between the radiation exposure of the MO (in μSv/s) and the use of the RADPAD was further analyzed in the dataset containing the individual fluoroscopy runs. The dataset contained multiple repeated fluoroscopy runs per patient, the amount of which varied per patient. Given this hierarchical data structure and the skewed data distribution, a generalized linear mixed effect model with Gamma error-distribution, logarithmic link-function, and patient as a random effect was used.[16] Radiation exposure

of the MO was defined as the measured dose rate. Based on theoretical grounds, we determined five potential independent predictors (fixed effects): 1) RADPAD versus no RADPAD, 2) one ceiling shield versus two ceiling shields, 3) DAP per second, 4) pulse rate per second, and 5) rotation angle of the C-arm. The validity of these hypothetical predictors was tested using likelihood-ratio tests of a model including the effect in question, against a model without the effect in question (backward elimination).

Significant predictors were added to the final model. Assumptions of the final generalized linear mixed effect model were checked using a visual inspection of qq-plots, residual plots, and testing for overdispersion. Beta estimates and 95% confidence intervals (CI) were extracted from the final mixed effect model to represent odds ratios (ORs).

RESULTS

Fourty-nine patients were included in the analysis: 25 patients in the study group (with RADPAD) and 24 patients in the control group (without RADPAD). Baseline and procedural characteristics are listed in *Table I*. Except for a significant difference in patient age, the baseline characteristics of the patients were comparable. Time required to position the RADPAD was negligible. The RADPAD appeared in the primary beam a few times but was easily repositioned. No acute deterministic skin effects were noted after the procedures.

Table 1: Patient and lesion characteristics at baseline.

Patient characteristics	Control group (n= 24)	Study group (n =25)	p-value
Age (year)	70.1	64.8	.04*
Male (%)	15 (63%)	12 (48%)	.46
BMI (kg/m²)	27.9 ± 2.8	25.5 ± 5.5	.06
Lesion location (%):			.49
• Iliac artery	9 (37.5%)	12 (48%)	
• Femoral artery	12 (50.0%)	12 (48%)	
• Popiteal and infrapopliteal	3 (12.5%)	1 (4%)	

Body Mass Index (BMI) is provided as mean ± SD. Gender and lesion location are provided as count with percentage.

Primary objective

The patient exposure (DAP) and staff exposure (E) are shown in *Table 2*. The deducted relative staff exposure (E/DAP) of the procedures are presented in *Figure 2*. Statistically significant reductions were found when comparing the relative staff exposure of the FO, SO, and MO of the study group with the control group; a median reduction of 66.5% for the FO (1.82 vs. 0.61 μSv/Gycm2, P < 0.0001), 68.3% for the SO (0.55 vs. 0.17 μSv/

Gycm2, P = 0.02), and 65.8% for the virtual MO (2.06 vs. 0.71 μSv/Gycm2, P < 0.0001). The absolute exposure levels of the SN were low, with medians of 0.0 μSv in both groups. Therefore, these measurements were excluded from further analyses.

Secondary objective

A total of 8,258 fluoroscopy runs were acquired throughout the 49 procedures. All runs with one or more missing potential fixed effects were removed. Of the 8,144 runs that remained, 3,567 were derived from the study group and 4,577 from the control group.

Likelihood-ratio tests confirmed the relevance of DAP/s, RADPAD, and ceiling screens as fixed effects in the generalized linear mixed effect model. This final multivariate mixed model showed a significant association between maximum operator exposure (μSv/s) and the presence of RADPADs (OR [95% CI] 0.51 [0.42–0.63], P ≤ 0.001). The presence of a second ceiling screen showed no significant association (P = 0.51). Complete data of the model are provided in Table III. Diagnostics of the mixed model confirmed normality of the residuals and showed no overdispersion or underdispersion of the model.

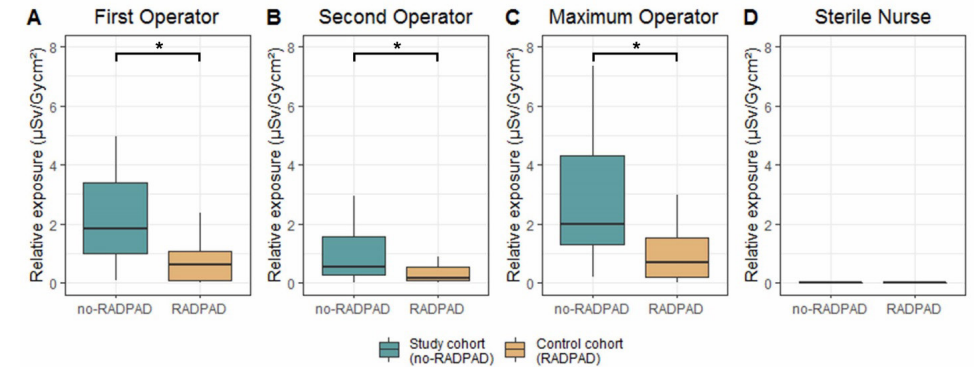*Figure 2:* Relative exposure data of staff members. Comparison the study group and control group in terms of relative exposure (E/DAP in μSv/Gycm²) of the first operator, second operator, maximum operator and sterile nurse. Significant reductions are indicated with an asterisk.

Table 2: Absolute exposure data of patient and staff members.

	Control group (n= 24)	Study group (n =25)
Patient exposure (DAP in Gycm²)	30.1 (IQR, 17.9 – 77.5)	26.4 (IQR, 8.0 – 47.5)
First operator exposure (E in μSv)	52.5 (IQR, 22.0-115.5)	11.1 (IQR, 1.1-25.4)
Second operator exposure (E in μSv)	25.0 (IQR, 8.8-33.0)	4.9 (IQR,0.4-18.1)
Maximum operator exposure (E in μSv)	70.4 (IQR, 42.9-123.9)	11.6 (IQR, 1.4-57.5)
Sterile nurse exposure (E in μSv)	0.0 (IQR, 0.0 – 0.0)	0.0 (IQR, 0.0 – 0.0)

Data provided in median with IQR.

Table 3: Outcomes of generalized linear mixed effect model to estimate maximum operator dose rate.

Fixed Effect	OR [95% CI]	p-value
Intercept dose rate of MO (μSv/s)	0.24 [0.20 – 0.28]	< .001*
DAP/s	4.42 [3.97 – 4.92]	< .001*
RADPAD vs no RADPAD	0.51 [0.42 – 0.63]	< .001*
Two ceiling screens vs one ceiling screen	0.88 [0.72 – 1.07]	0.51

OR = odds ratio, CI = confidence interval.

DISCUSSION

The results of this study demonstrate the efficacy of the RADPAD as a supplemental radiation protection device to shield operators during peripheral endovascular procedures. The RADPAD accounts for a 66–68% reduction of the relative chest exposure of the operators when used in addition to standard safety measures.

Conventional radiation protection strategies such as field size collimation and ceiling-mounted leaded glass shields have been proven highly effective, but these strategies require continuous effort.[17–19] Collimation needs to be adjusted repeatedly to maintain focus of the field of interest, while minimizing the area of exposure. Leaded glass shields require repositioning after virtually any change in C-arm geometry or operator position and their use is often restricted by their suspension system.

In contrast, the use of RADPADs requires minimal effort. Although the RADPAD is placed directly on top of the patient, the 'shadow zone' of the protection device is maximized. This allows operators to move more freely within this shadow zone and minimizes the need for reallocation of the RADPAD throughout the procedure. Furthermore, the RADPAD does not restrict operator movement nor sheath access.

Endovascular physicians are exposed to scatter radiation on a daily or weekly basis. With a maximum permitted dose limitation of 20 mSv per year in the European Union, a career in endovascular surgery can result in total accumulated doses of several hundreds of mSvs. The association between this type of protracted low-dose radiation exposure and carcinogenic effects remains a topic of heavy debate.[20] Epidemiological studies are limited by statistical power, inaccurate dose measurements, and undocumented confounders. While the insights in radiation-induced cellular and molecular responses

have evolved rapidly, the combined long-term effects of these responses remain poorly understood.[21] Despite these uncertainties, endovascular physicians should always use a precautionary approach when using radiation because the potential consequence of carcinogenesis can be fatal. In this basis, radiation exposure should be minimized when possible, unless doing so would compromise patient care. The use of RADPADs during endovascular treatment of PAD directly coincides with this objective. The RADPAD use is therefore recommended in all peripheral endovascular procedures, especially in those in which operators are not shielded properly by conventional radiation shields.

The strongly dominating mechanism of X-ray interaction in the RADPAD is photoelectric absorption. During photoelectric absorption, an incident X-ray photon interacts with an atom of the absorbing material and completely disappears; the energy of the photon is transferred to one of the orbital electrons of the atom. High atomic numbers and high density of the absorbing elements therefore form important properties for radiation shielding materials. As does the K-shell binding energy of the absorbing element, as each element is most effective at absorption of photons with energies equal or slightly higher than their K-shell binding energy. Bismuth K-edge lies around 90 keV and barium around 37 keV. Both with moderate atomic numbers (Ba = 56 and Bi = 83) and densities (Ba: 3.5 gm/cm³ and Bi 9.75 gm/cm³).

Prior studies with the RADPAD focussed on cardiac and abdominal procedures rather than peripheral procedures. In the thoracoabdominal region, the RADPAD was established as an effective radiation protection device responsible for relative operator dose (E/DAP) reduction rates of 20-89%.[7,11–13,22] Caution should be used when extrapolating these findings to the peripheral region. First, the efficacy of the RADPAD depends upon the photon energy of the scatter radiation. Although lead forms an effective shield for photons with energies in a wide diagnostic radiology range, the efficacy of composite materials such as bismuth and barium compounds (which are used in the RADPAD) are generally more energy-dependent and thus cover a smaller range of photon energies.[23–25] The energy spectrum of scatter photons depends on various semiautomatically regulated settings of the fluoroscopy system, including the X-ray tube voltage (kVp). Generally speaking, the X-ray energy increases along with tissue thickness and tissue density, which means that higher X-ray energies are used in the thorax and abdomen, compared to the lower limb. Second, the radiation protection drapes may be less suitable for peripheral procedures. The surface of the lower limb is narrow and patient movements under local anesthesia may cause undesired shifts of the drape.

The only existing study on the efficacy of the RADPAD in peripheral endovascular was provided by Power et al.[14] he study cohort and control cohort of this article differ significantly in terms of interventional region; the control cohort contained a high rate of iliac lesions (45.9 vs. 12.5%) and a low rate of popliteal and infrapopliteal lesions (10.8 vs. 25.0%) in comparison to the study cohort. This discrepancy is likely to cause bias because more radiation is needed to penetrate the pelvis and upper leg compared to the

knee or lower leg, hence creating more scatter radiation and increasing operator dose.[26] In the analysis of this study, the authors correct for these differences by the means of adjustment for the duration of patient exposure (expressed in FT) rather than adjustment for patient radiation dose itself (expressed in DAP). Although this is better than no correction at all, FT is known as a much weaker dose indicator than DAP, especially in peripheral procedures.[27]

There were certain limitations to this study. First, we exclusively measured radiation levels at the chest and did not assess dose to the hand, eye, or limbs.

Second, patient allocation was not randomized, meaning that the researchers decided whether the patient would be included in the study or control group. This was partially caused by logistics because the RADPADs were not always available at the starting phase of this study. To ensure that there would be an equal distribution of the procedural locations (iliac, femoral, popliteal, and infrapopliteal) in both groups, we allocated patients to specific groups in the last phase of this study.

Third, the study group was significantly younger than the control group. As we know, operator dose is strongly correlated with patient dose; the higher the patient exposure, the more scatter radiation will be produced. To ensure that discrepancies in patient exposure do not affect our study objectives, we used the DAP-adjusted operator dose given in E/DAP (mSv/Gycm2) rather than the absolute operator dose in E (mSv). By adjusting for DAP, we automatically compensate all intraprocedural differences that lead to differences in patient exposure.

Fourth, a generalized linear mixed model analysis was used to assess the effect of RADPAD use on maximum operator exposure while correcting for confounders. The distance between operator and radiation source could not be measured during this study, despite it being a known confounder for operator exposure (radiation exposure is inversely proportional to the square of the distance from the source). Although this explanatory fixed effect could not be taken into account, the final generalized linear mixed model showed an appropriate goodness of fit.

Finally, the visible presence of the RADPAD could bias the operator and trigger subtle behavioral differences.[7] Vlastra et al.[13] confirmed the existence of such bias in a randomized sham-controlled study that compared the effect of the RADPAD, a sham RADPAD, and no RADPAD. Surprisingly, the sham RADPAD was associated with a 43% higher relative dose than using no RADPAD at all (P = 0.009). The authors hypothesize that the visible presence of a radiation protection device causes a sense of security, which reduces the operator's tendency to maintain an appropriate distance.

CONCLUSION

In real-world situations, the RADPAD shields operators from radiation exposure during peripheral endovascular procedures. The use of the drape resulted in a median reduction of 66–68% of the relative procedural exposure of the primary and secondary operator. The drape was convenient in use, required minimal effort, and presented no drawbacks. We recommend the integration of the RADPAD in peripheral endovascular procedures.

REFERENCES

1. Hong MS, Beck AW, Nelson PR. Emerging national trends in the management and outcomes of lower extremity peripheral arterial disease. Ann Vasc Surg [Internet]. 2011;25(1):44–54. Available from: http://dx.doi.org/10.1016/j.avsg.2010.08.006

2. Goldsweig AM, Kennedy KF, Abbott JD, Jones WS, Velagapudi P, Rutar FJ, et al. Patient Radiation Dosage During Lower Extremity Endovascular Intervention. JACC Cardiovasc Interv. 2019;12(5):473–80.

3. Rajabi A, Noohi F, Hashemi H, Haghjoo M, Miraftab M, Yaghoobi N, et al. Ionizing radiation-induced cataract in interventional cardiology staff. Res Cardiovasc Med. 2015;4(1):4.

4. Grant EJ, Brenner A, Sugiyama H, Sakata R, Sadakane A, Utada M, et al. Solid Cancer Incidence among the Life Span Study of Atomic Bomb Survivors: 1958–2009. Radiat Res. 2017;187(5):513–37.

5. Kamiya K, Ozasa K, Akiba S, Niwa O, Kodama K, Takamura N, et al. From Hiroshima and Nagasaki to Fukushima 1 Long-term eff ects of radiation exposure on health. Lancet. 2015;386(9992):469–78.

6. National Research Council. Health Risks from Exposure to Low Levels of Ionizing Radiation [Internet]. BEIR VII , Phase 2. National Academies Press; 2006. 424 p. Available from: http://www.nap.edu/catalog/11340.html%5CnHEALTH%5Cnhttp://www.nap.edu/catalog/11340.html

7. Murphy JC, Darragh K, Walsh SJ, Hanratty CG. Efficacy of the RADPAD protective drape during real world complex percutaneous coronary intervention procedures. Am J Cardiol [Internet]. 2011;108(10):1408–10. Available from: http://dx.doi.org/10.1016/j.amjcard.2011.06.061

8. Politi L, Biondi-Zoccai G, Nocetti L, Costi T, Monopoli D, Rossi R, et al. Reduction of scatter radiation during transradial percutaneous coronary angiography: A randomized trial using a lead-free radiation shield. Catheter Cardiovasc Interv. 2011;79(1):97–102.

9. King JN, Champlin AM, Kelsey CA, Tripp DA. Using a sterile disposable protective surgical drape for reduction of radiation exposure to interventionalists. Am J Roentgenol. 2002;178(1):153–7.

10. Brambilla M, Occhetta E, Ronconi M, Plebani L, Carriero A, Marino P. Reducing operator radiation exposure during cardiac resynchronization therapy. Europace. 2010;12(12):1769–73.

11. Jones MA, Cocker M, Khiani R, Foley P, Qureshi N, Wong KCK, et al. The benefits of using a bismuth-containing, radiation-absorbing drape in cardiac resynchronization implant procedures. PACE - Pacing Clin Electrophysiol. 2014;37(7):828–33.

12. Kloeze C, Klompenhouwer EG, Brands PJM, Van Sambeek MRHM, Cuypers PWM, Teijink JAW. Editor's choice - Use of disposable radiation-absorbing surgical drapes results in significant dose reduction during EVAR procedures. Eur J Vasc Endovasc Surg [Internet]. 2014;47(3):268–72. Available from: http://dx.doi.org/10.1016/j.ejvs.2013.12.008

13. Vlastra W, Delewi R, Sjauw KD, Beijk MA, Claessen BE, Streekstra GJ, et al. Efficacy of the RADPAD Protection Drape in Reducing Operators' Radiation Exposure in the Catheterization Laboratory: A Sham-Controlled Randomized Trial. Circ Cardiovasc Interv. 2017;10(11):1–7.

14. Power S, Mirza M, Thakorlal A, Ganai B, Gavagan LD, Given MF, et al. Efficacy of a Radiation Absorbing Shield in Reducing Dose to the Interventionalist During Peripheral Endovascular Procedures: A Single Centre Pilot Study. Cardiovasc Intervent Radiol. 2014;573–8.

15. Taharim NK, Yeong CH, Ng KH, Abdullah BJJ. Evaluation of Occupational Dose Reduction in Interventional Radiology Using Lead-Free Protection Drape. In 2015. p. 1–13.

16. West B, Welch K, Galecki A. Linear Mixed Models: A Practical Guide Using Statistical Software. 1st ed. Chapman & Hall/CRC; 2007.

17. Sukupova L, Hlavacek O, Vedlich D. Impact of the Ceiling-Mounted Radiation Shielding Position on the Physician's Dose from Scatter Radiation during Interventional Procedures. Radiol Res Pract. 2018;2018(Cd):1–7.

18. Maeder M, Brunner-La Rocca HP, Wolber T, Ammann P, Roelli H, Rohner F, et al. Impact of a lead glass screen on scatter radiation to eyes and hands in interventional cardiologists. Catheter Cardiovasc Interv. 2006;67(1):18–23.

19. Abdelrahman MA, Abu Alfwares A, Alewaidat H, Alhasan M, Rawashdeh MA, Al Mousa DS. Compliance with Radiation Protection Practices among Radiologists. Health Phys. 2018;115(3):338–43.

20. Seong KM, Seo S, Lee D, Kim MJ, Lee SS, Park S, et al. Is the linear no-threshold dose-response paradigm still necessary for the assessment of health effects of low dose radiation? J Korean Med Sci. 2016;31:S10–23.

21. El-Sayed T, Patel AS, Cho JS, Kelly JA, Ludwinski FE, Saha P, et al. Radiation-Induced DNA Damage in Operators Performing Endovascular Aortic Repair. Circulation. 2017;136(25):2406–16.

22. Shah P, Khanna R, Kapoor A, Goel PK. Efficacy of RADPAD protection drape in reducing radiation exposure in the catheterization laboratory—First Indian study. Indian Heart J [Internet]. 2018;70(2018):S265–8. Available from: https://doi.org/10.1016/j.ihj.2018.03.008

23.   Kazempour M, Saeedimoghadam M, Shekoohi Shooli F, Shokrpour N. Assessment of the radiation attenuation properties of several lead free composites by monte carlo simulation. J Biomed Phys Eng. 2015;5(2):67–76.

24.   Murphy PH, Wu Y, Glaze SA. Attenuation properties of lead composite aprons. Radiology. 1993;186(1):269–72.

25.   Christodoulou EG, Goodsitt MM, Larson SC, Darner KL, Satti J, Chan HP. Evaluation of the transmitted exposure through lead equivalent aprons used in a radiology department, including the contribution from backscatter. Med Phys. 2003;30(6):1033–8.

26.   Ofori EK, Ofori-Manteaw BB, Gawugah JNK, Nathan JA. Relationship between patient anatomical thickness and radiographic exposure factors for selected radiologic examinations. J Heal Med Nurs [Internet]. 2016;23(August):150–62. Available from: https://iiste.org/Journals/index.php/JHMN/article/view/29048/29812

27.   Skripochnik E, Loh SA. Fluoroscopy time is not accurate as a surrogate for radiation exposure. Vascular. 2017;25(5):466–71.

3

3

CHAPTER | 4

Feasibility of Fresh Frozen Human Cadavers as a Research and Training Model for Endovascular Image Guided Interventions

Based on:

M.M. Jansen, C.E.V.B. Hazenberg, Q.M.B. de Ruiter,
R.W. van Hamersvelt, R. L.A.W. Bleys, J.A. van Herwaarden,

ABSTRACT

Objective

To describe the feasibility of a fresh frozen human cadaver model for research and training of endovascular image guided procedures in the aorta and lower extremity.

Methods

The cadaver model was constructed in fresh frozen human cadaver torsos and lower extremities. Endovascular access was acquired by inserting a sheath in the femoral artery. The arterial segment of the specimen was restricted by ligation of collateral arteries and, in the torsos, clamping of the contralateral femoral artery and balloon occlusion of the supratruncal aorta. Tap water was administered through the sheath to create sufficient intraluminal pressure to manipulate devices and acquire digital subtraction angiography (DSA). Endovascular cannulation tasks of the visceral arteries (torso) or the peripheral arteries (lower extremities) were performed to assess the vascular patency of the model. Feasibility of this model is based on our institute's experiences throughout the use of six fresh frozen human cadaver torsos and 22 lower extremities.

Results

Endovascular simulation in the aortic and peripheral vasculature was achieved using this human cadaver model. Acquisition of DSA images was feasible in both the torsos and the lower extremities. Approximately 84 of the 90 target vessels (93.3%) were patent, the remaining six vessels showed signs of calcified steno-occlusive disease.

Conclusions

Fresh frozen human cadavers provide a feasible simulation model for aortic and peripheral endovascular interventions, and can potentially reduce the need for animal experimentation. This model is suitable for the evaluation of new endovascular devices and techniques or to master endovascular skills.

INTRODUCTION

Rapid succession of catheter-based innovations in the last decade, has led to more sophisticated endovascular procedures and increased patient eligibility for endovascular treatment [1–4]. Preclinical models are essential to evaluate the feasibility, safety, and efficacy of any novel endovascular device or technique, and to obtain regulatory approval for their clinical application [5,6]. Preclinical models are also used in endovascular training and device instructions to stimulate safe and efficient implementation of novelties in clinical practice.

Various types of preclinical models are available for endovascular research and training purposes, each with its own advantages and disadvantages. Bench models, such as silicone aorta phantoms, provide a highly controlled environment but lack the complexity and tissue properties of clinical practice. Animal models, such as the well-established healthy swine model, allow in-vivo endovascular simulation, but the healthy, straight arteries of the swine differ considerably from the tortuous, calcified vessels of a typical vascular patient. Besides, the vasculature of the swine is narrower than that of humans, which can preclude the use of larger sheaths and devices. These anatomical and pathophysiological distinctions can compromise the translation from bench-to-bedside.[7–10]

Moreover, there are strong ethical grounds to look for alternatives for the use of living animals. Human cadaver reperfusion models have been reported as a suitable, although less familiar, alternative to animal models for endovascular device evaluation and training.[11–14] However, reperfusion of cadaveric tissue is a delicate and complex process, which may restrict widespread adoption of human cadaver models.

In contrast to these human cadaver reperfusion models, our institution has been using human cadaver models without arterial reperfusion, to our satisfaction. In this study, we present our human cadaver model, and aim to raise general awareness of the existence and feasibility of human cadaver models for endovascular simulation in the abdominal aorta and peripheral arteries.

MATERIALS AND METHODS

Human Cadavers

Body donations were regulated according to the national Dutch law on the disposal of the dead and the European legislations and ethical framework for body donation[15]. Written informed consent was obtained from the donors during life to use their cadavers for educational and research purposes. No additional approval of an ethics board was required for this study. Age, gender and serology report of the donors were provided. Other demographics and medical details were sealed to assure the anonymity of the

donors, as according to our institution's policy. The available data of 22 lower extremities and 6 fresh frozen human cadaveric torsos were used for the assessment of this cadaver model. Donors were predominantly male (75%) with a mean age of 74.4 ± 8.8.

Cadaveric specimen

The cadavers were dissected and frozen within 48 hours of post-mortem delay, at a temperature of -20°C. No additive preservation chemicals were used. The cadaveric torsos comprised the thorax, abdomen, pelvis and proximal part of the lower extremities until mid-femoral level. Two oblique dissection planes from axilla to sternum exposed the branches of the aortic arch, trachea, esophagus and cervical spine. Two axial dissection planes at mid-femoral level exposed the left and right femoral artery. The lower extremities comprised the foot, lower leg and part of the upper leg. An axial dissection plane at mid-femoral level exposed the femoral artery. The dissection planes of the torsos and lower extremities are illustrated in *Figure 1*.
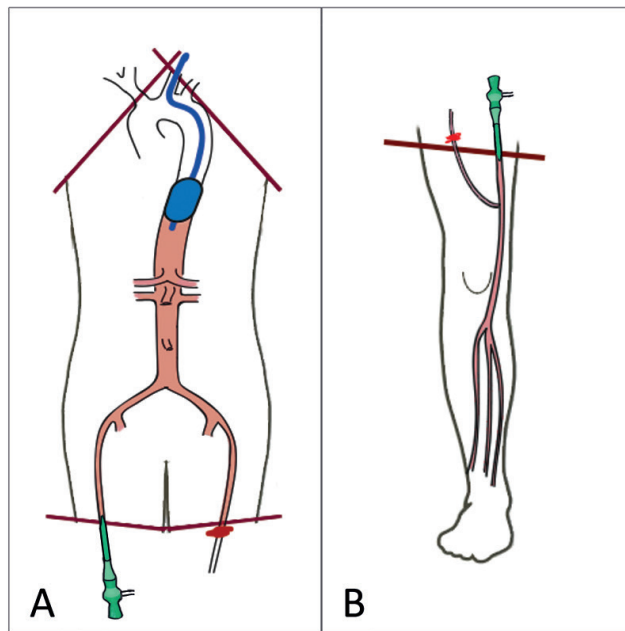
Figure 1: Schematic overview of the torso (A) and lower extremity (B) including dissection planes of the cadaveric specimen. Red lines indicate the dissection planes. The access sheath is indicated in green. Fluid leakage is prevented by ligation of the main collateral arteries in the dissection plane, and, in the torsos, by balloon occlusion of the proximal aorta and ligation of the contralateral femoral artery.

Cadaver preparation and storage

The cadaveric specimens were thawed at 15°C. Approximately one day of thawing was needed for the lower extremities and three days for torsos. The specimens were used for a maximum of four freeze-thaw cycles, due to deterioration of the soft tissues after prolonged use. No difference in quality of the specimen for endovascular use was noticed between first and last use of the specimen.

Vacant arteries in the intersection plane (typically the superficial femoral artery) were cannulated and flushed with a solution of warm tap water and non-oxidative laundry detergent (OMO®, Unilever, London, the UK) until clear liquid was recovered from the venous and arterial outflow. This process reduced odor and resolved post-mortem blood clots. The specimens were flushed with the same solution before restoring them, as low temperatures could cause crystallization of remnant contrast material[16].

Computed Tomography

After several initial experiments, it was decided to subject the specimens were subjected to a computed tomography (CT) scan prior to endovascular use. These scans allowed the identification of arterial pathology, calcifications and stenosis to select appropriate specimens for specific training or research purposes based on vascular pathology, as the medical records of the donors were sealed. The CT scans were acquired with a 64-detector CT scanner (IQon spectral CT, Philips®, Best, The Netherlands) using thin slice, high-dose settings to maximize image quality (slice thickness; 1 mm, spiral pitch; 0.39, tube voltage; 140 kVp, 100-400 mAs).

Endovascular interventions

The procedures were conducted in an experimental hybrid OR, equipped with a Philips Allura Xper FD20 fluoroscopy system (Philips Healthcare, Best, the Netherlands) and power injector (Mark 7 Arterion, Medrad, Whippany, USA). A vascular surgeon with > 5 years of experience in endovascular interventions performed the endovascular tasks.

Preparation

A 7 Fr introducer sheath was advanced in the femoral artery to provide either retrograde (torsos) or antegrade (lower extremities) arterial access, as shown in *Figure 2*. The sheath was secured to surrounding tissue with a nylon string or clamp. In all specimens, fluid leakage was prevented by ligation of the main collateral arteries in the dissection plane(s). Additionally, in the torsos, the contralateral femoral artery was clamped and the supratruncal aorta was occluded with a 40x30mm aortic valvuloplasty balloon (Z-MED; NuMED Inc®, Hopkinton). Within these restricted vascular segments, intraluminal pressure was created by injection 50cc (lower extremities) or 100cc (torso) of tap water through the sheath. *Figure 1* provides a schematic overview of the setup in the torsos and lower extremities.
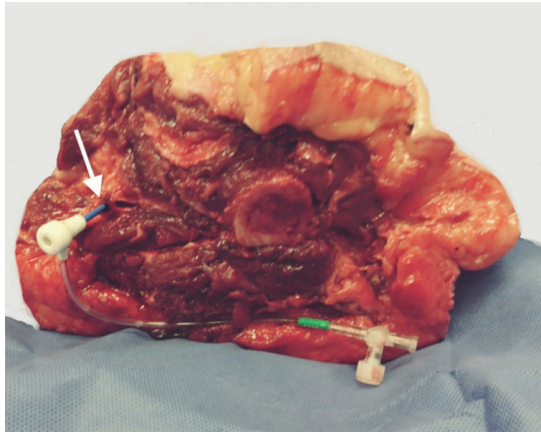
Figure 2: Cannulation of the femoral artery of a lower extremity. A 7Fr sheath is used to create antegrade access of the lower extremity through the vacant femoral artery (white arrow) in the axial dissection plane.

Procedures

Various endovascular procedures were performed using this fresh-frozen human cadaver model, both for both training and research purposes. These procedures included balloon angioplasty, stenting, and image optimization of cone beam computed tomography scans (CBCT). Throughout these experiments, the vascular patency of the fresh frozen cadavers was documented by means of cannulation of selected target vessels. These vessels comprised the celiac artery, superior mesenteric artery and left and right renal arteries in the torsos, and the anterior tibial artery, posterior tibial artery and peroneal artery in the lower extremities. These cannulations are comparable to the tasks performed during complex aortic interventions and peripheral interventions. In case of cannulation failure, a distinction was made between failure due to flaws in the cadaver model or failure due to steno-occlusive vascular disease.

Digital subtraction angiography

Digital subtraction angiography (DSA) was acquired using the following protocols.

DSA protocol lower extremity

Manual injection of 50 cc tap water through a Berenstein or Straight flush catheter to generate adequate intraluminal pressure, followed by injection of 20 cc of diluted (ratio 1:5) contrast agent (Ultravist® 300 mg/mL, Bayer Healthcare Pharmaceuticals Inc. Wayne, Germany). Remnant contrast material was flushed with 50 cc of tap water.

DSA protocol torso

Manual injection of 100 cc tap water through a pigtail catheter to generate adequate

intraluminal pressure, followed by injection of 120 cc diluted (ratio 1:5) contrast agent (Ultravist 300mg/mL) at 20 cc/s using a power injector. Remnant contrast material was flushed with 100 cc of tap water.

RESULTS

Feasibility of this model is based on our institute's experiences throughout the use of 6 fresh frozen human cadaver torsos and 22 lower extremities.

Computed tomography

Pre-procedural unenhanced computed tomography (CT) scans were available of 15 of the 22 lower extremities (68%) and 4 of the 6 torsos (66%). The CT scans allowed evaluation of the state of the vascular wall and arterial lumen, as visualized in Figure 3. The two most common port-mortem CT artefacts were decomposition artefacts (e.g. gas formation in the intestine and liver) and artefacts due to anatomical dissection (presence of air within vessels and compression of the aorta, iliac arteries and veins). However, none of these artefacts decreased the diagnostic value of the scan in terms of vascular disease.
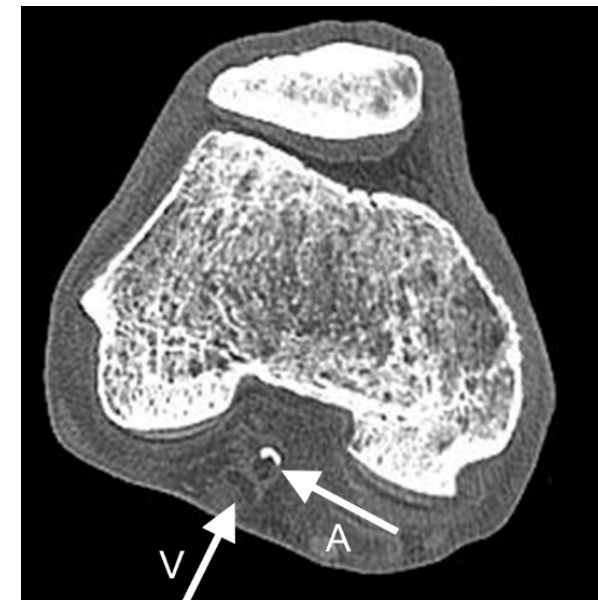
Figure 3: Unenhanced CT of frozen lower extremity of a human cadaver. The vein and artery are indicated with an arrow with 'A' and 'V' respectively. Differentiation between arterial lumen, vascular wall and calcifications are possible.

Endovascular interventions

The endovascular human cadaver model provided a realistic simulation setting for a variety of endovascular procedures. DSA imaging was realistic as shown in *Figure 4*. Air bubbles were visible in 23 of the 92 DSA's (25%), caused by insufficient prefilling of the vasculature (*Figure 5*). These bubbles had minimal impact on the diagnostic or navigational value of the DSAs, as the outline of the arteries remained visible.

The cadaver model demonstrated a high vascular patency. The celiac artery, superior mesenteric artery, and left and right renal artery could be successfully cannulated in all six torsos (100%). Cannulation of the posterior tibial artery, anterior tibial artery and peroneal artery was successful in 20 (91%), 21 (95%) and 19 (86%) specimens respectively. All six cases of cannulation failure were attributed to high grade stenosis or occlusions of the target vessel, as confirmed by available CTA or DSA imaging.

No visible tissue distortion or swelling of the specimen was observed, even after multiple hours of use. However, venous outflow and sheath leakage were noticeable. In the torsos, partial collapse of the infra-renal aorta was noticed after approximately half an hour, that impaired guidewire manipulation. The full range of guidewire motion could be retrieved by the injection of 100cc of tap water in the restricted arterial segment.

Figure 4: *DSA imaging of A) the trifurcation and crural arteries of a specimen with patent arteries, B) the trifurcation and crural arteries of a specimen with systemic atherosclerosis and C) the abdominal aorta and its visceral and renal branches.*

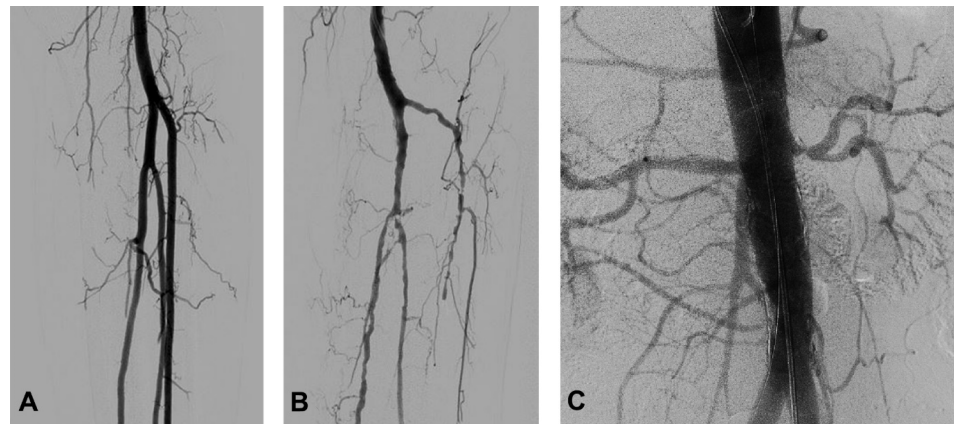**Figure 5**: *Air bubbles during angiography. Presence of air bubbles near the trifurcation, indicated with an arrow.*

DISCUSSION

Fresh frozen human cadavers form a suitable model to evaluate new endovascular devices and techniques or master endovascular skills. Human cadavers offer lifelike conditions with representative anatomy, pathophysiology and tactile feedback.

In contrast to previously reported (human) cadaver models [11–14,17–20], the current model does not employ arterial circulation. Arterial circulation is undeniably relevant for research that concerns hemodynamic processes such as stent deployment, or when maximal expansion of the arteries is desired to allow high-calibre devices. However, many research and training objectives may suffice in a model without circulation, especially since there are several disadvantages to post-mortem reperfusion. Extensive preparation of cadaver and fluid conduit, and an expensive extracorporeal pump are needed to generate stable circulatory flow and prevent conduit leakage. Extravasation of reperfusion fluid into the interstitial space and abdominal cavities forms another issue, as post-mortem decay increases the vascular permeability. Arterial circulation is therefore only sustainable for a limited period of time, and with low blood pressure levels, before resulting in massive edema and distortion of the soft tissues and organs [11–14,19,21].

In the current model, arterial circulation was omitted without compromising vessel patency or DSA quality. This allows us to maintain the anatomical and pathophysiolocal fidelity of fresh frozen human cadavers, while using less preparation time, fewer resources and causing significantly less edema than the existing cadaver reperfusion models.

This endovascular human cadaver model has several limitations. To start, the intraluminal pressure was not measured in these specimens. Arterial patency was assumed when guidewires and catheters could be manoeuvred freely, without movement restrictions due to arterial compression. These subjective observations were based on

tactile feedback of the devices, and their fluoroscopic feedback. However, maximum expansion of the arteries may not have been obtained, which may limit the use of large calibre devices.

Despite the existence of plenty of thriving body donation programs, it may be difficult to acquire the fresh frozen human cadavers. When available, the cadavers should be used as effectively as possible, as the preservation duration of fresh frozen tissue is limited. Our institution stimulates purposeful use of the cadavers by separating torso, head and extremities for use throughout different medical disciplines.

The specimen used in this study were reused for maximal four times. Chemical body preservation methods could extend the durability of the cadavers. However, fresh frozen preservation is the most lifelike conservation method currently available to preserve flexibility, color and texture of all tissues [22]. Chemical preservation using Thiel's method [23] provides similar levels of tissue flexibility, but may affect the elasticity of the arteries in a similar way as previously reported in tendons and ligaments [24,25].

Ideally, the vascular anatomy of the cadaveric specimen should match the intended research or training purpose to maximize the fidelity of the endovascular simulation. The privacy of donors is highly respected and therefore our all medical records, including cause of death, are sealed to secure the donors anonymity. However, this policy may be different in other institutions. Without medical records, we were forced to acquire CT scans of the frozen specimen to assess their vascular status. On CT assessment, plenty of lower extremities contained arteries with atherosclerosis and calcifications, however more uncommon pathology may be more difficult to find.

CONCLUSION

The endovascular fresh frozen human cadaver model presented in this study allows realistic simulation of endovascular procedures in the aorta and peripheral arteries. This model is suitable for preclinical research and development of endovascular technology, and to gain practical experience and master endovascular skills.

REFERENCES

1. Rafii-Tari, H., Payne, C. J. & Yang, G.-Z. Current and Emerging Robot-Assisted Endovascular Catheterization Technologies: A Review. *Annals of Biomedical Engineering* **42**, 697–715 (2014).
2. Henkes, H. & Weber, W. The Past, Present and Future of Endovascular Aneurysm Treatment. *Clinical Neuroradiology* **25**, 317–324 (2015).
3. Schneider, P. A. Evolution and current use of technology for superficial femoral and popliteal artery interventions for claudication. *Journal of Vascular Surgery* **66**, 916–923 (2017).
4. Chartrain, A. G. *et al.* Novel and emerging technologies for endovascular thrombectomy. *Neurosurgical Focus* **42**, E12 (2017).
5. Sorenson, C. & Drummond, M. Improving medical device regulation: the United States and Europe in perspective. *The Milbank quarterly* **92**, 114–50 (2014).
6. Kramer, D. B., Xu, S., Sc, M. & Kesselheim, A. S. Regulation of Medical Devices in the United States and European Union. *The New England Journal of Medicine* **366**, (2012).
7. Joffe, A. R., Bara, M., Anton, N. & Nobis, N. The ethics of animal research: a survey of the public and scientists in North America. *ATLA Alternatives to Laboratory Animals* **17**, 17 (2016).
8. Henrique Franco, N. Animal experiments in biomedical research: A historical perspective. *Animals* **3**, 238–273 (2013).
9. Prescott, M. J. & Lidster, K. Improving quality of science through better animal welfare: the NC3Rs strategy. *Lab Anim (NY)* **46**, 152–156 (2017).
10. Akhtar, A. The Flaws and Human Harms of Animal Experimentation. 407–419 (2015) doi:10.1017/S0963180115000079.
11. Arbatli, H. *et al.* Dynamic Human Cadaver Model for Testing the Feasibility of New Endovascular Techniques and Tools. *Ann Vasc Surg* **24**, 419–422 (2010).
12. Carey, J. N., Minneti, M., Leland, H. A., Demetriades, D. & Talving, P. Perfused fresh cadavers: Method for application to surgical simulation. *Am J Surg* **210**, 179–187 (2015).
13. Garrett, H. E. A human cadaveric circulation model. *J Vasc Surg* **33**, 1128–1130 (2001).
14. Chevallier, C. *et al.* Postmortem circulation: A new model for testing endovascular devices and training clinicians in their use. *Clinical Anatomy* **27**, 556–562 (2014).
15. McHanwell, S. *et al.* The legal and ethical framework governing Body Donation in Europe - A review of current practice and recommendations for good practice. *European Journal of Anatomy* **12**, 1–24 (2008).
16. Elisa, K. *et al.* Evaluation of contrast media submitted to ionizing radiation. *Radiol Bras.* **42**, 309–313 (2009).
17. Inglez De Souza, M. C. C. M. & Matera, J. M. Bleeding simulation in embalmed cadavers: Bridging the gap between simulation and live surgery. *Altex* **32**, 59–63 (2015).
18. Willaert, W., De Somer, F., Grabherr, S., D'Herde, K. & Pattyn, P. Post-mortem Reperfusion of a Pig: a First Step to a New Surgical Training Model? *Indian Journal of Surgery* **77**, 1–4 (2013).
19. Willaert, W. *et al.* Lifelike vascular reperfusion of a thiel-embalmed pig model and evaluation as a surgical training tool. *European Surgical Research* **56**, 97–108 (2016).
20. Grabherr, S. *et al.* Postmortem angiography after vascular perfusion with diesel oil and a lipophilic contrast agent. *AJR. American journal of roentgenology* **187**, 515–523 (2006).
21. Willaert, W., De Somer, F., Grabherr, S., D'Herde, K. & Pattyn, P. Post-mortem Reperfusion of a Pig: a First Step to a New Surgical Training Model? *Indian Journal of Surgery* **77**, 1–4 (2013).
22. Hayashi, S. *et al.* History and future of human cadaver preservation for surgical training: from formalin to saturated salt solution method. *Anatomical Science International* **91**, 1–7 (2016).
23. Thiel. The preservation of the whole corpse with natural color. *Annals of Anatomy* **174**, 185–195 (1992).
24. Steinke, H. *et al.* Deformation behavior of the iliotibial tract under different states of fixation. *Medical Engineering and Physics* **34**, 1221–1227 (2012).
25. Fessel, G. *et al.* Suitability of Thiel embalmed tendons for biomechanical investigation. *Annals of Anatomy* **193**, 237–241 (2011).

PART II

INTRAOPERATIVE IMAGE GUIDANCE
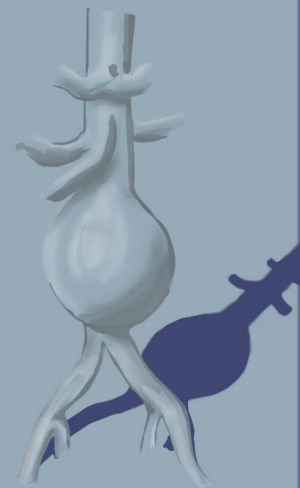
CHAPTER | 5

Current State in Intraoperative Navigation during Endovascular Treatment of Peripheral Artery Disease, a Systematic Review

ABSTRACT

Treatment of peripheral artery disease (PAD) has been shifting from an open surgical approach towards a more endovascular approach over the last decade. During endovascular interventions, intraoperative imaging is of crucial importance to provide optimal treatment. And as the entire field of endovascular surgery, imaging techniques are changing rapidly. With this systematic review we seek to provide broad overview of the current state of intraoperative image guidance and/or device navigation during the endovascular treatment of PAD, both for physicians well acquainted with the different imaging techniques and those seeking to become more familiar.

INTRODUCTION

Peripheral artery disease (PAD) is an obstructive atherosclerotic disease of the arteries that occurs most frequently in the lower extremities. The prevalence of PAD increases with age: globally, one in ten people aged ≥70 years is affected by PAD.[1]

In the last decades, the treatment of PAD has shifted from an open surgical approach to an endovascular approach, driven by the lower perioperative risks and faster hospital discharge associated with endovascular revascularization.[3,4] In the current international guidelines a prominent place is reserved for endovascular treatment of PAD, especially amongst patients who are unsuitable for open surgery due to comorbidities.[2,3] In this context, it is worth noting that a renewed debate has arisen regarding the role of endovascular treatment in addressing chronic limb-threatening ischemia, the most severe manifestation of PAD, due to the results of the BEST-CLI trial.

Endovascular treatment of PAD involves balloon angioplasty (with or without drug coating), stenting (covered /non-covered; with or without drug coating) and/or plaque debulking by means of mechanical or laser atherectomy or crossing devices. An elaborate scientific framework to determine the optimal treatment strategy for each individual patient or lesion is not yet available. Instead, the choice of treatment strategy is based largely on operator experience and preference, in combination with lesion characteristics such as recoil of the plaque, calcification grade and anatomical location.

Image guidance and navigation during endovascular treatment of PAD is conventionally provided by two-dimensional fluoroscopy and digital subtraction angiography (DSA). Both techniques require the use of X-ray radiation, and result in projection-based images which fail to provide three-dimensional (3D) information. The lack of 3D orientation can constrain device navigation, assessment of lesion severity and eccentricity, and/or the detection of treatment complications. These constraints can influence the technical success and long-term patency of the lesion, especially in technically challenging procedures, involving highly calcified or long lesions, tortuous anatomy, or chronic total occlusions (CTO).

To tackle these issues, new imaging technologies have been developed, aimed to improve intraprocedural diagnosis and device navigation, which in turn may have a positive effect on technical success, primary patency, procedure time, radiation exposure, use of contrast material or a combination of these. These imaging technologies are used on their own, or integrated in endovascular treatment devices to improve their performance (e.g. atherectomy devices, crossing devices or re-entry devices).

This review intends to summarize the latest developments in intraoperative image guidance and device navigation in endovascular treatment of PAD. To denominate these technologies, the collective term 'image guided navigation system' (IGNS) is used.

METHODS AND MATERIALS

Data search

This study was conducted according to the Preferred Reporting Items for Systematic Reviews and Meta-Analyses (PRISMA) guidelines for systematic reviews. On the 28th of July 2020, a database search in Medline and Embase was performed. Search strings are available in *Supplemental File A*. This systematic review was exempt from the need for Institutional Review Board review since the authors did not perform human or animal subject research.

Study selection

Original peer-reviewed research studies written in the English language focussing on multiplanar or 3D image guidance or device navigation in the peripheral arterial vasculature (iliac, femoral, popliteal and below the knee) in a clinical, phantom or animal study environment were included in this review. All patient populations and peripheral endovascular interventions were included. To exclude deprecated techniques that did not persevere in modern clinical practice, only studies published after 2010 were included.

Titles and abstracts were screened by two authors (RB and MJ). The same reviewers independently assessed full-article copies of references that were selected based on title/abstract, to determine final eligibility for inclusion. Disagreements between reviewers were discussed and a final decision was made based on consensus. All included studies underwent a reference list cross-check to identify studies that were not found in the initial database search.

Data collection

Of each of the selected studies, the following characteristics were collected: type of IGNS, study type, study purpose, lesion location and lesion type. Surrogate markers for clinical benefit were extracted when available including: technical success rate, complication rate, IGNS-related complication rate, procedure time (PT), contrast volume (CV), dose area product (DAP), air kerma (AK), fluoroscopy time (FT) and primary patency at follow-up. Primary patency was defined as 'uninterrupted patency over a specified length of follow-up', in concordance with the reporting standards of the Society for Vascular Surgery. IGNS-related complications were defined as all complications caused by vascular wall damage, such as perforations, dissections, pseudo-aneurysms. Where applicable, the accuracy of the IGNS was addressed with its registration error (RE). The RE was measured as the distance between actual position of the endovascular device and/or anatomical landmark and the position provided by the IGNS. Articles that did not report any of these measures were excluded from this review.

Risk of bias analysis

According to the PRISMA guidelines a risk of bias analysis was executed on the included randomized controlled trials and non-randomized controlled studies using the Cochrane Risk of Bias (ROB) tool[4] and the Risk Of Bias In Non-randomized Studies of Interventions (ROBINS-I) tool[5], respectively. Risk assessment was executed on the study level. No risk of bias analysis was conducted on single-arm observational studies (i.e. feasibility studies and retrospective studies).

RESULTS

The search generated 1932 results, of which 1642 remained after removal of duplicates. Eventually, 39 studies were included in this review. *Figure 1* illustrates the study inclusion in a flow chart, while the studies themselves are summarized in *Table 1*. The included articles encompass ten different types of IGNS, of which purpose and use varied per study: 1. magnetic particle imaging (MPI), 2. computed tomography (CT), 3. cone beam computed tomography (CBCT), 4. image fusion (IF) with preoperative CT/MR, 5. transcutaneous ultrasound (US), 6. intravascular ultrasound (IVUS), 7. intravascular photoacoustic ultrasound-IVUS (IVPA-IVUS), 8. optical coherence tomography (OCT), 9. robotic catheter systems and 10. fibre optic guidance.
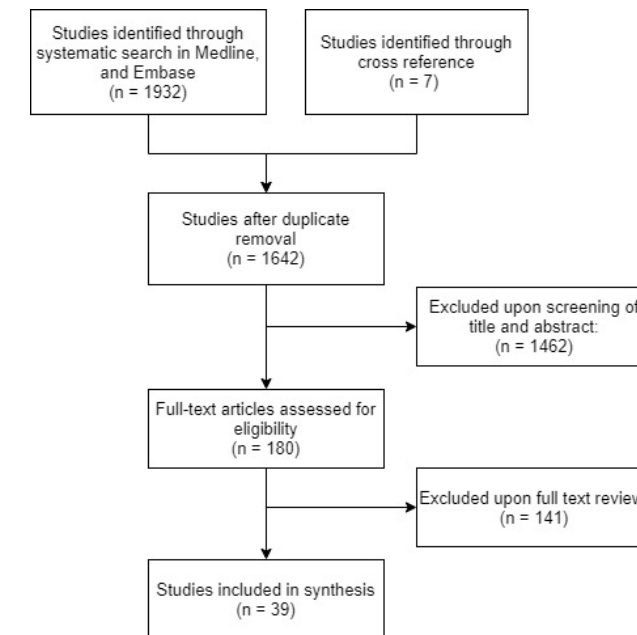
Figure 1: Flow chart of study inclusion

Table 1: *Complete overview of included studies.*

Author, Year	Study purpose	Study environment	Study type	Patients (lesions)	Device Type	Lesion characteristics
Magnetic particle imaging (MPI) guidance						
Herz[6], 2019	Preclinical feasibility of magnetic particle imaging (MPI) to guide angioplasty and stenting in peripheral stenotic lesions. MPI visualization requires MPI-visible contrast material (SPIO-based tracer agents) and MPI-visible markers on endovascular instruments	Phantom	Single-centre, prospective single-arm study	3 (3)	Custom-built magnetic particle imaging scanner (University Hospital Würzburg, Germany)	External iliac stenotic lesions (50% stenosis)
Computed tomography (CT) guidance						
Heidrich[7], 2018	Feasibility of intraprocedural CO_2 CTA (using hybrid angio-CT system) for diagnosis and planning in a patient with impaired renal function and excessive bowel gas	Clinical	Case report	1 (2)	Miyabi Angio-CT System (Siemens Medical Systems, Erlangen, Germany)	Iliac stenotic lesions
Cone beam computed tomography (CBCT) guidance						
Liang[8], 2016	Feasibility of CBCT-guided true lumen re-entry during iliac CTO crossing	Clinical	Single-centre, retrospective single-arm study	10 (10)	DynaCT (Siemens Medical Systems, Erlangen, Germany)	Iliac CTOs (TASCII B and D)
Image fusion (IF) guidance						
Sailer[9], 2015	Feasibility of 3D-3D IF-guidance during endovascular treatment of iliac, femoral, popliteal and BTK lesions	Clinical	Single-centre, prospective single-arm study	17 (20)	Allura Xper FD20 (Philips Healthcare, Amsterdam, The Netherlands)	Iliac, femoral, popliteal and BTK steno-occlusive lesions
Ierardi[10], 2016	Feasibility of 3D-3D IF-guidance during endovascular treatment of aortoiliac lesions	Clinical	Single-centre, prospective single-arm study	5 (N/A)	Allura Xper FD20 (Philips Healthcare, Amsterdam, The Netherlands)	Aortoiliac steno-occlusive lesions
Goudeketting[11], 2017	Feasibility of 3D-3D IF-guidance during endovascular treatment of iliac lesions	Clinical	Single-centre, prospective single-arm study	11 (15)	Allura Xper FD20 (Philips Healthcare, Amsterdam, The Netherlands)	Iliac steno-occlusive lesions
Stahlberg[12], 2019	Comparison of 2D-3D IF-guidance and conventional guidance during endovascular treatment of iliac lesions	Clinical	Retrospective non-randomized controlled trial	26 (N/A)	VesselNavigator (Philips Healthcare, Amsterdam, the Netherlands)	Iliac steno-occlusive lesions

Table 1: *Continued*

Author, Year	Study purpose	Study environment	Study type	Patients (lesions)	Device Type	Lesion characteristics
Transcutaneous ultrasound (US) guidance						
Banerjee[13], 2010	Feasibility of adjunctive US-guidance in intraluminal crossing of femoral CTOs, using a microdissection catheter	Clinical	Case series	1 (2)	N/A	Femoral CTOs
Nishino[14], 2012	Feasibility of adjunctive US-guidance in intraluminal crossing of femoropopliteal CTOs using a dual access approach	Clinical	Single-centre, prospective single-arm study	19 (19)	Sonosite 180 Plus (Sonosite Japan, Tokyo, Japan) with 5-10MHz transducer	Femoropopliteal CTOs, (TASCII B-D)
Krasznai[15], 2013	Feasibility of primary US-guidance during endovascular treatment of iliac lesions	Clinical	Single-centre, prospective single-arm study	31 (35)	Aloka Prosound Alfa7 (Aloka Co, Tokyo, Japan) with linear 3.5 MHz transducer	Iliac steno-occlusive lesions (TASCII A-C)
Bolt[16], 2019	To compare primary US-guidance with conventional fluoroscopic guidance during endovascular treatment of iliac lesions	Clinical	Single-centre, randomized controlled trial	142 (165)	Aloka Prosound Alfa7 (Aloka Co., Tokyo, Japan) with linear 3.5 MHz transducer	Iliac steno-occlusive lesions (TASCII A-B)
Intravascular ultrasound (IVUS) guidance						
Panaich[17], 2016	Evaluate the impact of adjunctive IVUS-assistance in terms of in-hospital complications during endovascular treatment of PAD	Clinical	Multi-centre, retrospective non-randomized controlled trial.	92714 (N/A)	N/A	Iliac, femoral, popliteal, BTK steno-occlusive lesions (TASCII A-D)
Iida[18], 2014	Evaluate the impact of adjunctive IVUS-assistance in terms of technical success and midterm patency during endovascular treatment of PAD	Clinical	Single-centre, retrospective propensity score-matched cohort study	468 (N/A)	N/A	Femoropopliteal steno-occlusive lesions (TASCII A-C)
Araki[19], 2014	Evaluate the impact of adjunctive IVUS-assistance in terms of midterm patency in the treatment of iliac CTOs using self-expandable stent grafts	Clinical	Single-centre, prospective single-arm study	82 (86)	N/A	Iliac CTOs (TASCII B-D)

Table 1: Continued

Author, Year	Study purpose	Study environment	Study type	Patients (lesions)	Device Type	Lesion characteristics
Kumakura[20], 2015	Evaluate the impact of adjunctive IVUS-assistance in terms of technical success and long-term patency in the treatment of de novo iliac lesions using self-expandable and balloon expandable stent grafts	Clinical	Single-centre, prospective single-arm study	455 (507)	Vision PV .018 20MHz (Philips Volcano, Amsterdam, the Netherlands) or Ultracross, 30MHz (Boston Scientific, Marlborough, MA, USA)	Iliac steno-occlusive lesions treated by primary stenting (TASCII A-D)
Krishnan[21], 2018	To compare IVUS-guided directional atherectomy with conventional fluoroscopy-guided directional atherectomy in the treatment of femoropopliteal in-stent restenosis	Clinical	Single-centre, retrospective non-randomized controlled trial.	114 (114)	N/A (Philips Volcano, Amsterdam, The Netherlands)	Femoropopliteal in-stent restenoses
Nakamura[22], 2020	Feasibility of retrograde revascularization of femoral CTOs using a Gogo catheter with IVUS to guide intraluminal crossing	Clinical	Single-centre, retrospective, single-arm study	31 (N/A)	Eagle Eye platinum ST (Philips Volcano, Amsterdam, the Netherlands) and Gogo inner-guiding catheter (Medikit, Tokyo, Japan)	Femoral CTOs
Tsubakimoto[23], 2020	To compare IVUS-guided crossing of femoropopliteal CTOs, with conventional fluoroscopy guidance, in terms of crossing pathways (intraluminal, subintimal, intramedial)	Clinical	Single-centre, retrospective, non-randomized controlled trial.	64 (71)	Eagle Eye short tip (Philips Volcano, Amsterdam, the Netherlands)	Femoropopliteal CTOs (TASCII B-D)
Kawasaki[24], 2011	Feasibility of contrast-free endovascular treatment of iliac and femoral lesions by means of IVUS-assisted guidance	Clinical	Single-centre, prospective single-arm study	36 (54)	Eagle Eye Gold (Philips Volcano, Amsterdam, the Netherlands)	Iliofemoral steno-occlusive lesions (TASCII A-D)
Kawasaki[25], 2012	To compare conventional guidance with contrast-free guidance (IVUS and CO_2 angiography) in iliac and femoral lesions	Clinical	Single-centre, retrospective non-randomized controlled trial.	107 (148)	N/A	Iliofemoral steno-occlusive lesions (TASCII A-D)
Kusuyama[26], 2012	Feasibility of contrast-free treatment of iliac and femoral lesions by means of IVUS-assisted guidance and CO_2-angiography	Clinical	Case study	1 (1)	Atlantis Pro Peripheral 40MHz (Boston Scientific, Boston Scientific, Marlborough, MA, USA)	Femoral CTO

Table 1: Continued

Author, Year	Study purpose	Study environment	Study type	Patients (lesions)	Device Type	Lesion characteristics
Higashimori[27], 2013	Feasibility of contrast-free treatment of iliac and femoral lesions by means of IVUS-assisted guidance and CO_2-angiography	Clinical	Case study	1 (1)	Eagle Eye Gold (Philips Volcano, Amsterdam, The Netherlands)	Femoropopliteal CTOs
Ephrem[28], 2016	Feasibility of contrast-free treatment of iliac and femoral lesions by means of NIRS-IVUS assisted guidance	Clinical	Case study	1 (1)	TVC catheter (InfraReDx, Burlington, MA, USA)	Femoral stenotic lesions
Baker[29], 2015	To evaluate the impact of the IVUS-guided Pioneer re-entry catheter in terms of technical success (true lumen re-entry) and midterm outcomes in the treatment of iliac and femoral CTOs	Clinical	Single-centre, retrospective propensity score-matched cohort study	40 (40)	Pioneer Plus (Philips Volcano, Amsterdam, The Netherlands)	Iliac, femoral CTOs (TASCII B-D)
Krishnamurthy[30], 2010	Feasibility of the IVUS-guided Pioneer re-entry catheter in terms of technical success (true lumen re-entry) in the treatment of iliac CTOs	Clinical	Single-centre, retrospective single-arm study	11 (11)	Pioneer Plus (Philips Volcano, Amsterdam, The Netherlands)	Iliac CTOs
Smith[31] 2011	To compare the IVUS-guided Pioneer re-entry catheter with the fluoroscopy-guided Outback re-entry catheter in terms of technical success (true lumen re-entry) the treatment of femoral CTOs	Clinical	Single-centre, retrospective non-randomized controlled trial	23 (23)	Pioneer Plus (Philips Volcano, Amsterdam, The Netherlands)	Femoral CTOs (TASC B-D)
Szymanski[32], 2011	Feasibility of the IVUS-guided Pioneer re-entry catheter in terms of technical success (true lumen re-entry) in the treatment of femoral CTOs	Clinical	Case study	1 (1)	Pioneer Plus (Philips Volcano, Amsterdam, The Netherlands)	Femoral CTO
Hishikari[33], 2015	Feasibility of adjunctive intravenous IVUS-guidance during intraluminal crossing of iliac CTOs	Clinical	Case study	1 (1)	AcuNav (Siemens Medical Solutions, Mountain View, CA, USA)	Iliac CTO
Takahashi[34], 2017	Feasibility of adjunctive intravenous IVUS-guidance during intraluminal crossing of femoropopliteal CTOs	Clinical	Single-centre, retrospective single-arm study	44 (50)	Visions PV .035 10MHz catheter (Philips Volcano, Amsterdam, The Netherlands)	Femoropopliteal CTOs
Optical coherence tomography (OCT) guidance						
Marmagkiolis[35], 2014	Feasibility of adjunctive OCT-guidance during endovascular treatment of femoral lesions	Clinical	Case series	2 (2)	C7-XR with FD-OCT catheter (St. Jude Medical Inc./Abbott)	Femoral steno-occlusive lesions

Table 1: Continued

Author, Year	Study purpose	Study environment	Study type	Patients (lesions)	Device Type	Lesion characteristics
Selmon[36], 2013 (CONNECT II trial)	Evaluation of the impact of an OCT-guided CTO crossing device (Ocelot™) in terms of safety and technical success in the treatment of de novo and restenotic femoropopliteal CTOs	Clinical	Multicentre, prospective, single-arm study	100 (100)	Ocelot™ (Avinger, Redwood, CA, USA)	Femoropopliteal CTOs (severely calcified lesions excluded)
Schaefers[37], 2018	Evaluation of the impact of an OCT-guided CTO crossing device (Ocelot™) in terms of safety, technical success and midterm outcomes in the treatment of femoropopliteal CTOs	Clinical	Single-centre, retrospective single-arm study	83 (84)	Ocelot™ (Avinger, Redwood, CA, USA)	Femoropopliteal CTOs (TASCII A-D),
Walters[38], 2018	Feasibility of an OCT-guided CTO crossing device (Ocelot™) in the treatment of iliac CTOs	Clinical	Case series	2 (2)	Ocelot™ (Avinger, Redwood, CA, USA)	Iliac CTOs
Schwindt[39], 2017 (VISION trial)	Feasibility of the OCT-guided atherectomy device (Pantheris™) in the treatment of patients with femopopliteal lesions	Clinical	Multicentre, prospective, single-arm study	158 (198)	Pantheris™ (Avinger, Redwood, CA, USA)	Femoropopliteal steno-occlusive lesions (TASCII A – C)
George[40], 2015	Feasibility of the OCT-guided atherectomy device (Pantheris™) and OCT-guided CTO crossing device (Ocelot™) in the treatment of a patients with a femopopliteal lesion	Clinical	Case study	1 (1)	Ocelot™ and Pantheris™ (Avinger, Redwood, CA, USA)	Femoropopliteal steno-occlusive lesions
Stavroulakis[41], 2019	Evaluation of the impact of the OCT-guided atherectomy device (Pantheris™) in terms of technical success and midterm outcomes in the treatment of patients with de novo and restenotic femopopliteal lesions	Clinical	Single-centre, retrospective, single-arm study	33 (37)	Pantheris™ (Avinger, Redwood, CA, USA)	Femoral CTOs
Intravascular photoacoustic-IVUS (IVPA-IVUS)						
Kole[42], 2019	Preclinical validation of IVPA-IVUS against NIRS-IVUS and histology in terms of identification and quantification of lipid-rich plaques	Ex-vivo porcine model	Single-centre, prospective, preclinical single-arm study	3 (3)	TVC Insight, Infraredx Inc, Bedford, MA, USA (NIRS-IVUS) and in-house developed IVPA-IVUS catheter	Iliac stenotic lesions (ex-vivo porcine)

Table 1: Continued

Author, Year	Study purpose	Study environment	Study type	Patients (lesions)	Device Type	Lesion characteristics
Robotic catheter guidance						
Bismuth[43], 2013	Feasibility of the Magellan robotic catheter in the treatment of iliofemoral steno-occlusive lesions	Clinical	Single-centre, prospective single-arm study	20 (41)	Magellan Robotic System with VC catheter (Auris Health, Redwood City, CA, USA)	Iliofemoral steno-occlusive lesions (TASC A-D)
Fibre optic guidance						
Jansen[44], 2020	Preclinical feasibility of fiber optic realshape (FORS) technology to enable real-time 3D device visualization and guidance in non-stenotic visceral, renal and peripheral arteries in phantom and porcine models	Phantom and porcine models	Preclinical, prospective, single-arm study	6 (144)	Fibre Optic RealShape platform (Philips Medical Systems Nederland, Best, the Netherlands)	Healthy, non-stenotic renal, visceral, iliac and femoral arteries.

Magnetic particle imaging

Magnetic particle imaging (MPI) uses magnetic fields to visualize superparamagnetic iron oxide (SPIO) nanoparticles in 3D space and therefore requires the use of SPIO-based contrast material to visualize the vasculature as well as SPIO-visible marker integration in the endovascular devices.[45] One preclinical study used MPI to guide angioplasty and stenting in phantom models of the iliac arteries, using an open-bore MPI-scanner, with a field of view of 2.9cm x 6.5mm, 8fps framerate and manually selectable imaging planes.[6] Despite successful angioplasty and stenting in all three phantom models, the road to clinical adoption is still long due to limitations in spatial resolution, narrow field of view and the absence clinically approved devices. Data from this study is summarized in *Table 2*.

CO$_2$ CT guidance

A case report described the feasibility of intraoperative CO$_2$ CTA using a hybrid OR with angio-CT system (Miyabi, Siemens Medical Systems, Erlangen, Germany) for diagnosis, planning and verification of stent placement.[7] This approach may improve navigation in selected patients, but widespread adoption is limited due to the required facilities. Data from this study is summarized in *Table 3*.

Cone beam computed tomography guidance

The feasibility of cone beam computed tomography (CBCT) to guide true lumen re-entry in guidewire resistant CTOs was assessed by Liang et al.[8] Aiming to provide an alternative for patients who are not eligible for reimbursement of conventional re-entry devices. This strategy proved to be safe and effective in all patients without procedure-related complications. As the acquisition of a CBCT is rather radiation intensive and lacks real-time guidance, this approach should be used when other alternatives are not available. Data from this study is summarized in *Table 4*.

Table 2: Magnetic particle imaging

Author, Year	Study purpose	Study type	Phantom models (lesions)	Lesion characteristics	Definition of technical success	Technical success	Complication rate
Herz[6], 2019	Preclinical feasibility of magnetic particle imaging (MPI) to guide angioplasty and stenting in peripheral stenotic lesions.	Preclinical (in-vitro), single-arm feasibility study	3 (3)	External iliac stenotic lesions (50% stenosis)	Successful crossing of lesion and stent placement	100%	0%

Table 3: Computed tomography guidance

Author, Year	Study purpose	Study type	Patients (lesions)	Lesion characteristics	CV (mL)	Definition of technical success	Technical success	Complication rate
Heidrich[7], 2018	Feasibility of intraprocedural CO$_2$ CTA (using hybrid angio-CT system) for diagnosis and planning in a patient with impaired renal function and excessive bowel gas.	Case report	1 (2)	Iliac stenotic lesions	160 mL CO$_2$	Visualization of lesion and successful crossing of lesion	100%	0%

Table 4: Cone beam computed tomography guidance

Author, Year	Study purpose	Study type	Patients (lesions)	Lesion characteristics	Definition of technical success	Technical success	Complication rate	Follow-up	Primary patency at follow up
Liang[8], 2016	Feasibility of CBCT-guided true lumen re-entry during iliac CTO crossing.	Retrospective, single-arm feasibility study	10 (10)	Iliac CTOs (TASCII B and D)	Successful true lumen re-entry and <30% residual stenosis	100%	0%	6 months (range, 3 - 45)	100%

Image fusion with preoperative CTA or MRA

Image fusion (IF) is the projection of preoperative datasets, such as magnetic resonance angiography (MRA) or computed tomography angiography (CTA) on top of conventional real-time fluoroscopy. The combined image visualizes the endovascular devices (in 2D, in real-time) in combination with the surrounding arterial structures (in 3D, preoperative). Data from the available studies is summarized in *Table 5*.

Two single-arm usability studies by Ierardi et al.[10] and Sailer et al.[9] on image fusion guidance were able to omit diagnostic angiography in respectively 80% and 48% of their patients. A third single-arm study by Goudeketting et al.[11] reported no reduction in number of angiographies. All three studies acquired an intraoperative cone beam computed tomography (CBCT) to perform initial image registration (3D-3D registration), which accounted for roughly one fifth of the procedural DAP.[46]

Stahlberg et al.[12] used more advanced 2D-3D registration methods, that require only two fluoroscopy images and a negligible amount of radiation. Consequently, the authors reported not only a significant reduction in CV (45 mL vs 120 mL, $p=.001$) but also in DAP (28.7 Gycm^2 vs 43.8 Gycm^2, $p<.05$) when comparing an IF cohort with a cohort with conventional image guidance.

Image registration of the image fusion overlay with the patient's on-table anatomy is essential for the performance of IF. Due to patient movements under local anaesthesia and the mobility of pelvis, hip and knee joints, this process is more challenging compared to other vascular beds such as the aorta. Average image registration durations between 2-5 minutes have been reported.[47,48] The accuracy of the registration was considered 'clinically acceptable' in all studies, although every study contained patient(s) in which severe inaccuracy was encountered, due to motion and vessel deformation[46–49]. Manual correction or re-registration can improve the accuracy, but inordinate movements in hip and knee joints were often too complex to dissolve completely.[46]

Transcutaneous ultrasound

Handheld transcutaneous US can visualize arterial composition, vessel layers and blood flow patterns from a wide range of viewing angles. Data from the available studies is summarized in *Table 6*.

Feasibility studies by Banerjee et al.[13] and Nishino et al.[14] successfully used adjunctive US-guidance to guide intraluminal revascularization of infrainguinal CTOs, by correcting device movement towards the arterial wall before damaging the intimal layer. When using this technique in combination with fluoroscopy, strong radiation hygiene principles are needed to protect the echographer from unnecessary radiation exposure. More recently, two studies explored the feasibility of US as primary image guidance for patients with chronic kidney disease. Meaning that the complete procedure including lesion crossing, sizing, angioplasty and stenting is performed exclusively using US-imaging. The initial single-arm feasibility study by Krasznai et al.[15] reported a technical

success rate of 94% in the iliac region, without complications. Technical failure was restricted to two TASCII-C lesions, in which the authors declined from difficult subintimal crossing under US-guidance at this early stage of research. Bolt et al.[16] succeeded this study with a randomized controlled trial in which patients were either treated using US guidance or conventional fluoroscopic guidance. This study demonstrated non-inferiority of US-guidance in terms of technical success (96.5% vs 98.8%, $p = .34$), although bail-out fluoroscopic guidance was needed during lesion crossing in 17% of the patients in the US-cohort. The use of ultrasound guidance led to a significant reduction in FT (0.7 min vs 6.0 min, $p<.01$), DAP (4.6 Gycm^2 vs 99.2 Gycm^2, $p<.01$) and CV (3.2 mL vs 67.5 mL, $p<.01$).

To summarize, transcutaneous US is an accessible and low-cost imaging technique that can be used in iliac, femoral and popliteal arteries. Image quality is strongly related to patient body habitus and lesion characteristics. Adjunctive use of transcutaneous US can aid intraluminal revascularization of difficult CTOs. In selected patients with TASCII A or B lesions and severe chronic kidney disease, transcutaneous US even forms a viable alternative to conventional fluoroscopy. Drawbacks of this technique are the need for a dedicated echographer and the limited field of view and occasional signal fall-out, as well as the need for bailout X-ray facilities.

Table 5: Image Fusion Guidance

Author, Year	Study purpose	Study type	Patients (lesions)	Lesion characteristics	DAP (Gy·cm²)	FT (mm:ss)	PT (min)	CV (mL)	RE (mm)	Definition of technical success	Technical success	Complication rate
Sailer[9], 2015	Feasibility of 3D-3D IF-guidance during endovascular treatment of iliac, femoral, popliteal and BTK lesions	Prospective single-arm feasibility study	17 (20)	Iliac, femoral, popliteal and BTK steno-occlusive lesions	67.8	N/A	102 (range 45 – 260)	58 ± 23	1.9 ± 2.0 mm	1. Successful crossing of lesion 2. Added value of IF during lesion crossing 3. Treatment of lesion without use of diagnostic angiography	1. 100% 2. 75% 3. 47%	0%
Ierardi[10], 2016	Feasibility of 3D-3D IF-guidance during endovascular treatment of aortoiliac lesions	Prospective single-arm feasibility study	5 (N/A)	Aortoiliac steno-occlusive lesions	60.2 (range, 55.0 – 63.8)	12:03 (range, 10:10 – 14:15)	32.2 (range, 27 – 38)	24 (range, 20 – 40)	Acceptable (100%), inacceptable (0%)	Successful crossing of lesion	100%	0%
Goudeketting[11], 2017	Feasibility of 3D-3D IF-guidance during endovascular treatment of iliac lesions	Prospective single-arm feasibility study	11 (15)	Iliac steno-occlusive lesions	54.1 (range, 18.0 – 159.0)	6:03 (range, 01:29 – 23:36)	49 (range, 13 – 111)	28 (range, 15 – 56)	4.0 ± 2.5mm, Accurate (27%), mismatch (55%), inaccurate (18%)	Residual stenosis of <30% on completion DSA	100%	0%
Stahlberg[12], 2019	Comparison of 2D-3D IF-guidance and conventional guidance during endovascular treatment of iliac lesions	Retrospective non-randomized controlled trial.	26 (N/A)	Iliac steno-occlusive lesions	*IF vs control cohort:* 28.7 (IQR, 19.7 – 42.2) vs :43.8 (IQR, 28.0 – 84.6) p<.05	*IF vs control cohort:* 05:18 (IQR, 03:06 – 06:12) vs 06:00 (IQR, 02:06 – 10:12). p= 0.38	N/A	*IF vs control cohort:* 45 (IQR, 30 – 90) vs 120 (IQR, 100 – 140). p <.01	N/A	Successful intra- or sub-intimal revascularization with residual stenosis of <30% on completion DSA	*IF vs control cohort:* 100% vs 100%	*IF vs control cohort:* Total: 9% (1 embolism) vs 0% IGNS-related: 0% vs 0%

Table 6: *Transcutaneous ultrasound*

Author, Year	Study purpose	Study type	Patients (lesions)	Lesion characteristics	DAP (Gy·cm²)	FT (mm:ss)	CV (mL)	Definition of technical success	Technical success	Complication rate	Follow-up	Primary patency at follow up	Freedom of re-intervention at follow up
Banerjee[13], 2010	Feasibility of adjunctive US-guidance in intraluminal crossing of femoral CTOs, using a microdissection catheter	Case series	1 (2)	Femoral CTOs	N/A	N/A	0	Successful CTO crossing	100%	0%	N/A	N/A	N/A
Nishino[14], 2012	Feasibility of adjunctive US-guidance in intraluminal crossing of femoropopliteal CTOs using a dual access approach	Single-centre, prospective single-arm study	19 (19)	Femoropopliteal CTOs, (TASCII B-D)	N/A	N/A	N/A	Successful CTO crossing and revascularization of at least one tibioperoneal vessel	95%	0%	3 years	63%	N/A
Krasznai[15], 2013	Feasibility of primary US-guidance during endovascular treatment of iliac lesions	Single-centre, prospective single-arm study	31 (35)	Iliac steno-occlusive lesions (TASCII A-C)	0	0	0	Successful CTO crossing	94%	Total: 3.2% IGNS-related: 0%	N/A	N/A	N/A
Bolt[16], 2019	To compare primary US-guidance with conventional fluoroscopic guidance during endovascular treatment of iliac lesions	Single-centre, randomized, controlled trial	142 (165)	Iliac steno-occlusive lesions (TASCII A-B)	*US cohort vs Control cohort:* 4.6 ± 15.1 vs 99.2 ± 133.2, p<.05	*US cohort vs Control cohort:* 0.7 ± 2 vs 6.0 ± 7.0, p<.01	*US cohort:* 3.2 ± 12.8	1. Crossing of lesion 2. Reduction of the peak systolic velocity to ≥50% (US cohort) or angiographic reduction of ≥50% (control cohort)	*US cohort vs control cohort:* 1. 96.5% vs 98.8%, p=.34 2. 91.7% vs 65.7%, p<.01	*US cohort vs control cohort* 2.8% (1 dissection, 1 pseudoaneurysm) vs 2.9% (2 dissections)	1 year	N/A	*US cohort vs control cohort:* 93.1% vs 95.7%, p=.72

Intravascular ultrasound

Intravascular ultrasound (IVUS) is a catheter-based ultrasound technique that provides real-time, cross-sectional views from within the artery. IVUS allows detailed 360° assessment of vessel layers, lesion composition, lesion eccentricity, calcification-grade and cross-sectional vessel size.[50] This morphological information can aid treatment selection and device sizing, which may decrease restenosis rates. Additionally, IVUS can be used to detect treatment flaws, such as residual stenosis, in-stent thrombus protrusion, stent malapposition or dissection. [51–53] Timely resolution of these issues positively affect intraprocedural outcomes and vascular patency.[17,21] Eighteen studies involving IVUS were included in this review, which were categorized in two groups: 1) standard IVUS catheters and 2) IVUS-integrated devices. Data from the available studies is summarized in Table 7.

1. IVUS catheters

Positive intraprocedural, short- and midterm outcomes were reported on adjunctive use of an IVUS catheter during treatment of PAD.[18,19,54,55] Lower rates of intra-procedural complication (11.8% vs 14.5%, $p<.001$), vascular complication (9.2% vs 11.4%, $p<.001$) and amputation (5.3% vs 9.8%, $p<.001$) where found by Panaich et al.[54] when comparing IVUS-assisted peripheral procedures to those performed without IVUS. During mid-term follow-up of femoropopliteal lesions, Iida et al.[56] reported a significant increase in primary patency (1-year patency: 90±2% vs 72±3%, 2-year patency: 77±3% vs 60±4% and 5-year patency: 65±6 vs 35±6%, $p<.001$). Araki et al.[57] reported even higher primary patency rates in the IVUS-assisted treatment of iliac CTOs (1-year patency: 98.7% and 2-year patency: 96.5%). Kumakura et al.[20] reported positive long-term primary patency rates of IVUS-assisted stent placement in iliac lesions (5 year: 87%, 10 years: 83% and 15 year: 75%). In comparison, the 15-year patency of TASCII C/D lesions achieved by Kumakura were more favourable than the 5-year patency rates reported in a meta-analysis by Ye et al.[58] in which patients were treated with a similar approach but without IVUS-guidance (75% vs 63%).

Krishnan et al.[55] showed that adjunctive IVUS guidance during directional atherectomy allowed more aggressive debulking in patients with femoropopliteal in-stent restenosis (18 vs 8 atherectomy passes, $p=.02$), resulting in higher primary patency rates at 12-month follow-up (83.1% vs 49%, $p=.03$).

Nakamura et al.[22] and Tsubakimoto et al.[23] demonstrated that IVUS-guidance can help avoid subintimal or intramedial crossing routes during CTO revascularization, by retracting and redirecting the guidewire when its path threatened to damage intimal and medial tissue. Nakamura et al.[59] reported feasibility and high revascularization success when using this approach during a retrograde intraluminal crossing of femoral CTOs. Moreover, Tsubakimoto et al.[60] was able to achieve clinically true lumen routes in 91.1% of the IVUS-guided procedures, as opposed to 51.3% of the fluoroscopy guided procedures ($p<.001$), leading to higher patency rates at 12 month compared to conventional fluoroscopy guidance (70.0% vs 52.2%, $p<.05$).

Additionally, three case reports and two prospective studies demonstrated the feasibility of IVUS imaging to reduce or avoid injection of contrast material in patients with severe chronic kidney disease or contrast allergy.[24–27,61] In the majority of the studies, IVUS was complemented with CO_2 angiography to visualize overall condition of the vascular tree.[62–64] Revascularization success was 100% in all five studies. Freedom from nephrotoxic contrast material was reported in all but three patients, whom required conventional angiography to evaluate infrapopliteal arteries or exclude arterial perforation.[26]

Two studies by Hishikari et al.[33] and Takahashi et al.[34] report the use of transvenous IVUS catheters to guide intraluminal crossing of iliac and femoropopliteal CTOs, respectively. These transvenous IVUS catheters are advanced in a vein that runs parallel to the artery of interest and aligned with the arterial devices using fluoroscopy. When IVUS imaging showed that the guidewire advanced the edge of the vessel, the guidewire was retracted and its path was corrected and centralized. Technical success rates of 100% and 96% were achieved without device related complications. Image quality varied with the anatomical position of the arteries and accompanying veins and the calcification grade of the artery. Even in severely calcified segments, (partial) visualization of the target artery could be achieved. Opposed to the subintimal approach, this intraluminal approach did not require stents in 42% of the cases, which is favourable in non-stenting zones such as the popliteal artery. Takahashi et al. [34] reported freedom from clinically driven reintervention at 1-year follow up of 77.9%.

2. IVUS-integrated devices

Re-entry devices are designed to create true lumen re-entry after subintimal crossing of a CTO. When conventional guidewire and catheter techniques fail to access the true lumen, a re-entry device can be used to puncture the intimal layer of the artery and gain luminal access. The Pioneer Plus re-entry device (Philips, Amsterdam, the Netherlands), formerly known as CrossPoint catheter, is the only re-entry device with an integrated IVUS transducer with colour Doppler application to guide needle deployment (*Figure 2*).

Baker et al.[29] compared a study cohort treated with the Pioneer Plus device, with a propensity score-matched control cohort in which conventional guidewire techniques were sufficient to access the true lumen. The study cohort, that used the re-entry device as bail-out strategy, reported lower technical success rates (90% vs 95%) and higher FT (42.6 ± 22.8 min vs 29.7 ± 20.1 min, $p = .12$), but neither finding was statistically significant. Indicating that this technique can be used when other methods fail. Primary patency of the study cohort after 1-year follow-up was congruent with the matched control cohort (67% vs 71%, $p = .82$), indicating that the Pioneer Plus device can accomplish technical success when conventional guidewire re-entry methods fail, without undermining short-term patency.
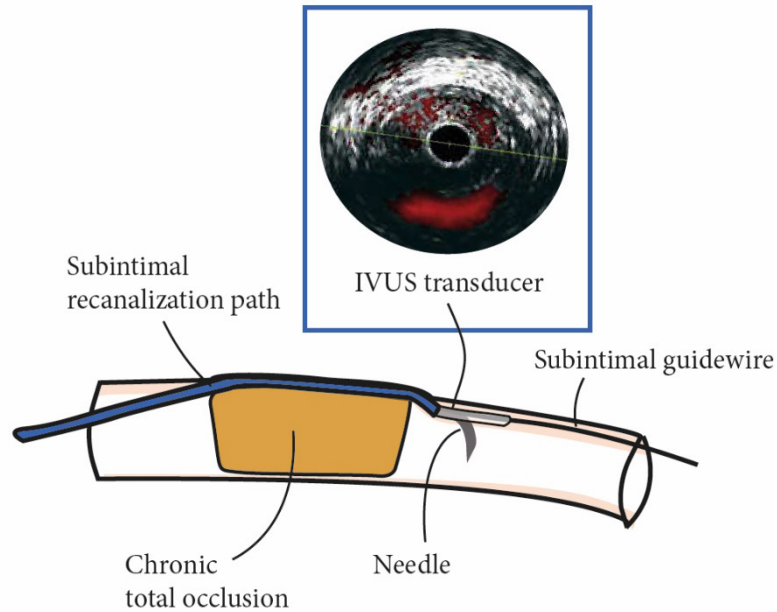
Figure 2: Re-entry device with IVUS transducer. These devices are used to support true-lumen re-entry after subintimal passage of a chronic total occlusion. This device contains an IVUS-transducer to guide needle-puncture of intimal layer to regain true lumen access. After successful puncture, a guidewire is advanced through the needle.

Smith et al.[31] compared the IVUS-guided Pioneer Plus re-entry catheter with the fluoroscopy-guided Outback re-entry catheter in the treatment of femoral CTOs. The IVUS-guided re-entry catheter was more effective in terms of technical success (100% vs 87%) and primary patency at 1-year follow-up (100% vs 86%). Costs of the Pioneer Plus re-entry catheter, however, were considerably higher than those of the Outback re-entry catheter ($3100 vs $1800).

In summary, IVUS allows intravascular assessment and guidance without requiring radiation exposure or nephrotoxic contrast, nor being limited by bowel gas and obese habitus. The adjunctive use of IVUS during endovascular treatment of PAD seems to positively affect intraprocedural, short- and midterm outcomes and can help to minimize intimal and medial damage during CTO crossing.[54–57,65,66] In selected patients with severe chronic kidney disease or contrast allergy, IVUS can form a viable alternative to angiography for diagnosis and treatment verification.[62–64,67,68]

Integration of IVUS in re-entry devices can aid subintimal revascularization of guidewire-resistant CTOs and lead to improved technical success and reduced complications by supporting true lumen re-entry.[69,70]

Intravascular optical coherence tomography

Intravascular optical coherence tomography (OCT) is in many ways comparable to IVUS: both are catheter-based imaging methods that provide cross-sectional imaging of the lumen and arterial wall. Instead of ultrasound waves, OCT utilizes near-infrared light waves that provide a superior image resolution and tissue discriminability compared to IVUS.[71] Intravascular OCT has a limited penetration depth of 1 – 3 mm. Due to the strong attenuation of light waves in blood, imaging is only possible in (balloon) occluded segments or when the blood is flushed with a hand-injected flush technique using contrast material, dextran or saline.[72,73] Although OCT guidance can be used on its own to assess lesion morphology[35], the technology is more frequently used as an integrated imaging tool in crossing devices (Ocelot™, Avenger Inc, Redwood City, CA, USA) or atherectomy devices (Pantheris™, Avenger Inc, Redwood City, CA, USA). Both these devices employ OCT to minimize damage to the tunica media and tunica adventitia or, in case of in stent restenosis, to the struts and fabric of the stent graft.

The Ocelot crossing device contains spiral flutes with adjustable rotation speed to advance through CTOs under OCT guidance (*Figure 3*). The Pantheris atherectomy device is equipped with a balloon system to achieve cutter apposition to the vessel wall (*Figure 4*). Data from the available studies is summarized in *Table 8*.
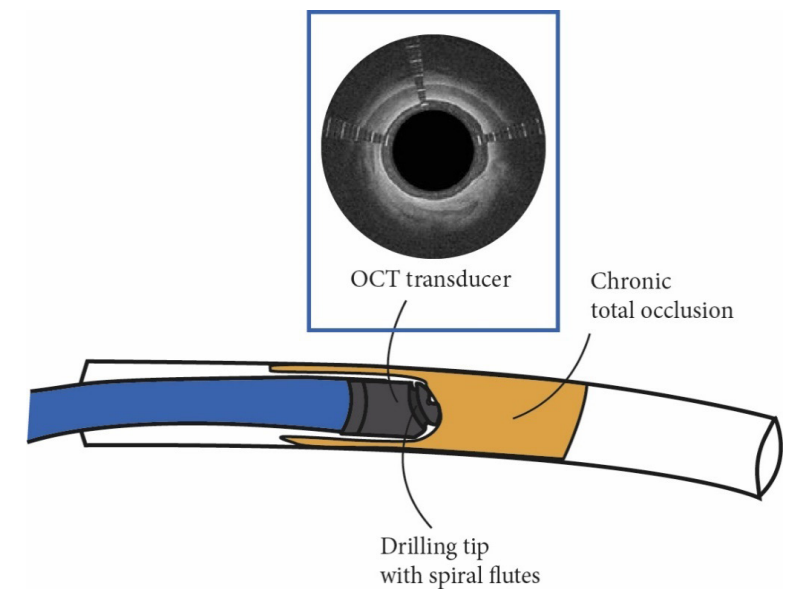
Figure 3: The Ocelot crossing device with OCT transducer. Rotation of the two spiral flutes in the tip of the device create an intraluminal channel through the chronic total occlusion. The device is equipped with an optical coherence tomography (OCT) transducer, that visualizes the different layers of the artery to prevent damage to the intimal and medial layers of the vessel during revascularization.

Table 7: Intravascular ultrasound

Author, Year	Study purpose	Study type	Patients (lesions)	Lesion characteristics	FT (mm:ss)	PT (min)	CV (mL)	Definition of technical success	Technical success	Complication rate	Follow-up	Primary patency at follow up	Freedom of re-intervention at follow up
Panaich[17], 2016	Evaluate the impact of adjunctive IVUS-assistance in terms of in-hospital complications during endovascular treatment of PAD	Multi-centre, retrospective non-randomized controlled trial	92714 (N/A)	Iliac, femoral, popliteal, BTK steno-occlusive lesions (TASCII A-D)	N/A	N/A	N/A	N/A	N/A	*IVUS vs control cohort:* Total: 9.2% vs 11.4%	N/A	N/A	N/A
Iida[18], 2014	Evaluate the impact of adjunctive IVUS-assistance in terms of technical success and midterm patency during endovascular treatment of PAD	Single-centre, retrospective propensity score-matched cohort study	468 (N/A)	Femoropopliteal steno-occlusive lesions (TASCII A-C)	N/A	N/A	N/A	N/A	N/A	N/A	23±18 months	*IVUS vs control cohort:* 65 ± 6% vs 35 ± 6% (12 months)	*IVUS vs control cohort:* 84 ± 3% vs 54 ± 6% (at 12 months)
Araki[19], 2014	Evaluate the impact of adjunctive IVUS-assistance in terms of midterm patency in the treatment of iliac CTOs using self-expandable stent grafts	Single-centre, single-arm, retrospective study	82 (86)	Iliac CTOs (TASCII B-D)	N/A	193 ± 63	210 ± 87	Successful CTO crossing	89.1%	Total: 2.4% IGNS-related: 0%	27.6 (range, 3-60)	98.7% (6 months), 98.7 (12 months), 97.5 (18 months), 96.5 (24 months)	N/A
Kumakura[20], 2015	Evaluate the impact of adjunctive IVUS-assistance in terms of technical success and long-term patency in the treatment of de novo iliac lesions using self-expandable and balloon expandable stent grafts	Single-centre, single-arm, prospective study	455 (507)	Iliac steno-occlusive lesions treated by primary stenting (TASCII A-D)	N/A	N/A	N/A	Residual stenosis of <30% on completion DSA	97.2%	Total: 4.0% IGNS-related: 1.8% (2 perforations, 1 dissection, 5 pseudoaneurysm)	63 months (range, 1 – 246)	87% (60 months), 83% (120 months), 75% (180 months)	N/A
Krishnan[21], 2018	To compare IVUS-guided directional atherectomy with conventional fluoroscopy-guided directional atherectomy in the treatment of femoropopliteal in-stent restenosis	Single-centre, retrospective, non-randomized controlled trial.	114 (114)	Femoropopliteal in-stent re-stenoses	N/A	N/A	N/A	Residual stenosis of ≤30% on completion DSA	*IVUS vs control cohort:* 100% vs 100%	*IVUS vs control cohort:* Total: 0% vs 0% IGNS-related: 0% vs 0%	12 months	N/A	*IVUS vs control cohort:* 82.1% vs 49% (at 12 months)
Nakamura[22], 2020	Feasibility of retrograde revascularization of femoral CTOs using IVUS to guide intraluminal crossing	Single-centre, retrospective, single-arm study	31 (N/A)	Femoral CTOs	44.7±30.9	45±41.2 (from vascular access until crossing of the CTO)	15.9±9.6	Successful CTO crossing	100%	Total: 6.5% IGNS-related: 0%	N/A	N/A	N/A

Table 7: Continued.

| Author, Year	Study purpose	Study type	Patients (lesions)	Lesion characteristics	FT (mm:ss)	PT (min)	CV (mL)	Definition of technical success	Technical success	Complication rate	Follow-up	Primary patency at follow up	Freedom of re-intervention at follow up
Tsubakimoto[23], 2020	To compare IVUS-guided crossing of femopopliteal CTOs, with conventional fluoroscopy guidance, in terms of crossing pathways (intraluminal, subintimal, intramedial)	Single-centre, retrospective, non-randomized controlled trial.	64 (71)	Femoropopliteal CTOs (TASCII B-D)	IVUS vs control cohort: 48.5±23.6 vs 58.2±29.1. p=.017	IVUS vs control cohort: 99 vs 113. p=.24	IVUS vs control cohort: 96 ± 40 vs 179 ± 66. p<.001	1. Successful CTO crossing with peak systolic velocity ratio of >2.4 on duplex ultrasound 2. Complete clinically true lumen route through CTO	IVUS vs control cohort: 1. 97.1% vs 94.8%. p=.49 2. 91.1% vs 51.3%. p<.001	N/A	12 months	IVUS vs control cohort: 70.0% vs 52.2%, p<.05	IVUS vs control cohort: 83.9% vs 62.8%, p<.05
Kawasaki[24], 2011	Feasibility of contrast-free endovascular treatment of iliac and femoral lesions by means of IVUS-assisted guidance	Single-centre, prospective feasibility study,	36 (54)	Iliofemoral steno-occlusive lesions (TASCII A-D)	N/A	Iliac: 60±21 Femoral: 74±22	0	Decrease of <10mmHg in the systolic gradient from the popliteal artery to the abdominal aorta measured with a multipurpose catheter and Doppler signal of the dorsal or posterior tibial artery	100%	Total: 0% IGNS-related: 0%	9.9±4.3 months (range 4-17)	N/A	5.5%
Kawasaki[25], 2012	To compare conventional guidance with contrast-free guidance (IVUS and CO_2 angiography) in iliac and femoral lesions	Single-centre, retrospective, non-randomized controlled trial.	107 (148)	Iliofemoral steno-occlusive lesions (TASCII A-D)	N/A	IVUS- vs control cohort: Iliac artery: 31±17 vs 45±24, p<.05 Femoral artery: 61±20 vs 53±18 p<.05	IVUS vs control cohort: Iliac artery: 0 vs 53±24 p<.01 Femoral artery: 2±6 vs 49±15 p<.01	Residual stenosis of ≤ 30% on completion DSA	IVUS vs control cohort: 100% vs 100%	IVUS vs control cohort: Total: 1.4% vs 0% IGNS-related: 1.4% vs 0% (1 perforation)	11.1 months (range, 3 – 18 months)	N/A	IVUS vs control cohort: 92.9% vs 93.6%
Kusuyama[26], 2012	Feasibility of contrast-free treatment of iliac and femoral lesions by means of IVUS-assisted guidance and CO_2-angiography	Case study	1 (1)	Femoral CTO	N/A	N/A	0	Successful revascularization as assessed on CO_2-angiography	100%	Total: 0% IGNS-related: 0%	N/A	N/A	N/A
Higashimori[27], 2013	Feasibility of contrast-free treatment of iliac and femoral lesions by means of IVUS-assisted guidance and CO_2-angiography	Case study	1 (1)	Femoropopliteal CTOs	32	92	0	Successful revascularization as assessed on CO_2-angiography	100%	Total: 0% IGNS-related: 0%	N/A	N/A	N/A

Table 7: Continued.

Author, Year	Study purpose	Study type	Patients (lesions)	Lesion characteristics	FT (mm:ss)	PT (min)	CV (mL)	Definition of technical success	Technical success	Complication rate	Follow-up	Primary patency at follow up	Freedom of re-intervention at follow up
Ephrem[28], 2016	Feasibility of contrast-free treatment of iliac and femoral lesions by means of NIRS-IVUS assisted guidance	Case study	1 (1)	Femoral stenotic lesions	N/A	113	0	Successful revascularization as assessed on CO_2-angiography	100%	Total: 0% IGNS-related: 0%	N/A	N/A	N/A
Baker[29], 2015	To evaluate the impact of the IVUS-guided Pioneer re-entry catheter in terms of technical success (true lumen re-entry) and midterm outcomes in the treatment of iliac and femoral CTOs.	Single-centre, retrospective propensity score-matched cohort study	40 (40)	Iliac, femoral CTOs (TASCII B-D)	*IVUS vs control cohort: 42.6±22.8 vs 29.7±20.1, p=.12*	N/A	N/A	Successful true lumen re-entry and residual stenosis of ≤ 30% on completion DSA	*IVUS vs control cohort:* 90% vs 95%	*IVUS vs control cohort:* Total: 0% vs 0% IGNS-related: 0% vs 0%	*IVUS cohort:* 4.3 months (range, 0.4 – 24)	*IVUS vs control cohort:* 62% vs 71% (at 12 months), p=.82	*IVUS vs control cohort:* 7.5% vs 0%
Krishnamurthy[30], 2010	Feasibility of the IVUS-guided Pioneer re-entry catheter in terms of technical success (true lumen re-entry) in the treatment of iliac CTOs	Single-centre, retrospective single-arm study	11 (11)	Iliac CTOs	N/A	N/A	N/A	Successful true lumen re-entry	100%	Total: 0% IGNS-related: 0%	Median: 9 months (range, 6-18)	100% (at 10 months)	100% (at 10 months)
Smith[31], 2011	To compare the IVUS-guided Pioneer re-entry catheter with the fluoroscopy-guided Outback re-entry catheter in terms of technical success (true lumen re-entry) the treatment of femoral CTOs	Single-centre, retrospective non-randomized controlled trial.	23 (23)	Femoral CTOs (TASC B-D)	*Pioneer cohort: vs Outback cohort 12.4 vs 15.6*	*Pioneer cohort vs Outback cohort: 53.1 vs 48.4*	N/A	Successful true lumen re-entry	*Pioneer cohort vs Outback cohort:* 100% vs 73.3%	*Pioneer cohort vs Outback cohort:* Total: 0% vs 0% IGNS-related: 0% vs 0%	12 months	*Pioneer cohort vs Outback cohort:* 100% vs 86%	N/A
Szymanski[32], 2011	Feasibility of the IVUS-guided Pioneer re-entry catheter in terms of technical success (true lumen re-entry) in the treatment of femoral CTOs	Case study	1 (1)	Femoral CTO	N/A	N/A	N/A	Successful true lumen re-entry	100%	Total: 0% IGNS-related: 0%	3 weeks	100% (3 weeks)	N/A

Table 7: Continued.

Author, Year	Study purpose	Study type	Patients (lesions)	Lesion characteristics	FT (mm:ss)	PT (min)	CV (mL)	Definition of technical success	Technical success	Complication rate	Follow-up	Primary patency at follow up	Freedom of re-intervention at follow up
Hishikari[33], 2015	Feasibility of adjunctive intravenous IVUS-guidance during intraluminal crossing of iliac CTOs	Case study	1 (1)	Iliac CTO	N/A	N/A	N/A	Successful intraluminal CTO crossing	100%	Total: 0% IGNS-related: 0%	N/A	N/A	N/A
Takahashi[34], 2017	Feasibility of adjunctive intravenous IVUS-guidance during intraluminal crossing of femoropopliteal CTOs	Single-centre, retrospective cohort study	44 (50)	Femoropopliteal CTOs	N/A	N/A	N/A	Successful intraluminal CTO crossing	100%	Total: 4.5% IGNS-related: 0%	12 months	N/A	77.9%
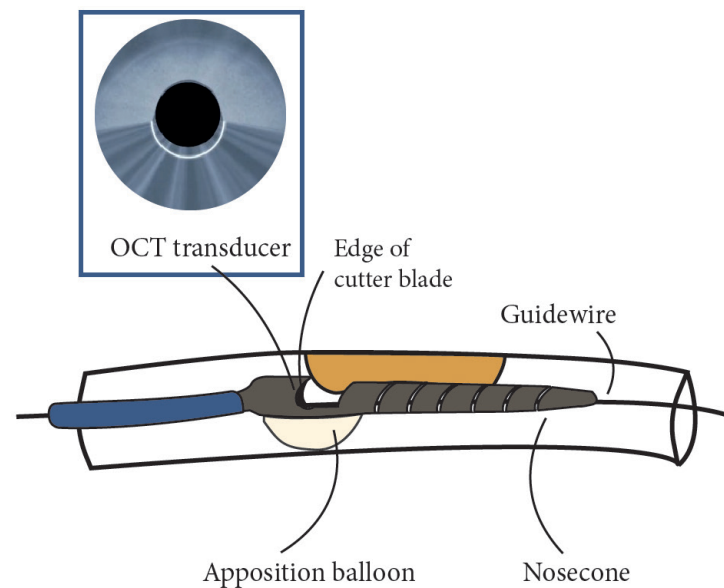
Figure 4: The Pantheris atherectomy device with OCT transducer. The OCT-transducer guides atherectomy and prevents damage to the intimal and medial vascular layers. Apposition of the cutter blade is obtained by inflation of the apposition balloon. Excised tissue is collected in the nosecone of the device, to enable multiple atherectomy passes prior to emptying the system.

OCT-guided crossing device

Selmon et al.[36] demonstrated the feasibility of the Ocelot device in patients with guidewire-resistant femoropopliteal CTOs without severe calcification.[74] Technical success of 97% was achieved with a IGNS-related complication rate of 2%. Assistance of an additional device was needed in 25% of the cases to puncture the topcap of the occlusion. A case series involving iliac CTOs showed similar use of additional devices to gain technical success.[38]

Schaefers et al.[37] did include severely calcified lesions in the study population and reported a technical success rates of 88.1% (15.5% with use of an additional device) and a IGNS-related complication rate of 4.8%.[75] Technical failure was associated with heavy calcification (diffuse calcifications on multiple sides of the arterial wall), presumably due to friction and the reduced capabilities to guide the drilling tip. Furthermore, bailout-use of the Ocelot device was suggested to increase the chance of technical failure and complications, as the drilling tip appeared to follow the false subintimal tracks created during prior crossing attempts.

A case study assessed the combined use of the Ocelot crossing device to surpass a CTO and the Pantheris atherectomy device to debulk the remaining spiral planes of eccentric plaque extending into the arterial lumen.[40] Histological examination of the excised plaque showed no traces of medial or adventitial tissue, indicating successful OCT-guidance.

OCT-guided atherectomy device

Schwindt et al.[39] established the feasibility of the Pantheris atherectomy device in the treatment of femoropopliteal steno-occlusive lesions, with a technical success rate

of 97%.[76] Patients with an occlusion were enrolled after successful intraluminal wire placement distal to the lesion, which was preferentially performed using the Ocelot crossing device. Despite OCT guidance, 18% of the lesion tissue samples contained >1% of adventitial tissue upon histological examination. Primary patency at 6 months follow-up was 92.1%.

Stavroulakis et al.[41] assessed the subsequent use of the Pantheris device and drug-coated balloon angioplasty in femoropopliteal steno-occlusive lesions. Technical success was achieved in 89% of the lesions. Device related complications were relatively high, with non-flow limiting dissections in 30% of the patients. During follow-up two treated vessels showed aneurysmatic degeneration, which was thought to be caused by the paclitaxel-coating. Primary patency rate was 93% at 12 months and 78% at 18 months.

To summarize, OCT can aid the identification of lesion morphology and composition and guide CTO crossing and stenosis debulking while limiting damage to the vascular wall. However, device-related adverse events were relatively high, with complication rates up to 8% and non-flow limiting dissections up to 30%.[74–77] Part of these issues are caused by the established learning curve to attain clinical aptitude in device handling and OCT interpretation.[74–76] Also, pre-existing false subintimal pathways may negatively affect complication rate and decrease technical success.[75]

OCT-guided atherectomy device

Schwindt et al.[39] established the feasibility of the Pantheris atherectomy device in the treatment of femoropopliteal steno-occlusive lesions, with a technical success rate of 97%.[39] Patients with an occlusion were enrolled after successful intraluminal wire placement distal to the lesion, which was preferentially performed using the Ocelot crossing device. Despite OCT guidance, 18% of the lesion tissue samples contained >1% of adventitial tissue upon histological examination. Primary patency at 6 months follow-up was 92.1%.

Stavroulakis et al.[41] assessed the subsequent use of the Pantheris device and drug-coated balloon angioplasty in femoropopliteal steno-occlusive lesions. Technical success was achieved in 89% of the lesions. Device related complications were relatively high, with non-flow limiting dissections in 30% of the patients. During follow-up two treated vessels showed aneurysmatic degeneration, which was thought to be caused by the paclitaxel-coating. Primary patency rate was 93% at 12 months and 78% at 18 months.

To summarize, OCT can aid the identification of lesion morphology and composition and guide CTO crossing and stenosis debulking while limiting damage to the vascular wall. However, device-related adverse events were relatively high, with complication rates up to 8% and non-flow limiting dissections up to 30%.[36,37,39,41,78] Part of these issues are caused by the established learning curve to attain clinical aptitude in device handling and OCT interpretation.[36,37,78] Also, pre-existing false subintimal pathways may negatively affect complication rate and decrease technical success.[37]

Near-infrared spectroscopy and photoacoustic ultrasound

Near-infrared spectroscopy intravascular ultrasound (NIRS-IVUS) is a validated catheter-based imaging strategy to identify vulnerable lipid-rich plaques in the coronary arteries.[79] NIRS-IVUS enables excellent assessment of lipid content in arterial segments, but the precise location of the lipid within the wall layers remains unknown due to the lack of depth resolution. The recently developed intravascular photoacoustic ultrasound (IVPA-IVUS) technique, may be able to detect lipid-rich compounds with depth resolution. Kole et al.[42] compares NIRS-IVUS and IVPA-IVUS imaging techniques and validates both techniques against histopathology in a preclinical studies involving swine iliac arteries. The study shows agreement between the lipid contents as measured by NIRS-IVUS and IVPA-IVUS, but only IVPA-IVUS was able to differentiate between superficial and deep lipid depots. Data from this study is summarized in *Table 9*. Clinical adoption of IVPA-IVUS for the detection of vulnerable plaques in peripheral procedures however, will require broad validation against human histopathological tissue.

Robotic catheter systems

One study described the use of a robotic catheter for endovascular treatment of PAD; the Magellan system (Auris Health Inc., Redwood City, CA, USA) that consists of a remotely operated steerable catheter with 6 degrees-of-freedom. The shape of the catheter tip is controlled by the operator, in contrast to conventional catheters who are limited to pre-formed shapes. Robotic actuators maintain stable catheter position, even when strong directional forces are exerted. In aortic and coronary vascular beds, the amount of wall hits, their contact force and the histopathological damage after target vessel cannulation were significantly reduced by the stable movements of the Magellan system.[80–82] After lesion crossing, the catheter functions as a conduit for third-party therapeutic devices. The operator is seated away from the X-ray source, which reduces operator exposure to radiation, but in-room assistance remains necessary to alter C-arm geometry or perform guidewire exchanges.

The clinical feasibility study by Bismuth et al.[43] demonstrated the safety of the Magellan system in aorta-iliac and femoropopliteal steno-occlusive lesions. Procedure times averaged 82±30 min, in which the Magellan system was used for 21±10 min. All lesions were successfully crossed with the robotic catheter except for one (95%), no complications occurred. The failed attempt was performed by a cardiac surgeon with no previous endovascular experience. All operators, regardless of experience, navigated the robotic catheter with ease, indicating that the Magellan system may shorten the path to endovascular proficiency.[83,84] Data from this study is summarized in *Table 10*.

Table 8: Optical coherence tomography

Author, Year	Study purpose	Study type	Patients (lesions)	Lesion characteristics	FT (mm:ss)	PT (min)	CV (mL)	Definition of technical success	Technical success	Complication rate (total and IGNS-related)	Follow-up	Primary patency at follow up	Freedom of re-intervention at follow up
Marmagkiolis[35], 2014	Feasibility of adjunctive OCT-guidance during endovascular treatment of femoral lesions	Case series	2 (2)	Femoral steno-occlusive lesions	N/A	N/A	N/A	Successful CTO crossing	100%	Total: 0% IGNS-related: 0%	1 month	100% (1 month)	100% (1 month)
Selmon[36], 2013 (CONNECT II trial)	Evaluation of the impact of an OCT-guided CTO crossing device (Ocelot™) in terms of safety and technical success in the treatment of de novo and restenotic femoropopliteal CTOs	Multicentre, single-arm prospective study	100 (100)	Femoropopliteal CTOs (severely calcified lesions excluded)	38.6 ± 29.1	107.3 ± 57.5 (lesion crossing time only: 32.9±42.9)	124.5 ± 100.3	Successful CTO crossing (with or without the use of other assisted devices)	72% (assisted technical success: 97%)	Total: 2.0% IGNS-related: 2.0% (2 vessel perforations)	30 days	98%	N/A
Schaefers[37], 2018	Evaluation of the impact of an OCT-guided CTO crossing device (Ocelot™) in terms of safety, technical success and midterm outcomes in the treatment of femoropopliteal CTOs	Single, centre, prospective registration study	83 (84)	Femoropopliteal CTOs (TASCII A-D), severely calcified lesions included	25.8 ± 11.7	87.9 ± 27.9	150.5 ± 53.4	Successful CTO crossing (with or without the use of other assisted devices)	72.6% (assisted technical success: 88.1%)	Total: 6.0% IGNS-related: 4.8% (4 vessel perforations)	Median 26, IQR: 20-32 months	54.2% (at 36 months)	N/A
Walters[38], 2018	Feasibility of an OCT-guided CTO crossing device (Ocelot™) in the treatment of iliac CTOs	Case series	2 (2)	Iliac CTOs	N/A	N/A	N/A	Successful CTO crossing	100%	Total: 0% IGNS-related: 0%	N/A	N/A	N/A
Schwindt[39], 2017 (VISION trial)	Feasibility of the OCT-guided atherectomy device (Pantheris™) in the treatment of patients with femopopliteal lesions	Multicentre, single-arm prospective study	158 (198)	Femoropopliteal steno-occlusive lesions (TASCII A – C)	30.2	N/A	N/A	Residual stenosis of ≤50% on completion DSA (with or without assisted devices)	52.5% (assisted technical success: 97.0%)	Total: 4.4% IGNS-related: 0.6% (1 dissections)	6 months	N/A	93.6%
George[40], 2015	Feasibility of the OCT-guided atherectomy device (Pantheris™) and OCT-guided CTO crossing device (Ocelot™) in the treatment of a patients with a femopopliteal lesion	Case study	1 (1)	Femoropopliteal steno-occlusive lesions	N/A	N/A	N/A	Residual stenosis of ≤10% on completion DSA	100%	Total: 0% IGNS-related: 0%	N/A	N/A	N/A
Stavroulakis[41], 2019	Evaluation of the impact of the OCT-guided atherectomy device (Pantheris™) in terms of technical success and midterm outcomes in the treatment of patients with de novo and restenotic femopopliteal lesions	Retrospective, single-centre, single-arm study	33 (37)	Femoral CTOs	N/A	N/A	N/A	Residual stenosis of ≤30% on completion DSA (with assistance of drug coated balloon angioplasty) in absence of arterial perforation	95%	Total: 60.1% IGNS-related: 33% (1 perforation, 11 non-flow limiting dissections)	Median: 15 months, IQR, 4-21	93% (12 months), 78% (16 months)	100% (12 months), 84% (16 months)

Fiber optic technology

The Fiber Optic RealShape (FORS) platform enables radiation-free tracking and navigation of guidewires and catheters in real-time and in 3D. Full-length shape reconstruction of these devices is based upon the concept of measuring strain in optical fibers, which are integrated in the devices itself. Device visualization is combined with images obtained by pre- or intra-operative imaging techniques such as CT, or fluoroscopy. One preclinical study described the use of FORS to track endovascular guidewires and catheters in phantom and animal models.[44] Target vessel cannulation was successful in 142 of the 144 cannulation tasks. Median registration accuracy of the device tip was 2.2mm (IQR; 1.2 - 3.8mm). Users judged FORS-based device visualization as superior to conventional fluoroscopic imaging, while not affecting their mechanical properties. Data from this study is summarized in *Table 11*.

Risk of bias analysis

Risk of bias analysis was executed on all randomized controlled trial (n = 1) and non-randomized controlled studies (n = 7) that were included in this review. Results of this analysis is provided in *Figure 5*.
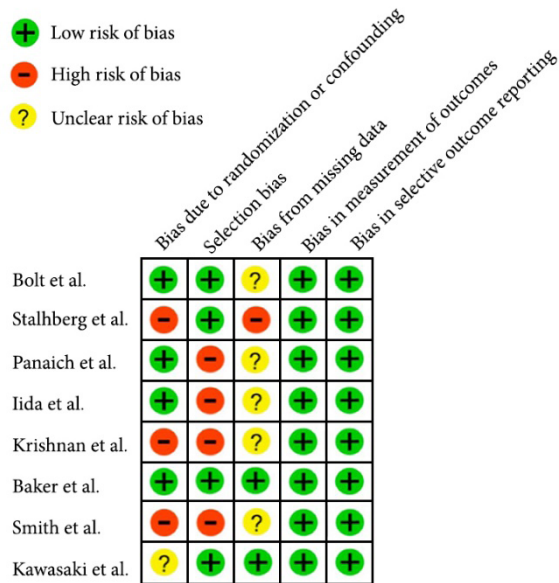
Figure 5: *Risk of Bias Analysis of the comparative studies included in this review.*

Table 9: Near-infrared spectroscopy and photoacoustic ultrasound

Author, Year	Study purpose	Study type	Patients (lesions)	Lesion characteristics	Technical success
Kole[42], 2019	Preclinical validation of IVPA-IVUS against NIRS-IVUS and histology in terms of identification and quantification of lipid-rich plaques. In order to identify vulnerable plaques	Preclinical single-arm feasibility study, in swine model.	3 (3)	Iliac stenotic lesions (ex-vivo porcine) and coronary stenotic lesions (ex-vivo human)	Accurate measurement of lipid content and lipid localization within atherosclerotic plaque

Table 10: Robotic catheter systems

Author, Year	Study purpose	Study type	Patients (lesions)	Lesion characteristics	AK (mGy)	FT (mm:ss)	PT (min)	Definition of technical success	Technical success	Complication rate
Bismuth[43], 2013	Feasibility of the Magellan robotic catheter in the treatment of iliofemoral steno-occlusive lesions	Prospective, single-arm study	20 (41)	Iliofemoral steno-occlusive lesions (TASC A-D)	621 ± 0.36	26 ± 14	82 ± 30 (lesion crossing time only: 21 ± 10)	1) accessing the lesion 2) successful revascularization of the limb	1) 100% 2) 95%	0%

Table 11: Fiber Optic Technology

Author, Year	Study purpose	Study type	Patients (lesions)	Lesion characteristics	RE (mm)	Definition of technical success	Technical success	Complication rate
Jansen[44], 2020	Preclinical feasibility of fiber optic technology to enable real-time 3D device visualization and guidance in non-stenotic visceral, renal and peripheral arteries in phantom and porcine models	Preclinical, prospective, single-arm study	6 (144)	Renal, visceral, iliac and femoral target vessels (no actual lesions)	2.2 (IQR: 1.2 – 3.8)	Successful cannulation of the dedicated target vessels	98.6%	0%

DISCUSSION

Major developments in catheter-based technology have led to increasingly complex endovascular procedures, long fluoroscopy times and high radiation doses. Parallel to these developments, new strategies are established to reduce radiation exposure and improve intraoperative image guidance. With this literature review we seek to provide broad overview of the latest developments in image guidance and device navigation during endovascular treatment of PAD, both for physicians well acquainted with these techniques and those seeking to become more familiar.

Ten different IGNS modalities were identified; MPI, intraoperative CTA, CBCT, IF, US, IVUS, PA-IVUS, OCT, robotic catheter technology and fibre optic technology. Each of these systems is designed to improve image guided navigation during (a specific part of) the endovascular procedure. Six of these ten IGNS (intraoperative CTA, CBCT, US, IVUS, IVPA-IVUS and OCT) provided additional intraprocedural assessment of vessel size and lesion morphology and lesion composition. Detailed information on these lesion characteristics can be pivotal for optimal device sizing and future choice of treatment strategy.

Comparison between different IGNS modalities is difficult, as each system serve different purposes and potential benefits. Variations in patient population, lesion morphology and combined use with adjunctive devices further complicate the comparison of outcome parameters between individual studies.

Only two studies intended to replace fluoroscopic guidance completely with another IGNS[85,86], while the IGNS in the remaining 37 studies served as an adjunctive imaging technique to supplement conventional fluoroscopic imaging.

Adjunctive techniques need to demonstrate clear advantages in procedural safety and/or procedural outcome in order to be cost-effective. However, the vast majority of the studies consisted of feasibility studies or retrospective database studies, whose design is unsuitable to address effectiveness, let alone cost-effectiveness. Only 8 studies had a comparative nature between study cohort (with IGNS-guidance) and control cohort (with conventional fluoroscopy guidance). Five of which showed high risk of bias due to confounding, selection bias or missing data.

Technical success (36/39 studies) and complication rate (34/39 studies) were the most frequently reported outcome parameters, although the definition of technical success shifted per study. In general, technical success rates were high and complication rates related to the IGNS were low, although several studies involving treatment devices with integrated IGNS showed a learning curve with relatively high complication rates at the start of use.[74,75,77,87]

Other outcome parameters such as FT (14/39), DAP (6/39 studies), PT (14/39 studies), CV (18/39 studies), primary patency at follow-up (14/39 studies) and freedom from reintervention (12/39) were reported more scarcely and showed large variations.

Future randomized controlled trials are needed to provide better evidence of advantages and cost-effectiveness, by comparing IGNS-assisted procedures with their conventional, less costly counterparts. As improvements in image guidance can be difficult to capture in quantifiable outcome measures such as DAP, CV and PT, these studies should try to incorporate more IGNS-specific outcomes, such as user-experience or registration error in their assessment. Additionally, long-term prospective studies are warranted to address the long-term effects of adjunctive imaging techniques on primary patency during follow-up.

CONCLUSION

Several promising systems for intraoperative image guidance and device navigation in the peripheral arteries have evolved throughout the last decade. Further research is required to provide framework guidance on the optimal IGNS for each individual procedure, and to provide insight on the cost-effectiveness of these IGNS for routine application in the management of PAD.

REFERENCES

1. Fowkes, F. G. R. et al. Comparison of global estimates of prevalence and risk factors for peripheral artery disease in 2000 and 2010: a systematic review and analysis. *Lancet* **382**, 1329–40 (2013).

2. Aboyans, V. et al. 2017 ESC guidelines on the diagnosis and treatment of peripheral arterial diseases, in collaboration with the european society for vascular surgery (ESVS). *Russian Journal of Cardiology* **23**, 164–221 (2018).

3. Gerhard-Herman, M. D. et al. 2016 AHA/ACC guideline on the management of patients with lower extremity peripheral artery disease: Executive summary: A report of the american college of cardiology/American Heart Association task force on clinical practice guidelines. *Circulation* vol. 135 (2017).

4. Sterne JAC, Savović J, Page MJ, Elbers RG, Blencowe NS, Boutron I, Cates CJ, Cheng H-Y, Corbett MS, Eldridge SM, Hernán MA, Hopewell S, Hróbjartsson A, Junqueira DR, Jüni P, Kirkham JJ, Lasserson T, Li T, McAleenan A, Reeves BC, Shepperd S, Shrier I, Stew, H. JPT. RoB 2: A revised Cochrane risk-of-bias tool for randomized trials. *BMJ* 1–24 (2019).

5. Sterne, J. A. et al. ROBINS-I: A tool for assessing risk of bias in non-randomised studies of interventions. *BMJ (Online)* **355**, 4–10 (2016).

6. Herz, S. et al. Magnetic Particle Imaging-Guided Stenting. *J Endovasc Ther* **26**, 512–519 (2019).

7. Heidrich, J., Nguyen, J., Florescu, C. & Steward, A. Carbon dioxide CT angiography during endovascular treatment of bilateral common iliac disease with angio-CT utilisation. *J Med Imaging Radiat Oncol* **62**, 798–802 (2018).

8. Liang, H. L. et al. The use of a Colapinto TIPS Needle under cone-beam computed tomography guidance for true lumen re-entry in subintimal recanalization of chronic iliac artery occlusion. *Journal of the Chinese Medical Association* **80**, 371–375 (2017).

9. Sailer, A. M. et al. Fusion Guidance in Endovascular Peripheral Artery Interventions: A Feasibility Study. *Cardiovasc Intervent Radiol* **38**, 314–321 (2015).

10. Ierardi, A. M. et al. Fusion of CT Angiography or MR Angiography with Unenhanced CBCT and Fluoroscopy Guidance in Endovascular Treatments of Aorto-Iliac Steno-Occlusion: Technical Note on a Preliminary Experience. *Cardiovasc Intervent Radiol* **39**, 111–116 (2016).

11. Goudeketting, S. R. et al. The use of 3D image fusion for percutaneous transluminal angioplasty and stenting of iliac artery obstructions: validation of the technique and systematic review of literature. *Journal of Cardiovascular surgery* **58**, (2017).

12. Stahlberg, E. et al. Fusion Imaging Reduces Radiation and Contrast Medium Exposure During Endovascular Revascularization of Iliac Steno-Occlusive Disease. *Cardiovasc Intervent Radiol* (2019) doi:10.1007/s00270-019-02250-5.

13. Banerjee, S., Das, T. S. & Brilakis, E. S. Transcutaneous ultrasound-guided endovascular crossing of infrainguinal chronic total occlusions. *Cardiovascular Revascularization Medicine* **11**, 116–119 (2010).

14. Nishino, M. et al. Bidirectional endovascular treatment for chronic total occlusive lesions of the femoropopliteal arterial segment using a hand-carried ultrasound device and a retrograde microcatheter. *J Vasc Surg* **56**, 113–117 (2012).

15. Krasznai, A. G. et al. Duplex-guided percutaneous transluminal angioplasty in iliac arterial occlusive disease. *European Journal of Vascular and Endovascular Surgery* **46**, 583–587 (2013).

16. Bolt, L. J. J. et al. Duplex-guided versus Conventional Percutaneous Transluminal Angioplasty of Iliac TASC II A and B Lesion: A Randomized Controlled Trial. *Ann Vasc Surg* **55**, 138–147 (2019).

17. Panaich, S. S. et al. Intravascular Ultrasound in Lower Extremity Peripheral Vascular Interventions: Variation in Utilization and Impact on In-Hospital Outcomes From the Nationwide Inpatient Sample (2006-2011). *Journal of endovascular therapy* **23**, 65–75 (2016).

18. Iida, O., Takahara, M., Soga, Y. & Suzuki, K. Efficacy of Intravascular Ultrasound in Femoropopliteal Stenting for Peripheral Artery Disease With TASC II Class A to C Lesions. *Journal of Endovascular Therapy* **21**, 485–492 (2014).

19. Araki, M. et al. Long-term outcome of the self-expanding stents for chronic total occlusion of the iliac artery. *EuroIntervention* **9**, 287 (2013).

20. Kumakura, H. et al. 15-Year Patency and Life Expectancy after Primary Stenting Guided by Intravascular Ultrasound for Iliac Artery Lesions in Peripheral Arterial Disease. *JACC Cardiovasc Interv* **8**, 1893–1901 (2015).

21. Krishnan, P. et al. Intravascular ultrasound guided directional atherectomy versus directional atherectomy guided by angiography for the treatment of femoropopliteal in-stent restenosis. *Ther Adv Cardiovasc Dis* **12**, 17–22 (2018).

22. Nakamura, S., Rokutanda, T., Kurokawa, H. & Onoue, Y. Endovascular Treatment of Long Superficial Femoral Artery-Chronic Total Occlusions Using the Gogo Catheter With IVUS Via a Popliteal Puncture Method Is Effective, Safe, and Useful. *Vasc Endovascular Surg* **54**, 225–232 (2020).

23. Tsubakimoto, Y. et al. IVUS-Guided Wiring Improves the Clinical Outcomes of Angioplasty for Long Femoropopliteal CTO Compared with the Conventional Intraluminal Approach. *J Atheroscler Thromb* (2020) doi:https://doi.org/10.5551/jat.57166.

24. Kawasaki, D. et al. Preprocedural Evaluation and Endovascular Treatment of Iliofemoral Artery Disease Without Contrast Media for Patients With Pre-Existing Renal Insufficiency. *Circulation Journal* **75**, 179–184 (2011).

25. Kawasaki, D. et al. Safety and efficacy of endovascular therapy with a simple homemade carbon dioxide delivery system in patients with ileofemoral artery diseases. *Circ J* **76**, 1722–1728 (2012).

26. Kusuyama, T., Iida, H. & Mitsui, H. Intravascular ultrasound complements the diagnostic capability of carbon dioxide digital subtraction angiography for patients with allergies to iodinated contrast medium. *Catheter Cardiovasc Interv* **80**, E82-6 (2012).

27. Higashimori, A., Yokoi, Y., A., H. & Y., Y. Stent implantation for chronic total occlusion in the iliac artery using intravascular ultrasound-guided carbon dioxide angiography without iodinated contrast medium. *Cardiovasc Interv Ther* **28**, 415–418 (2013).

28. Ephrem, G., Garikipati, S. & Hanson, I. D. The fluoro-less and contrast-less peripheral endovascular intervention: Halfway there. *Cardiovascular Revascularization Medicine* **17**, 418–420 (2016).

29. Baker, A. C. et al. Technical and early outcomes using ultrasound-guided reentry for chronic total occlusions. *Ann Vasc Surg* **29**, 55–62 (2015).

30. Krishnamurthy, V. N., Eliason, J. L., Henke, P. K. & Rectenwald, J. E. Intravascular Ultrasound-Guided True Lumen Reentry Device for Recanalization of Unilateral Chronic Total Occlusion of Iliac Arteries: Technique and Follow-Up. *Ann Vasc Surg* **24**, 487–497 (2010).

31. Smith, M., Pappy, R. & Hennebry, T. A. Re-entry Devices for Peripheral Chronic Occlusions. *Texas Heart Institute journal / from the Texas Heart Institute of St. Luke's Episcopal Hospital, Texas Children's Hospital* **38**, 392–7 (2011).

32. Szymański, R. et al. Successful recanalization of total chronic occlusion of the superficial femoral artery by antegrade subintimal angioplasty with stenting using the Pioneer Plus Re-Entry Catheter. *Postepy w Kardiologii Interwencyjnej* **7**, 91–94 (2011).

33. Hishikari, K. et al. Intravenous Intravascular Ultrasound Using the AcuNav Ultrasound Catheter for Guiding Recanalization of Aortoiliac Chronic Total Occlusions. *Journal of Endovascular Therapy* **22**, 269–271 (2015).

34. Takahashi et al. Successful trans-collateral approach for chronic total occlusion of the superficial femoral artery using a side-hole sheath. *J Am Coll Cardiol* **69**, S329–S331 (2017).

35. Marmagkiolis, K., Lendel, V., Leesar, M. A., Feldman, M. D. & Cilingiroglu, M. Use of optical coherence tomography during superficial femoral artery interventions. *Journal of Invasive Cardiology* **26**, 220–223 (2014).

36. Selmon, M. R. et al. Final results of the Chronic Total Occlusion Crossing with the Ocelot System II (CONNECT II) study. *J Endovasc Ther* **20**, 770–781 (2013).

37. Schaefers, J. F. et al. Outcome After Crossing Femoropopliteal Chronic Total Occlusions Based on Optical Coherence Tomography Guidance. *Vasc Endovascular Surg* **52**, 27–33 (2018).

38. Walters, D., Al Khiami, B., Mahmud, E. & Patel, M. Use of the Ocelot catheter in iliac chronic total occlusion intervention. *Cardiovascular Revascularization Medicine* **19**, 795–798 (2018).

39. Schwindt, A. G. et al. Lower Extremity Revascularization Using Optical Coherence Tomography-Guided Directional Atherectomy: Final Results of the EValuatIon of the PantheriS OptIcal COherence Tomography ImagiNg Atherectomy System for Use in the Peripheral Vasculature (VISION) St. *Journal of Endovascular Therapy* **24**, 355–366 (2017).

40. George, J. C., Varghese, V., J.C., G. & V., V. Utility of Image-Guided Atherectomy for Optimal Treatment of Ambiguous Lesions by Angiography. *Vascular Disease Management* **12**, 140–144 (2015).

41. Stavroulakis, K. et al. Optical coherence tomography guided directional atherectomy with antirestenotic therapy for femoropopliteal arterial disease. *J Cardiovasc Surg (Torino)* **60**, 191–197 (2019).

42. Kole, A. et al. Comparative Quantification of Arterial Lipid by Intravascular Photoacoustic-Ultrasound Imaging and Near-Infrared Spectroscopy-Intravascular Ultrasound. *J Cardiovasc Transl Res* **12**, 211–220 (2019).

43. Bismuth, J. et al. A first-in-man study of the role of flexible robotics in overcoming navigation challenges in the iliofemoral arteries. *J Vasc Surg* **57**, 14S-19S (2013).

44. Jansen, M. et al. Three Dimensional Visualisation of Endovascular Guidewires and Catheters Based on Laser Light instead of Fluoroscopy with Fiber Optic RealShape Technology: Preclinical Results. *European Journal of Vascular and Endovascular Surgery* **0**, (2020).

45. Panagiotopoulos, N. et al. Magnetic particle imaging : current developments and future directions. *Int J Nanomedicine* 3097–3114 (2015) doi:10.2147/IJN.S70488.

46. Sailer, A. M. et al. Fusion Guidance in Endovascular Peripheral Artery Interventions: A Feasibility Study. *Cardiovasc Intervent Radiol* **38**, 314–321 (2015).

47. Goudeketting, S. R. et al. The use of 3D image fusion for percutaneous transluminal angioplasty and stenting of

iliac artery obstructions: validation of the technique and systematic review of literature. *Journal of Cardiovascular surgery* **58**, (2017).

48. Stahlberg, E. *et al.* Fusion Imaging Reduces Radiation and Contrast Medium Exposure During Endovascular Revascularization of Iliac Steno-Occlusive Disease. *Cardiovasc Intervent Radiol* (2019) doi:10.1007/s00270-019-02250-5.

49. Ierardi, A. M. *et al.* Fusion of CT Angiography or MR Angiography with Unenhanced CBCT and Fluoroscopy Guidance in Endovascular Treatments of Aorto-Iliac Steno-Occlusion: Technical Note on a Preliminary Experience. *Cardiovasc Intervent Radiol* **39**, 111–116 (2016).

50. Shammas, N. W. *et al.* The role of precise imaging with intravascular ultrasound in coronary and peripheral interventions. *Vasc Health Risk Manag* **15**, 283–290 (2019).

51. Shammas, N. W., Torey, J. T., Shammas, W. J., Jones-Miller, S. & Shammas, G. A. Intravascular Ultrasound Assessment and Correlation With Angiographic Findings Demonstrating Femoropopliteal Arterial Dissections Post Atherectomy: Results From the iDissection Study. *J Invasive Cardiol* **30**, 240–244 (2018).

52. Kashyap, V. S. *et al.* Angiography underestimates peripheral atherosclerosis: Lumenography revisited. *Journal of Endovascular Therapy* **15**, 117–125 (2008).

53. Shammas, N. W. *et al.* The role of precise imaging with intravascular ultrasound in coronary and peripheral interventions. *Vasc Health Risk Manag* **15**, 283–290 (2019).

54. Panaich, S. S. *et al.* Intravascular Ultrasound in Lower Extremity Peripheral Vascular Interventions: Variation in Utilization and Impact on In-Hospital Outcomes From the Nationwide Inpatient Sample (2006-2011). *Journal of endovascular therapy* **23**, 65–75 (2016).

55. Krishnan, P. *et al.* Intravascular ultrasound guided directional atherectomy versus directional atherectomy guided by angiography for the treatment of femoropopliteal in-stent restenosis. *Ther Adv Cardiovasc Dis* **12**, 17–22 (2018).

56. Iida, O., Takahara, M., Soga, Y. & Suzuki, K. Efficacy of Intravascular Ultrasound in Femoropopliteal Stenting for Peripheral Artery Disease With TASC II Class A to C Lesions. *Journal of Endovascular Therapy* **21**, 485–492 (2014).

57. Araki, M. *et al.* Long-term outcome of the self-expanding stents for chronic total occlusion of the iliac artery. *EuroIntervention* **9**, 287 (2013).

58. Ye, W. *et al.* Early and late outcomes of percutaneous treatment of TransAtlantic Inter-Society Consensus class C and D aorto-iliac lesions. *J Vasc Surg* **53**, 1728–1737 (2011).

59. Nakamura, S., Rokutanda, T., Kurokawa, H. & Onoue, Y. Endovascular Treatment of Long Superficial Femoral Artery-Chronic Total Occlusions Using the Gogo Catheter With IVUS Via a Popliteal Puncture Method Is Effective, Safe, and Useful. *Vasc Endovascular Surg* **54**, 225–232 (2020).

60. Tsubakimoto, Y. *et al.* IVUS-Guided Wiring Improves the Clinical Outcomes of Angioplasty for Long Femoropopliteal CTO Compared with the Conventional Intraluminal Approach. *J Atheroscler Thromb* (2020) doi:https://doi.org/10.5551/jat.57166.

61. Ephrem, G., Garikipati, S. & Hanson, I. D. The fluoro-less and contrast-less peripheral endovascular intervention: Halfway there. *Cardiovascular Revascularization Medicine* **17**, 418–420 (2016).

62. Kusuyama, T., Iida, H. & Mitsui, H. Intravascular ultrasound complements the diagnostic capability of carbon dioxide digital subtraction angiography for patients with allergies to iodinated contrast medium. *Catheter Cardiovasc Interv* **80**, E82-6 (2012).

63. Higashimori, A. & Yokoi, Y. Stent implantation for chronic total occlusion in the iliac artery using intravascular ultrasound-guided carbon dioxide angiography without iodinated contrast medium. *Cardiovasc Interv Ther* **28**, 415–418 (2013).

64. Kawasaki, D. *et al.* Safety and efficacy of endovascular therapy with a simple homemade carbon dioxide delivery system in patients with ileofemoral artery diseases. *Circ J* **76**, 1722–1728 (2012).

65. Hishikari, K. *et al.* Intravenous Intravascular Ultrasound Using the AcuNav Ultrasound Catheter for Guiding Recanalization of Aortoiliac Chronic Total Occlusions. *Journal of Endovascular Therapy* **22**, 269–271 (2015).

66. Takahashi, Y. *et al.* Transvenous Intravascular Ultrasound-Guided Endovascular Treatment for Chronic Total Occlusion of the Infrainguinal Arteries. *Journal of Endovascular Therapy* **24**, 718–726 (2017).

67. Kawasaki, D. *et al.* Preprocedural Evaluation and Endovascular Treatment of Iliofemoral Artery Disease Without Contrast Media for Patients With Pre-Existing Renal Insufficiency. *Circulation Journal* **75**, 179–184 (2011).

68. Ephrem, G., Garikipati, S. & Hanson, I. D. The fluoro-less and contrast-less peripheral endovascular intervention: Halfway there. *Cardiovascular Revascularization Medicine* **17**, 418–420 (2016).

69. Baker, A. C. *et al.* Technical and early outcomes using ultrasound-guided reentry for chronic total occlusions. *Ann Vasc Surg* **29**, 55–62 (2015).

70. Smith, M., Pappy, R. & Hennebry, T. A. Re-entry Devices for Peripheral Chronic Occlusions. *Texas Heart Institute journal / from the Texas Heart Institute of St. Luke's Episcopal Hospital, Texas Children's Hospital* **38**, 392–7 (2011).

71. Eberhardt, K. M. *et al.* Prospective evaluation of optical coherence tomography in lower limb arteries compared with intravascular ultrasound. *J Vasc Interv Radiol* **24**, 1499–1508 (2013).

72. Secco, G. G. *et al.* Optical Coherence Tomography Guidance during Peripheral Vascular Intervention. *Cardiovasc Intervent Radiol* **38**, 768–772 (2015).

73. Kendrick, D. E. *et al.* Dextran or Saline Can Replace Contrast for Intravascular Optical Coherence Tomography in Lower Extremity Arteries. *Journal of Endovascular Therapy* **23**, 723–730 (2016).

74. Selmon, M. R. *et al.* Final results of the Chronic Total Occlusion Crossing with the Ocelot System II (CONNECT II) study. *J Endovasc Ther* **20**, 770–781 (2013).

75. Schaefers, J. F. *et al.* Outcome After Crossing Femoropopliteal Chronic Total Occlusions Based on Optical Coherence Tomography Guidance. *Vasc Endovascular Surg* **52**, 27–33 (2018).

76. Schwindt, A. G. *et al.* Lower Extremity Revascularization Using Optical Coherence Tomography-Guided Directional Atherectomy: Final Results of the EValuatIon of the PantheriS OptIcal COherence Tomography ImagiNg Atherectomy System for Use in the Peripheral Vasculature (VISION) St. *Journal of Endovascular Therapy* **24**, 355–366 (2017).

77. Stavroulakis, K. *et al.* Optical coherence tomography guided directional atherectomy with antirestenotic therapy for femoropopliteal arterial disease. *J Cardiovasc Surg (Torino)* **60**, 191–197 (2019).

78. Schwindt, A. G. *et al.* Lower Extremity Revascularization Using Optical Coherence Tomography-Guided Directional Atherectomy: Final Results of the EValuatIon of the PantheriS OptIcal COherence Tomography ImagiNg Atherectomy System for Use in the Peripheral Vasculature (VISION) St. *J Endovasc Ther* **24**, 355–366 (2017).

79. Gardner, C. M. *et al.* Detection of Lipid Core Coronary Plaques in Autopsy Specimens With a Novel Catheter-Based Near-Infrared Spectroscopy System. **1**, (2008).

80. Duran, C., Lumsden, A. B. & Bismuth, J. A randomized, controlled animal trial demonstrating the feasibility and safety of the Magellan endovascular robotic system. *Ann Vasc Surg* **28**, 470–478 (2014).

81. Bismuth, J., Kashef, E., Cheshire, N. & Lumsden, A. B. Feasibility and safety of remote endovascular catheter navigation in a porcine model. *Journal of Endovascular Therapy* **18**, 243–249 (2011).

82. Rafii-Tari, H. *et al.* Reducing contact forces in the arch and supra-aortic vessels using the Magellan robot. *J Vasc Surg* **64**, 1422–1432 (2016).

83. Riga, C. V. *et al.* Advanced catheter technology: Is this the answer to overcoming the long learning curve in complex endovascular procedures. *European Journal of Vascular and Endovascular Surgery* **42**, 531–538 (2011).

84. Bismuth, J. *et al.* A first-in-man study of the role of flexible robotics in overcoming navigation challenges in the iliofemoral arteries. *J Vasc Surg* **57**, 14S-19S (2013).

85. Krasznai, A. G. *et al.* Duplex-guided percutaneous transluminal angioplasty in iliac arterial occlusive disease. *European Journal of Vascular and Endovascular Surgery* **46**, 583–587 (2013).

86. Bolt, L. J. J. *et al.* Duplex-guided versus Conventional Percutaneous Transluminal Angioplasty of Iliac TASC II A and B Lesion: A Randomized Controlled Trial. *Ann Vasc Surg* **55**, 138–147 (2019).

87. Schwindt, A. G. *et al.* Lower Extremity Revascularization Using Optical Coherence Tomography-Guided Directional Atherectomy: Final Results of the EValuatIon of the PantheriS OptIcal COherence Tomography ImagiNg Atherectomy System for Use in the Peripheral Vasculature (VISION) St. *J Endovasc Ther* **24**, 355–366 (2017).

CHAPTER | 6

Target Vessel Displacement during Fenestrated and Branched Endovascular Aortic Repair and its Implications for the Role of Image Fusion Roadmaps

Based on:
Marloes M. Jansen, Merel van der Stelt, Stefan P.M. Smorenburg, Cornelis H. Slump, Joost A. van Herwaarden, Constantijn E.V.B. Hazenberg.

ABSTRACT

Objective
This retrospective study quantifies target vessel displacement during fenestrated and branched endovascular aneurysm repair due to the introduction of stiff guidewires and stent graft delivery systems. The effect that intraoperative vessel displacement has on the usability of computed tomography angiography (CTA) roadmaps is also addressed.

Methods
Patients that underwent fenestrated or branched EVAR were included in this retrospective study. Two imaging datasets were collected from each patient: (I) preoperative CTA and (II) intraoperative contrast-enhanced cone beam computed tomography (ceCBCT) acquired after the insertion of the stiff guidewire and stent graft delivery system. After image registration, the 3D coordinates of the ostium of the celiac artery, superior mesenteric artery, right renal artery and left renal artery were recorded in both the CTA and the ceCBCT dataset by two observers. The three-dimensional displacement of the ostia of the target vessels was calculated by subtracting the coordinates of CTA and ceCBCT from one another. Additionally, the tortuosity index and the maximum angulation of the aorta were calculated.

Results
In total 20 patients and 77 target vessels were included in this study. The ostium of the celiac, superior mesenteric, right renal and left renal artery underwent non-uniform three-dimensional displacement with mean absolute displacement of 8.2, 7.7, 8.2 and 6.2 mm, respectively. The average displacement of all different target vessels together was 7.8 mm. A moderate correlation between vessel displacement and the maximum angulation of the aortoiliac segment was found (Spearman's $\rho=0.45$, $P<0.05$).

Conclusion
The introduction of stiff endovascular devices during fenestrated or branched EVAR causes significant, non-uniform displacement of the ostium of the visceral and renal target vessels. Consequently, preoperative CTA roadmaps based on bone registration are suboptimal to guide target vessel catheterization during these procedures.

INTRODUCTION

Fenestrated and branched endovascular aneurysm repair (FEVAR and BEVAR) provide minimal invasive treatment to patients with complex juxta-renal and supra-renal aortic aneurysms.[1] The procedure involves a main stent graft body that contains fenestrations or branches which are connected to the visceral and renal arteries with bridging stents. This method ensures that the aneurysm sack is excluded from circulation, while the blood flow towards the vital organs is preserved.[2] Catheterization of these visceral and renal arteries, with a mean diameter of 6 – 8 mm,[3-5] can be challenging due to the size of the aneurysm, vessel tortuosity, stenosis of the vessel origin or misalignment of the main stent body. The technical complexity of target vessel catheterization can lead to high radiation exposure, high contrast volumes and long procedure times. Optimal visualization of the target vessels and their orientation in three-dimensional (3D) space plays a key role in the catheterization process.

Image fusion is one of the techniques that enables 3D visualization of the target vessels during FEVAR and BEVAR.[6] Image fusion allows its user to combine intraoperative fluoroscopy with patient-specific preoperative imaging, typically computed tomography angiography (CTA). The resulting image contains real-time visualisation of the endovascular devices (in 2D) in combination with a high-resolution projection of the arteries of interest (in 3D) which can be a powerful tool to improve image guidance. Throughout this paper, the term 'image fusion' will be used to refer to this imaging technique.

Image fusion relies on rigid image registration (i.e., alignment) of the preoperative CTA with the patient's on-table anatomy. This process requires an intraoperative cone beam computed tomography (CBCT) scan (3D/3D registration) or, two biplane fluoroscopy images (2D/3D registration). The main landmarks for alignment of the scans are the pelvis, vertebrae and arterial calcifications. After initial image registration, a status quo of the patient anatomy is assumed. In reality the use of endovascular devices, such as stiff guidewires and stent graft delivery systems, causes the arteries to stretch and elongate.[7] This geometrical deformation leads to a mismatch between actual position of target vessels and their representation on the roadmap.

This study assesses target vessel displacement due to the introduction of a stiff guidewire and stent graft delivery system during FEVAR and BEVAR procedures. The displacement of the four target vessels in relation to each other is assessed in closer detail. Additionally, anatomical factors were identified to predict the extent of vessel displacement prior to the procedure.

MATERIALS AND METHODS

Patient data

The study was conducted in accordance with the Declaration of Helsinki (as revised in 2013). The study was approved by the ethics board of the METC Utrecht (Protocol No.: 19-381/C) and individual consent for this retrospective analysis was waived. All patients that had undergone FEVAR or BEVAR within our institution between January 2015 and January 2017 were screened for this study, and their data was anonymized.

All patients had undergone preoperative CTA to assess suitability for endovascular intervention, and to design the custom-made fenestrated or branched stent graft. Additionally, all patients had received an intraprocedural contrast-enhanced CBCT (ceCBCT) as part of our institution's standard protocol for complex endovascular treatment of juxta- and suprarenal aneurysms. We excluded patients with preoperative CTA scans that deviated from our own in-house protocol for visualization of the abdominal aorta, since we wanted to assure homogenous image quality. Patients with pre-existing aortic or thoracic stent graft were also excluded from the study, as the presence of a rigid stent graft could influence vessel deformation.

Imaging

CTA scans

The preoperative CTA scan of the patient was acquired 1–7 months prior to the FEVAR or BEVAR procedure, with a Philips Brilliance ICT 256 Slice Scanner (Philips, Best, the Netherlands). To minimize motion artefacts, the scans were acquired with ECG-triggering and breath-hold after inhalation. The scan parameters were: tube voltage, 100–120 kV; mAs, 183–189; reconstructed voxel size, ≤0.98 mm × 0.98 mm × 1 mm (range, 0.45 mm × 0.45 mm × 1 mm–0.98 mm × 0.98 mm × 1 mm). Intravenous contrast was injected with a solution of 80 cc (patient weight <70 kg) or 100 cc (patient weight >70 kg) of contrast fluid (Ultravist-300 mg/mL, Bayer AG, Leverkusen, Germany) and 40 cc saline at an injection rate of 5 cc/s. Scan delay was based on prior bolus triggering with a threshold level of 125 HU at the level of the renal arteries.

Ce-CBCT scan

The ceCBCT scan was performed during an endovascular procedure performed in a hybrid operating room with Philips Allura FD-20 fixed fluoroscopy system (Philips, Best, the Netherlands). All patients were treated under general anaesthesia, laying in a supine position with their left arm abducted at an angle of approximately 90°. Both femoral arteries and, when necessary the left brachial artery, were surgically exposed to obtain vascular access. A pigtail catheter was positioned above the level of the celiac artery through one femoral artery, and the fenestrated or branched stent-graft (custom-made Zenith® stent graft, Cook Medical, Bloomington, IN, USA) was advanced over a

0.035" stiff guidewire (Backup Meier, Marlborough, MA, USA) from the contralateral femoral artery. The Backup Meier is one of the 'stiffer' stiff guidewires with a flexural modulus of 139.6 GPA.[8] Prior to stent graft deployment, the ceCBCT was acquired. To minimize motion artefacts, a respiratory arrest was induced during the scan at positive end-expiratory pressure (PEEP) of 5 cmH2O. Contrast injection comprised of a patient-specific volume of contrast fluid (Ultravist-300 mg/mL) depending on the patient's BMI, kidney function and aortic lumen (range, 35–50 cc). The contrast agent was diluted with saline to a total of volume of 100 cc and injected with an injection rate of 8 cc/s. A scan delay of 2 seconds was set to ensure vessel enhancement of the arteries of interest during the complete rotation. Acquisition parameters include: tube voltage; 120 kVp, rotation; 180°, images; scan time; 10.2 s. Image reconstruction was performed using metal artefact reduction to reduce metal streak artefacts caused by the stent graft and its markers. Resolution was 384 mm × 297 mm × 384 mm with 1 mm × 1 mm × 1 mm voxel size.

Analysis of vessel displacement

Image registration

Image registration of the CTA with the ceCBCT was based on the bone landmarks of the vertebrae in the open-source programme ITK-SNAP 3.6.0[9] as shown in *Figure 1*.

First, the ceCBCT dataset was scaled to match the spatial resolution of the CTA dataset, using an automated function of the software, after which rigid transformation (rotation and translation) was used to align the ceCBCT dataset with the CTA dataset. Correct registration of the bone landmarks is a crucial requirement for the measurement in this study. Whenever image registration failed (inability to align all vertebrae correctly) the patients were excluded from the study.
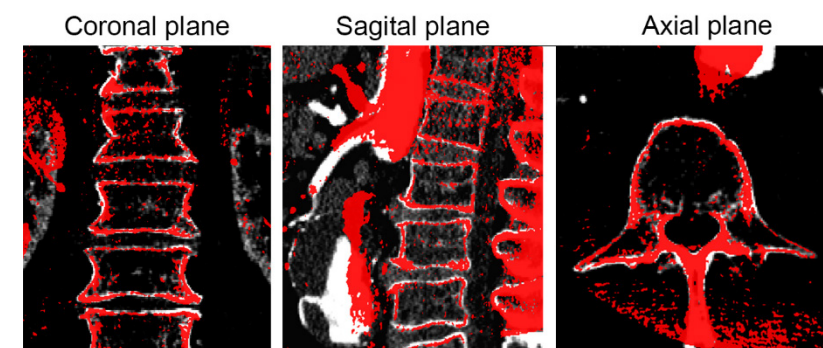
Figure 1: Image registration based on the bony structures of the vertebrae. The vertebrae of both imaging datasets were aligned using automatic scaling and manual translation and rotation. The computed tomography angiography (CTA) dataset is displayed in black-and-white, and the contrast-enhanced cone beam computed tomography (ce-CBCT) dataset is superimposed in red including the outline of the (undeployed) stent graft. Coronal, sagittal and axial reconstructions were used to confirm successful alignment of both imaging datasets, as seen here.

Landmarking of the ostium of the target vessels

The ostium of the celiac artery (CA), superior mesenteric artery (SMA), left renal artery (LRA) and right renal artery (RRA) were landmarked in both the CTA dataset and the ceCBCT dataset. Landmarking was performed by two researchers: one vascular surgeon who performed >250 FEVAR and BEVAR procedures and one experienced researcher involved in clinical imaging during >100 FEVAR and BEVAR procedures. The landmarks were placed in the caudal edge of the ostium of the vessel, as this edge could be distinguished consistently. This landmark was placed by first selecting the centre of the ostium of the target vessel in an axial reconstruction plane, followed by selection of the distal edge of the ostium of the vessel in the sagittal (for CA and SMA) or coronal reconstruction plane (for RRA and LRA) as shown in *Figure 2*. All measurements were performed using an enlarged zoom of 5px/mm to keep measurements consistent. Each of these landmarks was recorded as a 3D coordinate. Inter observer variability was checked using the inter class correlation of both observers.
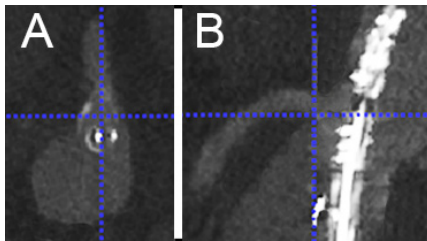
Figure 2: *Placement of the landmark in the ostium of the superior mesenteric artery (SMA) in a contrast-enhanced cone beam computed tomography (ce-CBCT scan).* **Figure 2A:** *selecting the center of the ostium of the vessel in the axial reconstruction plane.* **Figure 2B:** *selecting the distal edge of the ostium in the sagittal reconstruction plane. The undeployed stent graft is visible in both imaging planes.*

Calculation of the displacement of the ostium of the target vessels: The displacement of the ostium of the target vessels was determined by calculating the difference between the two coordinates of the CTA dataset and the ceCBCT dataset. The displacement was calculated in the x-, y- and z- direction, as according to Eq. [1]. The x-, y- and z-coordinates were defined as: x-coordinate; left to right, y-coordinate; anterior to posterior, z-coordinate; caudal to cranial.

$$\begin{bmatrix} x_d \\ y_d \\ z_d \end{bmatrix} = \begin{bmatrix} x_{CTA} \\ y_{CTA} \\ z_{CTA} \end{bmatrix} - \begin{bmatrix} x_{CBCT} \\ y_{CBCT} \\ z_{CBCT} \end{bmatrix} \qquad\qquad Eq.\ 1$$

Subsequently, the 3D displacement was calculated as the Euclidean distance between the two coordinates using the law of Pythagoras, as according to *Eq. 2*.

$$d = \sqrt{x_d{}^2 + y_d{}^2 + z_d{}^2} \qquad\qquad Eq.\ 2$$

Calculation of the uniformity of target vessel displacement in a patient

To assess the uniformity of the displacement of the renal and visceral target vessels, we calculated the intraclass correlation of the four target vessels in terms of displacement in x-, y- and z-axis.

The effect of aortic geometry on vessel displacement

Secondary aim of this study was to assess the influence of aortic geometry on the extent of vessel displacement. The tortuosity index and the maximum tortuosity angle were chosen for this purpose, as both required minimum measurement time during preoperative work-up.

Maximum tortuosity angle

The maximum tortuosity angle of aorto-iliac segment was measured using a 3D adaption of the technique described by van Keulen et al.[10], available in the 3Mensio workstation (3Mensio Medical Imaging, Bilthoven, the Netherlands). This function measures the angulation between two line-elements of 15 mm along the central lumen line (Figure 3A). The highest angulation in the aortoiliac segment (from left subclavian artery until the origin of the common femoral artery) was recorded as maximum tortuosity angle.
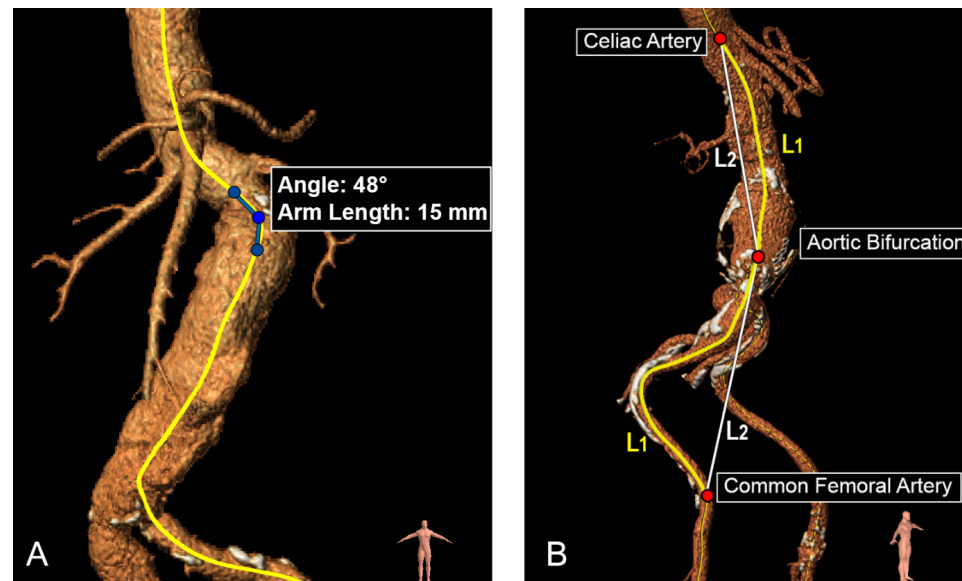
Tortuosity index

The tortuosity indices of the aortic and iliac segment were calculated using a function available in the 3Mensio workstation. The aortic segment ranged from the left subclavian artery until the aortic bifurcation. The iliac segment ranged from the aortic bifurcation until the origin of the common femoral artery and was measured unilaterally on the side of stent graft introduction. The tortuosity index was calculated by dividing the distance along the central lumen line (L1) of the arterial segment, by the straight-line distance between the start and endpoint of the segment (L2).[11,12] These measurements are shown in *Figure 3B*.

Statistical analysis

The data was analysed using R version 3.1.3, using the packages: ggplot, tableGrob, gtable, data.table, qqnorm, xlsx, multcomp, psych.[13] Inter observer agreement was tested using the intraclass correlation (ICC), with 95% confidence interval, using a 2-way mixed effect model with absolute agreement and single measurements. Values of <0.5, between 0.5 and 0.75, between 0.75 and 0.9 and >0.9 are indicative of poor, moderate, good and excellent reliability (14). Intraclass correlation of the target vessel displacement of the four vessels on the x-, y-, z- axis were also performed using ICC calculation. In which values of <0.5,

between 0.5 and 0.75, between 0.75 and 0.9 and >0.9 were indicative of poor, moderate, good and excellent correlation of the movement of all four vessels.[14] Vessel displacement, tortuosity indices and maximum tortuosity angles were represented as median with range. Missing data was handled by case deletion. Correlations between the target vessel displacement and (I) the tortuosity index or (II) the maximum tortuosity angle were tested using the nonparametric Spearman's correlation test. To meet the assumption of observation independence, the independent variable comprised of the mean displacement of all four target vessels. All tests were powered to find moderate to strong linear associations only (effect size >0.31) with a power of ≥0.8 and a confidence level of 0.95.

Figure 3: Calculation of tortuosity index and maximum tortuosity angle. Figure 3A) Calculation of the maximum tortuosity angle. The tortuosity angle was measured along the central lumen line (in yellow) using two 15 mm long line segments (in blue). The highest angulation in the aortoiliac segment was reported as the maximum tortuosity angle. Figure 3B) Calculation of the tortuosity index of the aortic and the iliac segment. The tortuosity index of the aortic segment and the iliac segment were calculated by dividing the distance along the central lumen line of the segment (L1: yellow line), by the straight-line distance between the start- and endpoint of the segment (L2: white line).

RESULTS

Patients

Imaging data of 74 patients were screened for eligibility, of which 43 patients were excluded due to inappropriate CTA resolution and image quality. After CTA examination

another 9 patients were excluded due to pre-existing stent grafts. The remaining 22 patients were confirmed eligible for this study. Two patients were excluded during the study because of unsuccessful image registration of the vertebrae. No identifiable reason for failure of image registration could be identified, apart from differences in patient positioning. Additionally, 3 target vessels were excluded due to occlusions of the vessel origin that made it impossible to identify the distal edge of the ostia. A total of 77 target vessels from 20 patients remained available for analysis, consisting of 18 CAs, 20 SMAs, 20 RRAs, and 19 LRAs. Procedural characteristics are represented in *Table I*.

Analysis of vessel displacement

The measured displacement between preoperative CTA and intraoperative ceCBCT of the ostia of the CA, SMA, RRA and LRA are provided in *Table II*. Inter observer agreement was good with an ICC of 0.89 (0.84–0.92). The median 3D displacement of the CA, SMA, RRA and LRA were 8.2, 7.7, 8.2 and 6.2 mm, respectively. An example of the intraoperative displacement of the arteries is visualized in *Figure 4*.

The displacement of the four target vessels showed a poor correlation to each other, meaning that the vessels all moved in different directions and to different extents. The intraclass correlation was 0.37 (0.18–0.58), 0.16 (0.00–0.38) and 0.56 (0.38–0.74) in terms of x-, y- and z-axis displacement, respectively. This non-uniformity of the target vessel movement is further visualized in *Figure 5*.

Table I: Procedural characteristics.

Characteristics	Number of patients (%)
Stent graft configuration:	
- 3 branches with scallop	2 (10%)
- 3 fenestrations with scallop	9 (45%)
- 4 branches	2 (10%)
- 4 fenestrations	4 (20%)
- 3 fenestrations and 1 branch	2 (10%)
- 2 fenestrations and 2 branches	1 (5%)
Side of stent graft introduction	
- Right	17 (85%)

Table 2: Overview of target vessel displacement.

Target Vessel	Right - Left (x-axis)	Anterior - Posterior (y-axis)	Cranio - Caudal (z-axis)	Total 3D vector
Celiac trunk	5.2 mm (range: 0 – 17.6)	3.9 mm (range: 0 – 8.5)	3.0 mm (range: 0 – 13.0)	8.2 mm (range: 3.1 – 19.6)
Superior mesenteric artery	4.3 mm (range: 0 – 13.7)	3.2 mm (range: 0 – 7.1)	3.0 mm (range: 0 – 9.0)	7.8 mm (range: 2.3 – 14.1)
Right renal artery	4.5 mm (range: 0 – 9.9)	3.1 mm (range: 0 – 6.7)	4.0 mm (range: 1.0 – 11.0)	8.2 mm (range: 1.8 – 13.6)
Left renal artery	2.9 mm (range: 0 – 13.7)	2.4 mm (range: 0 – 10.7)	3.5 mm (range: 0 – 14.0)	6.2 mm (range: 2.1 – 17.6)
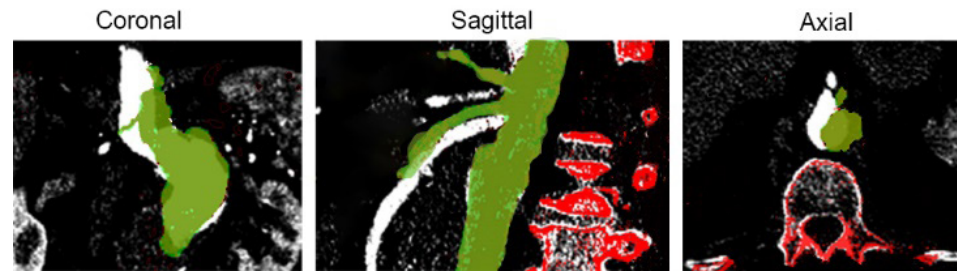
Figure 4: Target vessel displacement visualized by over-projection of the intraoperative contrast-enhanced cone beam computed tomography (ce-CBCT) on top of preoperative computed tomography angiography (CTA). The CTA scan is displayed in black-and-white and the ce-CBCT is superimposed in green (arteries) and red (vertebrae and bone markers). Axial, sagittal and coronal views show the intraoperative displacement of the ostia of the target vessels.
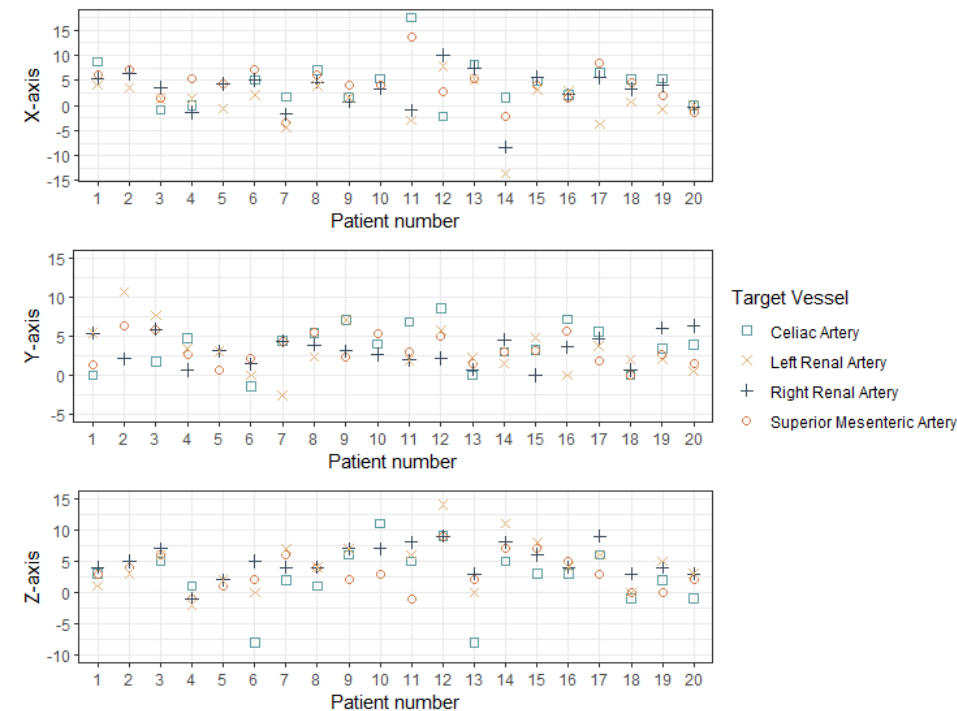
Figure 5: Non-uniform target vessel displacement. Target vessel displacement visualized in the x-, y- and z-axis of all twenty patients. Notice that the four target vessels in a single patient do not move as a single unit in all three axes. Instead, the displacement varies strongly amongst the different target vessels, indicating non-uniform displacement of the renal and visceral arteries. This implies that a single realignment of the roadmap to adjust for all intraoperative vascular deformation will not suffice, and that the roadmap will need to be realigned for each individual target vessel. For clarity, this scatter plot was limited to the first five patients of this study.

The effect of aortic geometry on vessel displacement

Maximum tortuosity angle

The median maximum tortuosity angle of the aortoiliac segment was 58° (range, 31°–84°). A moderate monotonic relationship (Spearman's ρ=0.45, P<0.05) was found between the extend of vessel displacement and the maximum tortuosity angle of the aortoiliac segment. The scatterplot is provided in *Figure 6*.

Tortuosity index

The median tortuosity index of the aortic and iliac segment were 1.24 (range, 1.08–1.37) and 1.37 (range, 1.11–1.62) respectively. Based on this study, there was no significant correlation between the extend of target vessel displacement and the tortuosity index of the aortic segment (P=0.93), nor the iliac segment (P=0.15).
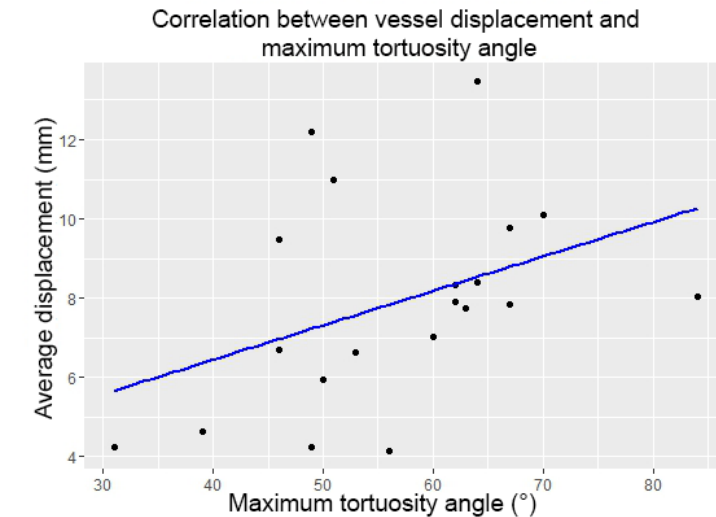
Figure 6: Association between vessel displacement and maximum tortuosity angle of the aortoiliac segment. Scatter plot of the mean vessel displacement per patient plotted against the maximum tortuosity angle of the aortoiliac segment.

DISCUSSION

This study demonstrates that the insertion of a stiff guidewire and stent graft delivery system during FEVAR or BEVAR causes significant displacement of the ostia of the visceral and renal target vessels. Selective realignment of the roadmap using an angiogram can help reduce the initial mismatch, but due to the poor correlation of the displacement across the four target vessels, the individual vessels will move differently which makes it

impossible to align all target vessels at once.

Image fusion guidance is a topic of broad interest in endovascular surgery, and its feasibility has been evaluated in a variety of procedures. Two meta-analyses have shown that the use of image fusion results in a significant reduction in radiation dose[15] and contrast material[16] during FEVAR and BEVAR procedures. However, both meta-analyses report high heterogeneity in procedural outcomes, both amongst the included studies and within these studies themselves. We postulate that the variation within the studies themselves could be related to the strong diversity in roadmap accuracy. An accurate image fusion roadmap provides guidance during target vessel catheterization and thereby reduces contrast, radiation dose and procedure time, but these procedural effects degrade quickly when the roadmap needs to be realigned repeatedly using angiography. In turn, the roadmap accuracy is affected by the extent of intraoperative vessel displacement, which differs strongly per patient: in this study, the displacement of the target vessel ostia ranged from 1.8 to 19.6 mm. Prediction of the extent of intraoperative vessel displacement prior to the procedure, could aid patient selection for the use of image fusion. According to our findings, the maximum tortuosity angle seems to be related to the extent of target vessel displacement. However, we were unable to establish a clear cut-off point, thus making the predictive value of this measure limited.

Surgeons could consider alternative imaging methods to guide target vessel catheterization during FEVAR and BEVAR. The alternative we use in our institution, is a roadmap based on a segmented ceCBCT rather than the conventional roadmaps based on pre-operative CTA, to guide target vessel catheterization in FEVAR and BEVAR. In fact, all patients in this study were treated using the ceCBCT roadmap, rather than an actual CTA-roadmap. When acquired after the insertion of the stent graft delivery system, the ceCBCT takes into account the majority of the intraoperative deformation of the arteries. As a result, the ceCBCT roadmap accurately visualizes 1) the 3D position of all four ostia of the visceral and renal target vessels and 2) the run-off of these target vessels and their branches to allow stable placement of the guidewire in the distal artery. In our experience (>150 procedures), these ceCBCT roadmaps seem to be more accurate than conventional CTA roadmaps. The main drawbacks of ceCBCT roadmaps are their limited field of view, the need for an additional injection of 35–50 cc contrast, and the need for intraoperative segmentation of the arteries of interest to prevent over-projection of bone and soft tissue on the roadmap. An example protocol for acquisition of ceCBCT is provided by Törnqvist et al.[17]

Another fast-developing strategy to resolve the mismatch between the real-time anatomy and the image fusion roadmap, is the use of deformable (dynamic) image fusion applications.[18–21] These applications generate a deformable model of the vascular geometry, in which the distance between certain subsections can be modified or stretched to allow dynamic corrections to match with the real-time anatomy. These modifications can be initiated manually, or with computerized algorithms that detect and

predict the interactions between stiff guidewires and vessel structures based on finite-element simulations of the interaction between stiff guidewires and vessel structures.[18–21] Validation studies of these technologies with preclinical data seems promising, but clinical prospective studies are not yet available.

Several studies have previously assessed vessel displacement due to the insertion of stiff endovascular devices using 2D angiography, but these measurements hold limited validity in the three dimensional domain.[7,22,23] To date, only one other study reported vessel displacement in 3D. This study by Maurel et al.[24], used similar methods to assess the 3D vessel displacement of the SMA, RRA and LRA during EVAR (n=13) and FEVAR (n=7) resulting in a median vessel displacement of 6.7, 6.2 and 6.4 mm for the SMA, RRA and LRA, respectively. In the current study, slightly higher target vessel displacements of these target vessels were observed, which may be caused by the more proximal position of the stiff delivery system in the aorta (near the target vessels) during FEVAR and BEVAR when compared to EVAR procedures.

The present study is in accordance with the work undertaken by Kauffmann et al.[7] who previously reported non-uniformity displacement of the left and right renal artery during EVAR. A persisting mismatch of one renal artery remained visible on the image fusion roadmap after previously having aligned the contralateral renal artery.

The present study has some limitations. Firstly, the introduction of stiff endovascular devices influences the geometry of the complete vascular tree. In this study, however, we limited our analysis to the displacement of structures that are of critical importance during target vessel catheterization in FEVAR and BEVAR; the ostia of the CA, SMA, RRA and LRA.

Secondly, this study measures the displacement of the vessel ostia immediately after bone-based image registration. In clinical practice, most centres would perform additional adjustments based on a selective angiogram or arterial calcifications, prior to utilization of the roadmap. These adjustments are likely to reduce the overall mismatch between the image fusion roadmap and the on-table anatomy. As we aim for a robust and reproducible initial registration, we chose not to include arterial calcifications as registration markers in this study. Registration based on combination of bone markers and calcifications requires compromise and thus may have more than one possible solution. Besides, as the ostia of the different target vessels each move in different directions, realignment based on repeated angiography might be needed when alternating between target vessels. Relying on these (selective) angiograms can be disadvantageous in the unfortunate case that a main stent graft blocks the flow to one of the target vessels after deployment. In which case it is left up to estimated guessing to find the target vessel and reposition the main stent graft.

Thirdly, none of the patients in this study actually received treatment based on guidance of a CTA-roadmap, as our institution uses a different approach using an intraoperative ceCBCT a roadmap. The routine acquisition of these intraoperative

ceCBCT scans, formed the basis of this unique dataset, in which the position of target vessels after the insertion of the main stent graft could be selected. In combination with a preoperative CTA this forms the opportunity to measure the intraoperative displacement between the preoperative setting and the intraoperative setting. While this study shows implications for the use of preoperative CTA roadmaps, it is important to note that the procedures themselves involved a different navigation strategy using only this intraoperative ceCBCT as a roadmap. We were therefore unable to report the effect of roadmap accuracy on procedural outcomes.

Lastly, although the rigid 3D/3D registration of the spine was excellent in 20 patients, alignment of the bones does not guarantee alignment of the soft tissues. Differences in respiratory phase and patient position could result in displacement of the aorta and its side branches. Pathologic disease progression between the time of CTA acquisition and intervention may also alter the vascular anatomy. Note, that during clinical use of image fusion roadmaps, these same issues would occur during image registration. In fact, discrepancies in respiratory phase are technically unavoidable when performing image fusion roadmaps in procedures performed under general anaesthesia. Preoperative CTAs/MRAs are generally acquired during self-controlled breath-hold (negative pressure ventilation), whilst intraoperative images are frequently acquired using a respiratory arrest of the mechanical ventilation (positive pressure ventilation) at positive end-expiratory pressure (PEEP). The breathing mechanisms of positive and negative pressure ventilation are different and therefore their respiratory phases are non-comparable.

According to Sailer et al.[25] the respiration induced displacement of the visceral and renal target vessels during a normal, self-controlled breathing cycle is on average 1.4 mm, oriented in exclusively the cranio-caudal direction (z-axis). Thus, while our study outcomes may have been affected by respiratory movements, but the contribution will be small and only oriented in the cranio-caudal direction.

CONCLUSION

The introduction of stiff endovascular devices during FEVAR and BEVAR causes significant displacement of the ostia of the CA, SMA, RRA and LRA. The displacement of the individual target vessels within a patient show a poor correlation to each other. Consequently, the use of preoperative CTA roadmaps will require repeated realignment when alternating between target vessels or projection angles and therefore provide suboptimal guidance for target vessel catheterization during FEVAR and BEVAR procedures.

REFERENCES

1   Anderson JL, Adam DJ, Berce M, Hartley DE. Repair of thoracoabdominal aortic aneurysms with fenestrated and branched endovascular stent grafts. *J Vasc Surg* 2005;**42**(4):600–7. Doi: 10.1016/j.jvs.2005.05.063.

2   Verhoeven ELG, Katsargyris A, Fernandes E Fernandes R, Bracale UM, Houthoofd S, Maleux G. Practical points of attention beyond instructions for use with the Zenith fenestrated stent graft. *J Vasc Surg* 2014;**60**(1):246–52. Doi: 10.1016/j.jvs.2014.01.065.

3   Mohiuddin M, Mansoor A, Ali M, Hassan N. Analysis of renal artery morphometry in adults: A study conducted by using multidetector computed tomography angiography. *Pakistan J Med Sci* 2017;**33**(4):943–7. Doi: 10.12669/pjms.334.13063.

4   Majos M, Stefańczyk L, Szemraj-Rogucka Z, Elgalal M, De Caro R, Macchi V, et al. Does the type of renal artery anatomic variant determine the diameter of the main vessel supplying a kidney? A study based on CT data with a particular focus on the presence of multiple renal arteries. *Surg Radiol Anat* 2018;**40**(4):381–8. Doi: 10.1007/s00276-017-1930-z.

5   Pinal-Garcia DF, Nuno-Guzman CM, Gonzalez-Gonzalez ME, Ibarra-Hurtado TR. The Celiac Trunk and Its Anatomical Variations: A Cadaveric Study. *J Clin Med Res* 2018;**10**(4):321–9. Doi: 10.14740/jocmr3356w.

6   Jones DW, Stangenberg L, Swerdlow NJ, Alef M, Lo R, Shuja F, et al. Selected Technique Image Fusion and 3-Dimensional Roadmapping in Endovascular Surgery. *Ann Vasc Surg* 2018;**52**(May):302–11. Doi: 10.1016/j.avsg.2018.03.032.

7   Kauffmann C, Douane F, Therasse E, Lessard S, Elkouri S, Gilbert P, et al. Source of errors and accuracy of a two-dimensional/three-dimensional fusion road map for endovascular aneurysm repair of abdominal aortic aneurysm. *J Vasc Interv Radiol* 2015;**26**(4):544–51. Doi: 10.1016/j.jvir.2014.12.019.

8   Harrison GJ, How T V., Vallabhaneni SR, Brennan JA, Fisher RK, Naik JB, et al. Guidewire stiffness: What's in a name? *J Endovasc Ther* 2011;**18**(6):797–801. Doi: 10.1583/11-3592.1.

9   Paul A. Yushkevich, Joseph Piven, Heather Cody Hazlett, Rachel Gimpel Smith, Sean Ho, James C. Gee and GG. ITK-snap 3.6.0 2006.

10 van Keulen JW, Moll FL, Tolenaar JL, Verhagen HJM, van Herwaarden JA. Validation of a new standardized method to measure proximal aneurysm neck angulation. *J Vasc Surg* 2010;**51**(4):821–8. Doi: 10.1016/j.jvs.2009.10.114.

11 Chaikof EL, Fillinger MF, Matsumura JS, Rutherford RB, White GH, Blankensteijn JD, et al. Identifying and grading factors that modify the outcome of endovascular aortic aneurysm repair. *J Vasc Surg* 2002;**35**(5):1061–6. Doi: 10.1067/mva.2002.123991.

12 Chaikof EL, Blankensteijn JD, Harris PL, White GH, Zarins CK, Bernhard VM, et al. Reporting standards for endovascular aortic aneurysm repair. *J Vasc Surg* 2002;**35**(5):1048–60. Doi: 10.1067/mva.2002.123763.

13 R Core Team. R: A language and environment for statistical computing 2014. Available from: http://www.r-project.org/

14 Koo TK, Li MY. A Guideline of Selecting and Reporting Intraclass Correlation Coefficients for Reliability Research. *J Chiropr Med* 2016;**15**(2):155–63. Doi: 10.1016/j.jcm.2016.02.012.

15 Ruiter QMB De, Reitsma JB, Moll FL, Herwaarden JA Van. Meta-analysis of Cumulative Radiation Duration and Dose During EVAR Using Mobile, Fixed, or Fixed/3D Fusion C-Arms. *J Endovasc Ther* 2016;**23**(6):944–56. Doi: 10.1177/1526602816668305.

16 Goudeketting SR, Heinen SGH, Ünlü Ç, van den Heuvel DAF, de Vries J-PPM, van Strijen MJ, et al. Pros and Cons of 3D Image Fusion in Endovascular Aortic Repair: A Systematic Review and Meta-analysis. *J Endovasc Ther* 2017;**24**(4):595–603. Doi: 10.1177/1526602817708196.

17 Törnqvist P, Dias N, Sonesson B, Kristmundsson T, Resch T. Intra-operative cone beam computed tomography can help avoid reinterventions and reduce CT follow up after infrarenal EVAR. *Eur J Vasc Endovasc Surg* 2015;**49**(4):390–5. Doi: 10.1016/j.ejvs.2015.01.009.

18 Gindre J, Bel-Brunon A, Rochette M, Lucas A, Kaladji A, Haigron P, et al. Patient-Specific Finite-Element Simulation of the Insertion of Guidewire During an EVAR Procedure: Guidewire Position Prediction Validation on 28 Cases. *IEEE Trans Biomed Eng* 2017;**64**(5):1057–66. Doi: 10.1109/TBME.2016.2587362

19 Kaladji A, Dumenil A, Castro M, Cardon A, Becquemin JP, Bou-Saïd B, et al. Prediction of deformations during endovascular aortic aneurysm repair using finite element simulation. *Comput Med Imaging Graph* 2013;**37**(2):142–9. Doi: 10.1016/j.compmedimag.2013.03.002.

20 Roy D, Holzapfel GA, Kauffmann C, Soulez G. Finite element analysis of abdominal aortic aneurysms: Geometrical and structural reconstruction with application of an anisotropic material model. *IMA J Appl Math (Institute Math Its Appl* 2014;**79**(5):1011–26. Doi: 10.1093/imamat/hxu037.

21 Mouktadiri G, Bou-Saïd B, Walter-Le-Berre H. Aortic endovascular repair modeling using the finite element

method. *J Biomed Sci Eng* 2013;**06**(09):917–27. Doi: 10.4236/jbise.2013.69112.

22   Fukuda T, Matsuda H, Doi S, Sugiyama M, Morita Y, Yamada M, et al. Evaluation of Automated 2D-3D Image Overlay System Utilizing Subtraction of Bone Marrow Image for EVAR: Feasibility Study. *Eur J Vasc Endovasc Surg* 2013;**46**(1):75–81. Doi: 10.1016/j.ejvs.2013.04.011.

23   Ahmad W, Obeidi Y, Majd P, Brunkwall JS. The 2D-3D Registration Method in Image Fusion Is Accurate and Helps to Reduce the Used Contrast Medium , Radiation , and Procedural Time in Standard EVAR Procedures. *Ann Vasc Surg* 2018;**51**(March):177–86. Doi: 10.1016/j.avsg.2018.01.098.

24   Maurel B, Hertault A, Gonzalez TM, Sobocinski J, Roux M Le, Delaplace J. Evaluation of Visceral Artery Displacement by Endograft Delivery System Insertion. *J Endovasc Ther* 2014;(21):339–47. Doi: 10.1583/13-4471MR.1.

25   Sailer AM, Wagemans BAJM, Das M, de Haan MW, Nelemans PJ, Wildberger JE, et al. Quantification of Respiratory Movement of the Aorta and Side Branches. *J Endovasc Ther* 2015;**22**(6):905–11. Doi: 10.1177/1526602815605325.

6

6

CHAPTER | 7

Three–Dimensional Visualization of Endovascular Devices based on Laser Light instead of Fluoroscopy with Fiber Optic RealShape (FORS) Technology: Preclinical Results

ABSTRACT

Objective
Fiber Optic RealShape (FORS) is a new technology platform that enables real time three-dimensional (3D) visualisation of endovascular guidewires and catheters, based on the concepts of fibre optic technology instead of fluoroscopy. Anatomical context is provided by means of co-registered prior anatomical imaging, such as digital subtraction angiography or computed tomography. This preclinical study assesses the safety and feasibility of FORS technology.

Methods
Six physicians performed endovascular tasks in a phantom model and a porcine model using FORS enabled floppy guidewires, Cobra-2 catheters and Berenstein catheters. Each physician performed a set of predefined tasks in both models, including setup of the FORS system, device registration, and 12 aortic and peripheral target vessel cannulation tasks. The evaluation of the FORS system was based on (i) target vessel cannulation success; (ii) safety assessment; (iii) the accuracy of the FORS based device visualisation; and (iv) user experience.

Results
Successful cannulation was achieved in 72 of the 72 tasks (100%) in the phantom model and in 70 of the 72 tasks (97%) in the porcine model. No safety issues were reported. The FORS based device visualisation had a median offset at the tip of 2.2 mm (interquartile range 1.2-3.8 mm). The users judged the FORS based device visualisation to be superior to conventional fluoroscopic imaging, while not affecting the mechanical properties (torquability, pushability) of the FORS enabled guidewire and catheters.

Conclusion
The combined outcomes of high cannulation success, positive user experience, adequate accuracy, and absence of safety issues demonstrate the safety and feasibility of the FORS system in a preclinical environment. FORS technology has great potential to improve device visualisation in endovascular interventions.

INTRODUCTION

In the last decade, the treatment strategy of vascular pathology has shifted from an open surgical to an endovascular approach. The growing popularity of the endovascular approach has led to new endovascular treatment options, which are often complex in nature. An increase in procedure complexity is especially visible in endovascular aortic repair and endovascular treatment of stenotic lesions in lower limbs.[1,2] The treatment of these more complex patients leads to longer procedures, with high contrast volumes and high radiation exposure for both patients and medical staff.[3]

Fluoroscopy is the standard imaging and navigation guiding technique in endovascular surgery. Despite its long-lasting and widespread use, fluoroscopy has several disadvantages. Extensive exposure to fluoroscopy can lead to long-term health effects and DNA damage[4]. Current radiation guidelines aim to decrease unnecessary radiation exposure for patients and medical staff wherever possible.[4,5] These guidelines are especially relevant for physicians who perform endovascular procedures on a day-to-day basis and thereby accumulate a significant amount of radiation during their careers.

Another disadvantage of fluoroscopy is its two-dimensional (2D) character. Fluoroscopy converts three-dimensional (3D) structures into 2D projections and thereby depletes the perception of depth and tortuosity from the images. This lack of volumetric information makes navigation of endovascular devices more difficult, thereby increasing the risk of procedural failure.

In the last decade, several interventional imaging tools have been designed to address these limitations.[6–9] These imaging tools combine (i.e. coregister) real-time 2D fluoroscopy with static 3D anatomical images, such as computed tomography angiography (CTA) or magnetic resonance angiography (MRA). The resulting image provides real-time visualization of the in-body devices (in 2D) superimposed onto the surrounding vascular anatomy (in 3D). The use of these imaging tools has been shown to decrease radiation dose[6,7], contrast volume[6–9], and procedure time[7,8] of several endovascular interventions. However, it should be noted that while these imaging tools improve anatomical guidance, they do not improve the visualization of the endovascular devices themselves.

In this study, we evaluated a new guidance platform that combines these existing imaging tools with a brand-new technology that allows visualization of endovascular devices in 3D in real-time. The visualization of these specially designed guidewires and catheters relies on a new-to-the-world technology in the medical field: Fiber Optic RealShape (FORS). This study evaluated the performance and safety of FORS-technology in a preclinical environment.
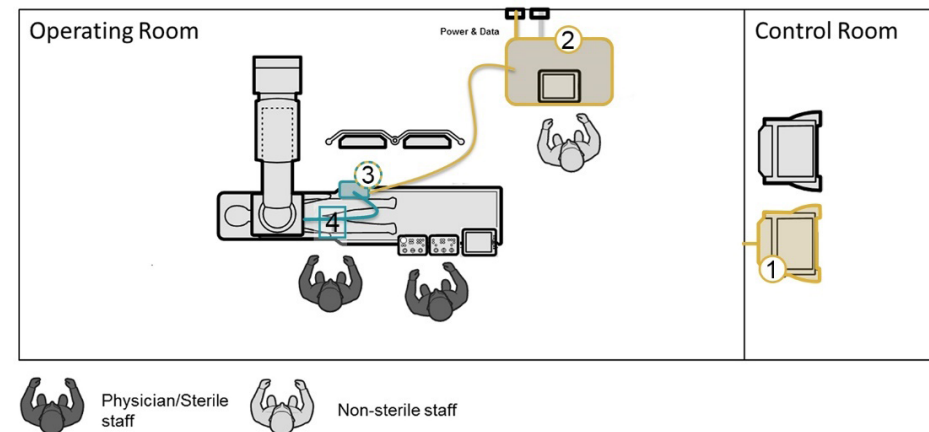
MATERIALS AND METHODS
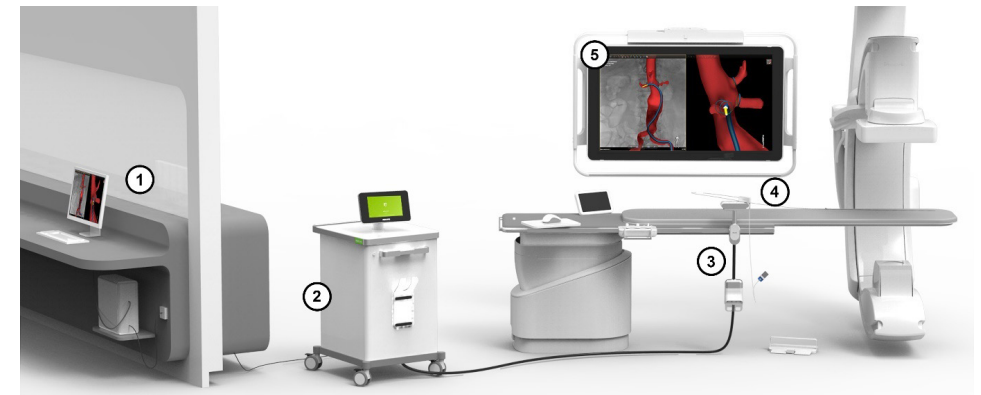
Fiber Optic RealShape technology

The FORS technology platform consists of equipment that sends laser light through a multicore optical fiber integrated in specially designed guidewires and catheters. Twists and bends in the optical fiber influence the wavelength spectrum of the reflected light. By analyzing the wavelength spectra of the reflected light in real-time, it is possible to reconstruct the 3D shape of the full length of the optical fiber. Integration of these optical fibers in guidewires and catheters allows radiation-free visualization of the endovascular devices.[10]

Visualization of these FORS-enabled devices alone, without anatomical surroundings, has limited use. Therefore, FORS works in conjunction with a commercially available fixed fluoroscopy system; either the Philips Allura Xper FD20 system or the Philips Azurion 7 FD20 system (Philips Medical Systems Nederland B.V., Best, the Netherlands). The fluoroscopy system is used to generate static anatomical roadmaps of the vessels, by means of either the acquisition of a digital subtraction angiography (DSA) or coregistered preoperative CTA.
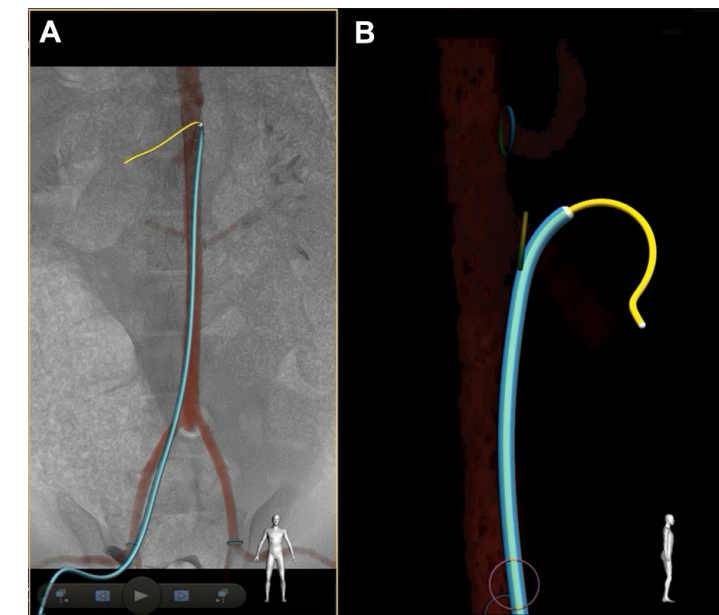
The FORS system consists of four main parts: (1) the single-use devices, (2) the docking top and docking base, (3) the trolley, and (4) the workstation. These components are visualized and numbered in Figure 1. Figure 2 provides an impression of the FORS system, and Figure 3 shows the FORS-enabled device visualization combined with an anatomical roadmap. A comprehensive explanation of the FORS system and its components is provided in Supplemental File A.

Figure 2: *Artist impression of the Fiber Optic RealShape (FORS) system. Copyright (2018) by Philips Medical Systems Nederland. The FORS system comprises a workstation (1), trolley (2), docking base and docking top (3), and the FORS-enabled devices (4). The FORS-enabled devices are visualized in context of an anatomical roadmap on the screen (5).*

Figure 3: *Device visualization based on Fiber Optic RealShape (FORS) in a porcine model. The FORS-enabled guidewire (yellow) and Cobra-2 catheter (light blue) are shown in biplane view setting. Panel A shows the FORS-based device visualization in anterior-posterior projection, rendered onto a roadmap of computed tomography (CTA) and previously acquired fluoroscopy. Panel B simultaneously shows the FORS-based device visualization in a 90° left anterior oblique lateral projection. The facing direction of the guidewire and catheter are visible due to a white marking at the tip of the device. Note 1: The iliac portion of the FORS-enabled devices is partly projected outside the CTA roadmap. This is caused by differences in porcine positioning and vessel deformation due to the insertion of the stiff sheath. Note 2: The fluoroscopy image has been previously acquired and the FORS wire have been moved in the meantime. The FORS visualization is updated but no new fluoroscopy images have been acquired.*

Figure 1: *Illustration of the Fiber Optic RealShape (FORS) system components. Copyright (2018) by Philips Medical Systems Nederland. The yellow components represent the non-sterile components, consisting of the workstation (1), FORS trolley (2) and nonsterile docking base (3). The blue components represent the sterile components, including the docking top (3), which is placed on top of the sterile drape and the FORS single-use devices (4).*

Three endovascular devices equipped with FORS technology were available during this study (Figure 4):

- A 0.035" angled, floppy hydrophilic angiographic guidewire equipped with a torque aid tool. This guidewire has an in-body working length of 120 cm.
- A 5.5F Cobra C2 angiographic catheter with an in-body working length of 80 cm. This catheter is compatible with a 0.035" guidewire.
- A 5.5F Berenstein angiographic catheter with an in-body working length of 80 cm. This catheter is also compatible with a 0.035" guidewire.

Each device contains a sensor lumen, this is a secluded lumen that contains a multicore optical fiber. The fiber runs through the full length of the device and is tethered to the docking top, which is at the table side. The docking top is connected to the docking base, which makes the optical connection to the laser source. Because the devices are tethered at the table side, the guidewire is only front loadable, whereas the catheters are front and back loadable. The FORS-enabled devices have similar radiopacity and mechanical properties as their commercially available counterparts. The FORS-enabled guidewire is fully compatible with conventional catheters, and FORS-enabled catheters are fully compatible with conventional guidewires.
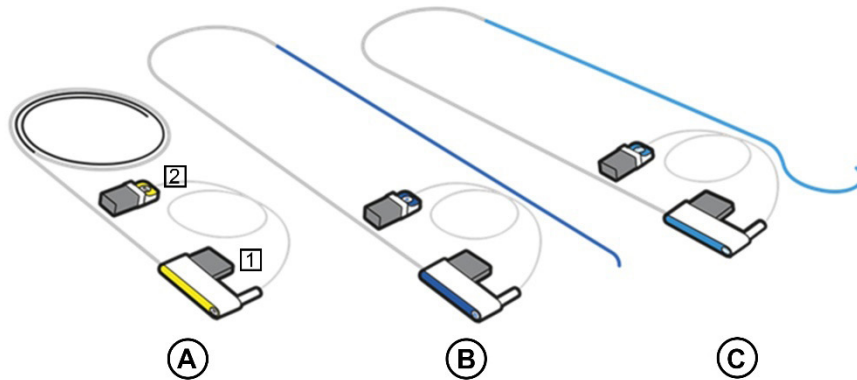
Figure 4: *The Fiber Optic RealShape (FORS) enabled devices. Copyright (2018) by Philips Medical Systems Nederland. In this study, three types of FORS-enabled devices were used: floppy guidewires (A), Berenstein catheters (B), and Cobra-2 catheters (C). Each device has a sensor lumen that contains a multicore optical fiber. The devices are tethered, and are connected to the docking top using a docking fin (1) and to the docking base using an optical connector (2).*

FORS workflow

Step 1. Visualization of anatomical context

An anatomical roadmap is created to visualize the anatomy of interest during FORS-based (fluoroscopy-free) navigation. This roadmap consists of preprocedural CTA imaging or intraprocedural static X-ray imaging such as a single-shot exposure or DSA.

Step 2. FORS-enabled device registration

To align the coordinate system of the FORS-enabled devices with the coordinate system of the X-ray system (including anatomical roadmap), two fluoroscopy images are acquired from different C-arm orientations ($^3\Delta30°$). The user manually marks the tip of the FORS-enabled device on both fluoroscopy images, after which automated software performs registration of the full length of the device. The system displays the fluoroscopy images overlaid with the registered FORS-enabled devices. The user can confirm this final registration or perform manual corrections to achieve agreement between the two modalities.

Step 3. Device navigation

After device registration, the FORS-enabled devices are rendered onto the anatomical roadmap. This visualization contains 3D features, such as shading and a white marker at the distal tip, to indicate the facing direction of the device (Figure 3). Virtual biplane viewing can be used to display the images from two different angles simultaneously to provide volumetric information. The FORS system supports the simultaneous visualization of a maximum of one FORS-enabled guidewire and one FORS-enabled catheter. Alternatively, a FORS-enabled device can be combined with a conventional device.

Preclinical models

The study used two preclinical models: a phantom model and a porcine model.

Phantom Model

The phantom consisted of a 3D silicone model of an abdominal aortic aneurysm with renal and iliac arteries (Elastrat, Geneva, Switzerland), as shown in Figure 5. A non-pulsatile pump was used to perfuse the model with a solution of water and soap, to reduce wall friction. Vascular access was provided by hemostatic valves in both external iliac arteries. A contrast-enhanced CTA scan of the model was available for roadmap purposes.
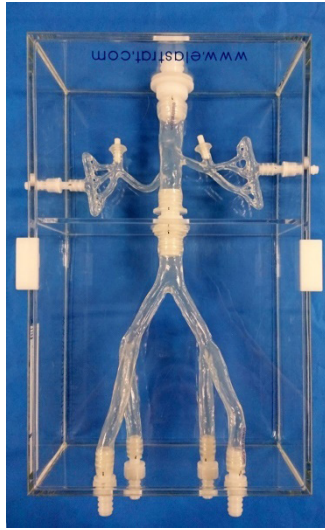
Figure 5: Phantom model. Silicone phantom model of the aorta with renal and iliac arteries.

Porcine Model
The porcine model consisted of three female Topvigs Norsvin swine (van Beek, Lelystad, the Netherlands) of approximately 60 kg. The experimental protocol was approved by the local Animal Welfare Body. Preoperative CTA scans were acquired under general anesthesia with the swine in supine position. The CTA was acquired with a SOMATOM Definition Flash (Siemens, München, Germany), with tube voltage of 80 kV and slice thickness of 0.5 mm. A mixture of 28 mL saline and 120 mL Optiray-320 contrast material (Mallinckrodt Pharmaceuticals, Staines-upon-Thames, United Kingdom) was injected in the jugular vein, at a speed of 6 mL/s and a scan delay of 20 to 40 seconds. The experiments were performed with the swine in similar position as during CTA acquisition to minimize registration errors. Unilateral femoral access was acquired using surgical cutdown, followed by the placement of a 6F sheath (Arrow; Teleflex Inc, Morrisville, NC, USA) in the femoral artery.

Study protocol
This study was performed in a hybrid operating theater equipped with a Philips Allura FD20 FlexMove X-ray system and a FORS system (Philips Medical Systems Nederland B.V., Best, the Netherlands).

Six physicians with varying degrees of experience were recruited to participate in this study, consisting of two experienced vascular surgeons, one less experienced vascular surgeon, two experienced interventional radiologists and one less experienced interventional radiologist. The experienced physicians had >5 years of working experience in the endovascular domain, with a caseload of >60 complex cases per year.

The less experienced physicians had ≤5 years of working experience, with a total caseload of at least 325 cases. All physicians had prior experience with static anatomical roadmaps and followed a hands-on training of the FORS system before this study.

In each session, a predefined protocol was executed by two physicians. One physician had the role of primary operator and performed device setup and registration, followed by 12 cannulation tasks. Each cannulation task started at the level of the bifurcation of the common iliac artery. The other physician assisted in the role of secondary operator. After completion of these tasks, the two physicians switched roles and repeated the protocol.

The cannulation tasks consisted of (1) the right renal artery, (2) the left renal artery, (3) the contralateral common iliac artery (CIA), (4) the superior mesenteric artery (SMA), and (5) the contralateral superficial femoral artery (SFA). Tasks 1, 2, and 3 were executed in the phantom model, whereas the tasks in the porcine model depended on the executed scenario: tasks 1, 2, and 3, or tasks 1, 2, and 4, or 1, 2, and 5. Each physician repeated these three tasks throughout four different scenarios, to assess various functionalities of the FORS system. A flowchart of this protocol is shown in Figure 6.

The scenarios consisted of:
- Scenario 1: Two conjoined FORS-enabled devices and a CTA roadmap
- Scenario 2: Two conjoined FORS-enabled devices and an X-ray roadmap
- Scenario 3: One FORS-enabled device and one conventional device and a CTA roadmap
- Scenario 4: One FORS-enabled device and one conventional device and an X-ray roadmap

In scenario 3 and 4, the physicians used either a conventional 0.035" hydrophilic Radifocus guidewire (Terumo, Somerset, New Jersey, USA) or a conventional 5F catheter of the physician's preference. The physicians used the following catheters: Berenstein (Merit Medical, South Jordan, Utah, USA), SIM2 (Cook, Bloomington, Indiana, USA), Cobra-2 OptiTorque and Cobra-2 GlideCath (Terumo, Somerset, New Jersey, USA) and SOS-2 (Angiodynamics, Lantham, New York, USA).

End points
Target vessel cannulation success
The primary end point of this study was technical success of target vessel cannulation, scored as "success" or "failure". Successful cannulation was achieved when a guidewire and catheter were placed in a stable position inside the target vessel. The correct position of the devices was confirmed with X-ray imaging.

Safety
The occurrence of hazards and adverse events was monitored. A hazard was defined as situation where patient or user safety may be negatively affected (e.g. sterility breach,

vessel damage). Hazards were identified by the physician and by the observing research team, consisting of FORS-technicians and specialists. Vessel damage is difficult to identify during navigation, therefore angiography was employed to detect dissections or perforations of the vascular wall. Furthermore, the FORS-enabled devices were inspected macroscopically after use.
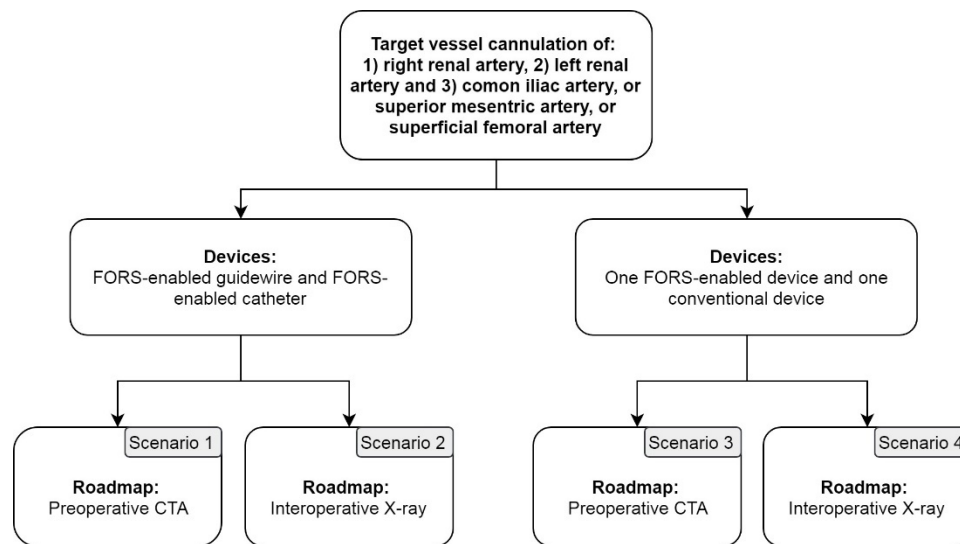
Figure 6: *Cannulation protocol performed in phantom and porcine model. Each physician repeated three cannulation tasks during four different scenarios, leading to a total of 12 cannulation tasks per physician. FORS = Fiber Optic RealShape. CTA = Computed Tomography Angiography.*

Accuracy
The accuracy of the FORS system was measured using a dedicated software tool (Philips Medical). Measurements were performed on the available fluoroscopy and DSA images, acquired to confirm (1) FORS-enabled device registration or (2) target vessel cannulation success or failure. Two metrics were measured; the tip-to-tip distance and the maximum lateral offset. Both metrics are relevant to assess, because physicians rely both on the tip position and the overall catheter shape to navigate their devices to the target vessels.

The tip-to-tip distance encompasses the 3D offset of the tip of the device. This was measured by manual selection of the tip of the device on fluoroscopy, followed by selection of tip in the FORS-based device visualization. The software tool subsequently calculated the 3D offset between these two points, based on the underlying geometrical settings of the C-arm and the 3D shape computation of the FORS-enabled device.

The maximum lateral offset encompasses the maximum lateral displacement (perpendicular to the centerline) of the FORS-based visualization in the distal segment

of the device (2 to 10 cm from the distal tip). Both measurements are shown in Figure 7.

To enhance the visibility of the devices, the FORS system visualizes its guidewire and catheter as 50% wider than their actual width. When the fluoroscopy projection of the device was located within the FORS-based visualization, the offset was measured as 0. When two FORS-enabled devices were used in conjunction, the accuracy of the guidewire was measured exclusively, because the shape of the guidewire plays a leading role in the visualization of conjoined devices.
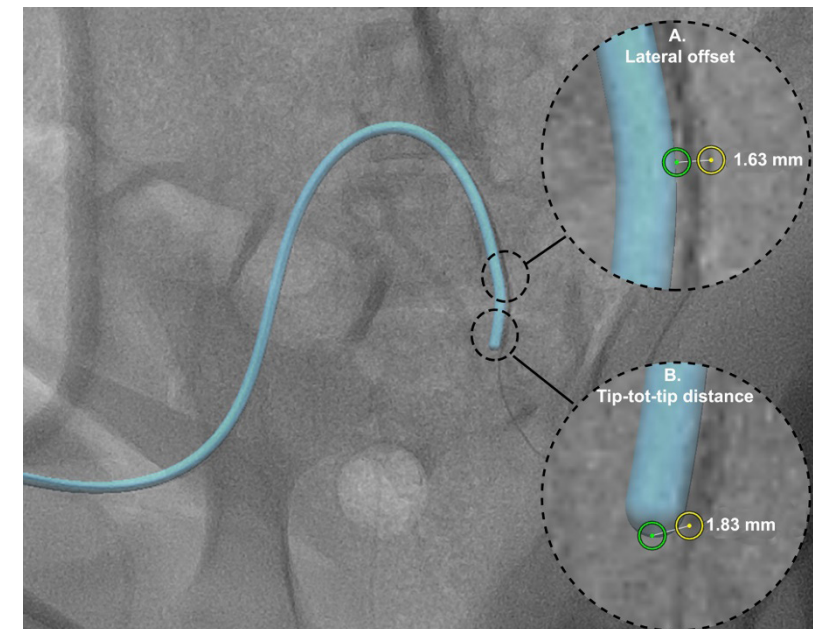
Figure 7: *Accuracy measurements of the Fiber Optic RealShape (FORS) based visualization in a porcine model. The FORS-based visualization of a Cobra-2 catheter rendered onto fluoroscopic imaging during cannulation of the contralateral common iliac artery in a porcine model. Accuracy measurements were performed at the proximal section of the device (A) to measure the maximum lateral offset, and at the tip of the device (B) to measure the tip-to-tip distance. The yellow circle marks the device on fluoroscopy, and the green circle marks the corresponding point in the FORS-based visualization of the device.*

User experience
At the end of each scenario, each physician individually filled in a user experience questionnaire to reflect on the performance of the FORS system (to the best of their knowledge), including:
- Usefulness of the FORS-based visualization of the devices and the anatomical roadmap (better, at par, or worse than current clinical practice)
- Quality of the FORS-based device visualization and registration (accurate or slightly

off but acceptable, or not accurate)

- Responsiveness of the FORS-based device visualization (responsive enough or not responsive enough)
- Mechanical properties of FORS-enabled devices (better, at par, or worse than current clinical practice)
- Compatibility of FORS-enabled devices with ancillary devices (good, adequate, or poor)
- Ability to manually inject contrast agent through the FORS-enabled catheter (good, adequate, or poor)

Data collection and statistical analysis:

The target vessel cannulation success and user experience questionnaire are presented as descriptive data. The accuracy data is represented as median with the interquartile range (IQR). The Mann-Whitney U test was used to test for significant differences (p < .05) in accuracy between the phantom model and the porcine model.

RESULTS

Target vessel cannulation success

A total of 144 cannulation tasks were performed. In the phantom model, 72 of the 72 cannulation tasks (100%) were completed successfully. In the porcine model, 70 of 72 cannulations (97.2%) were successful. The physicians attributed the two cannulation failures to the anatomy of the swine and catheter shape rather than to the functionality of the FORS system. Both cannulation failures involved the cannulation of the SMA in the porcine model with a FORS-enabled guidewire and a FORS-enabled catheter (scenario 1 and 2). The swine in question had relatively narrow aortas and steep downward-facing SMAs that were incompatible with the Cobra-2 or Berenstein configuration.

Safety

No adverse events or hazards occurred during this study. Neither vascular damage nor damage to the devices was found. All users commented that the system was easy and safe to use.
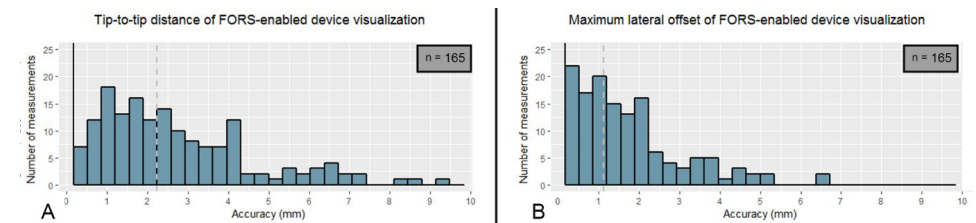
Accuracy

Approximately 121 fluoroscopy and 49 DSA images were available for measurement. Five images were excluded retrospectively because the tip of the device was not visible within the field of view. The median tip-to-tip distance of the device was 2.2 mm (IQR, 1.2 - 3.8 mm). The median maximum lateral offset measured of the device was 1.1 mm (IQR, 0.3 - 2.0 mm). Both metrics were non-normally distributed (Figure 8). No

significant difference was found between the accuracy measurements in the phantom and the porcine model (tip-to-tip distance, p = .08; lateral offset, p = .74).

User experience

During the in-depth interview, the physicians gave their impression of the FORS system. Each of the six physicians mentioned that the system felt safe and intuitive to use.

Figure 8: *Accuracy of the Fiber Optic RealShape (FORS) based device visualization in phantom and porcine models. Panel A shows the distribution of the tip-to-tip accuracy of the FORS-based visualization. Panel B shows the distribution of the maximum lateral accuracy of FORS-based visualization. In both figures, the grey dashed line indicates median.*

All physicians believed that the FORS system could have a clinical benefit, because it may result in a simplification of endovascular device navigation and a reduction in fluoroscopy time. In addition, several physicians thought that the use of FORS technology could result in a reduction the contrast volume (2 physicians) and procedure time (4 physicians) in complex procedures, as FORS enhanced the 3D understanding of the guidewire's and catheter's shape, position and direction in its anatomical context.

The usefulness of the FORS-based device visualization in combination with CTA roadmaps was rated as "better than standard guidance" in 10 of the 12 times and "at par with standard guidance" in the remaining 2 times. Users referred to severe inaccuracy of the CTA roadmap as their main motivation for the "at par" rating. The usefulness of the FORS-based device visualization in combination with DSA roadmaps was rated as "better than standard guidance" at all times (100%). The virtual biplane viewing option and the white mark at the tip of the devices were mentioned as valuable additions because these features created multidimensional insight in the anatomy and the orientation of the devices. The physicians rated the quality of the FORS-based device visualization and registration as "accurate" in 7 cases (58%) or "slightly off, but acceptable" in 5 (42%), despite some slight deviations from fluoroscopy from time to time. All physicians rated the responsiveness of the FORS-based visualization was as "good," although several

physicians mentioned slight jitter[1] in the FORS-based visualization during part of the procedure and that the jitter could be distracting during a long case.

Five of six physicians rated the mechanical properties (torquability, pushability) of the FORS-enabled devices as "at par" with the best commercially available devices in current clinical practice. One physician experienced the FORS-enabled Cobra-2 catheter as stiffer than the GlideCath Cobra-2 (Terumo) catheter that he conventionally used. Compared with these GlideCath catheters, he rated the mechanical properties of the devices as "worse." All physicians felt that the compatibility of the FORS-enabled devices with conventional devices was "good" as well as the ability to inject contrast agent. The results of the user experience questionnaire in the phantom model and the porcine model are summarized in Supplementary File B.

DISCUSSION

This study evaluated FORS, a new medical technology that offers real-time 3D visualization of specially designed endovascular guidewires and catheters based on fiber optic technology instead of fluoroscopy. FORS-based device navigation distinguishes itself from conventional fluoroscopy by providing insight in the 3D shape of the device using shading, simultaneous biplane viewing modes, and a tip marker that clearly shows the facing direction of the devices. Due to these features, FORS-based guidance appears to be more intuitive than standard fluoroscopic guidance.

This preclinical study was conducted with a heterogeneous team of users, comprising of vascular surgeons and interventional radiologists with different experience levels. We believe that this heterogeneity is critical to assess the ease of use and safety of the system. No hazardous situations were observed by the research team, or by the physicians themselves. All users were unanimously satisfied with the accuracy of the FORS-based visualization, while the design of the FORS-enabled guidewires and catheters did not compromise the mechanical properties of the devices.

In the past, electromagnetic tracking (EM) has been proposed as an alternative method to track endovascular devices. The tracking ability of EM systems is limited to the tip of the device, instead of its full length, as with FORS-technology. Details on the in-vivo accuracy of EM tracking are based on animal studies of Manstad-Hulaas et al.[11] and Abi-Jaoudeh et al[12] that report a mean tip-to-tip distance of 4.2 ± 1.8 mm and 4.3 ± 1.0 mm respectively, measured in 3D. The current study measured a mean tip-to-tip distance of 2.7 ± 2.2 mm. However, these measurements were conducted in a 2D image, which may underestimate the actual discrepancy in 3D space. Furthermore, this study did not examine whether the tip-to-tip distance was influenced by the position of device-registration, nor if the larger discrepancies occurred when the devices were removed further from their registration-position. Future studies are required to provide more information on this subject.

In the current study, several in-vitro experiments were executed in a phantom model without pulsatile circulation, which might reduce the clinical fidelity of these experiments. However, we found no significant differences in accuracy between in-vitro and in-vivo use of the FORS system, indicating that active blood flow does not influences the performance of the FORS system.

The FORS system is not without limitations. Firstly, the number of FORS-enabled guidewire and catheter configurations is currently limited. Despite this limitation, 98.6% of the cannulation tasks could be fulfilled successfully with FORS-enabled devices. In a clinical setting, physicians can always resort to a combination of a FORS-enabled guidewire and a conventional catheter with the desired shape, to achieve cannulation success while maintaining benefits of FORS-guidance.

Secondly, the FORS system supports the use anatomical roadmaps based on preoperative CTA imaging. This functionality is widely used in commercial products such as Philips' VesselNavigator, GE's Innova Vision's, and Siemens' EVAR-3D Guidance.[6,13,14] However, differences in patient positioning, patient motion and device induced vessel deformation can cause this roadmap to become less accurate. In fact, roadmap deviations of 4 to 11 mm have been reported, depending on the procedural phase and the region of interest.[15–17]

Consequently, the accuracy of the CTA roadmaps needs to be monitored occasionally and modified accordingly. As an alternative, the FORS system also supports intraprocedural DSA images as an anatomical roadmap. Although 2D, these DSA roadmaps provide a more recent representation of the patient's on-table anatomy.

Currently, FORS technology functions exclusively in combination with a Philips high-end X-ray system, although future development may allow the integration of FORS technology in other brands of fluoroscopy systems. The FORS system thereby forms an expansion of current clinical practice rather than a complete replacement of fluoroscopic imaging. For now, the use of fluoroscopy remains inevitable during various diagnostic and interventional phases of the procedure, including angiography and stent deployment. In fact, the setup of the FORS system requires a few fluoroscopy images to create an anatomical roadmap and to perform device registration. While FORS cannot completely eliminate the use of radiation, it does offer great potential to reduce the cumulative radiation dose of endovascular procedures. In this study, however, we did not assess radiation dose or cannulation time, as these parameters would have been biased by the physician's learning curve.

Despite its limitations, this work establishes proof of concept of the FORS system, that provides full length visualization of FORS-enabled devices in three-dimensional space,

---

1   By the term jitter, small (around 0.5mm) irregular movement around the median position of the visualized shape is meant. This is primarily a function of the signal to noise of the system.

without the need for active fluoroscopy. The safety and feasibility of the FORS system in a preclinical setting was demonstrated by the combined outcomes of high cannulation success, lack of hazards, positive user experience, and adequate accuracy. Clinical studies are necessary to explore the effect of FORS technology on technical success rates, radiation parameters, contrast volume, and procedure times of endovascular procedures in patients.

REFERENCES

1   Gonzalez L, Chen A, Lin PH, Pisimisis G, Barshes NR, Bechara CF, et al. Latest recanalization techniques for complex superficial femoral artery occlusions. J Cardiovasc Surg (Torino) 2012;**53**(4):487–94.

2   Castelli P, Piffaretti G, Lomazzi C, Rivolta N, Riva F, Maida S, et al. Fenestrated and branched endovascular grafts for complex aortic aneurysms. A review. Ital J Vasc Endovasc Surg 2008;**15**(1):63–8.

3   Thakor AS, Winterbottom A, Mercuri M, Cousins C, Gaunt ME. The radiation burden from increasingly complex endovascular aortic aneurysm repair. Insights Imaging 2011;**2**(6):699–704. Doi: 10.1007/s13244-011-0120-5.

4   National Research Council. Health Risks from Exposure to Low Levels of Ionizing Radiation: BEIR VII Phase 2. Washingt DC Natl Acad Press 2006:424. Doi: 10.17226/11340.

5   Ortiz López P, Dauer LT, Loose R, Martin CJ, Miller DL, Vañó E, et al. ICRP Publication 139: Occupational Radiological Protection in Interventional Procedures. Ann ICRP 2018;**47**(2). Doi: https://doi.org/10.1177/0146645317750356.

6   Stangenberg L, Shuja F, Carelsen B, Elenbaas T, Wyers MC, Schermerhorn ML. A novel tool for three-dimensional roadmapping reduces radiation exposure and contrast agent dose in complex endovascular interventions. J Vasc Surg 2015;**62**(2):448–55. Doi: 10.1016/j.jvs.2015.03.041.

7   McNally MM, Scali ST, Feezor RJ, Neal D, Huber TS, Beck AW. Three-dimensional fusion computed tomography decreases radiation exposure, procedure time, and contrast use during fenestrated endovascular aortic repair. J Vasc Surg 2015;**61**(2):309–16. Doi: 10.1016/j.jvs.2014.07.097.

8   Sailer AM, de Haan MW, Peppelenbosch AG, Jacobs MJ, Wildberger JE, Schurink GWH. CTA with Fluoroscopy Image Fusion Guidance in Endovascular Complex Aortic Aneurysm Repair. Eur J Vasc Endovasc Surg 2014;**47**(4):349–56. Doi: 10.1016/j.ejvs.2013.12.022.

9   Tacher V, Lin M, Desgranges P, Deux J-F, Grünhagen T, Becquemin J-P, et al. Image Guidance for Endovascular Repair of Complex Aortic Aneurysms: Comparison of Two-dimensional and Three-dimensional Angiography and Image Fusion. J Vasc Interv Radiol 2013;**24**(11):1698–706. Doi: 10.1016/j.jvir.2013.07.016.

10 Froggat ME, Klein JW, Gifford DK, Kreger ST. United States Patent No. US 8773650 B2, 2014.

11 Manstad-Hulaas F, Tangen GA, Gruionu LG, Aadahl P, Hernes TAN. Three-Dimensional Endovascular Navigation With Electromagnetic Tracking: Ex Vivo and In Vivo Accuracy. J Endovasc Ther 2011;**18**(2):230–40. Doi: 10.1583/10-3301.1.

12 Abi-Jaoudeh N, Glossop N, Dake M, Pritchard WF, Chiesa A, Dreher MR, et al. Electromagnetic Navigation for Thoracic Aortic Stent-graft Deployment. J Vasc Interv Radiol 2010;**21**(6):888–95. Doi: 10.1016/j.jvir.2009.12.402.

13 Schulz CJ, Schmitt M, Böckler D, Geisbüsch P. Fusion Imaging to Support Endovascular Aneurysm Repair Using 3D-3D Registration. J Endovasc Ther 2016;**23**(5):791–9. Doi: 10.1177/1526602816660327.

14 Sadek M, Berland TL, Maldonado TS, Rockman CB, Mussa FF, Adelman MA, et al. Use of preoperative magnetic resonance angiography and the Artis zeego fusion program to minimize contrast during endovascular repair of an iliac artery aneurysm. Ann Vasc Surg 2014;**28**(1):261.e1-261.e5. Doi: 10.1016/j.avsg.2013.07.001.

15 Steuwe A, Geisbüsch P, Schulz CJ, Böckler D, Kauczor H-U, Stiller W. Comparison of Radiation Exposure Associated With Intraoperative Cone-Beam Computed Tomography and Follow-up Multidetector Computed Tomography Angiography for Evaluating Endovascular Aneurysm Repairs. J Endovasc Ther 2016;**23**(4):583–92. Doi: 10.1177/1526602816649588.

16 Schulz CJ, Schmitt M, Böckler D, Geisbüsch P. Feasibility and accuracy of fusion imaging during thoracic endovascular aortic repair. J Vasc Surg 2016;**63**(2):314–22. Doi: 10.1016/j.jvs.2015.08.089.

17 Goudeketting SR, Heinen SG, van den Heuvel DA, van Strijen MJ, de Haan MW, Slump CH, et al. The use of 3D image fusion for percutaneous transluminal angioplasty and stenting of iliac artery obstructions: Validation of the technique and systematic review of literature. J Cardiovasc Surg (Torino) 2018;**59**(1):26–36. Doi: 10.23736/S0021-9509.17.10224-7.

SUPPLEMENTAL FILE A: FORS SYSTEM COMPONENTS

The FORS system consists of four main parts: (1) the single-use devices, (2) the docking top and docking base, (3) the trolley, and (4) the workstation.

1. Single use devices

The FORS-enabled devices are sterile and single use. Each device contains a sensor lumen, which is a secluded lumen located in the center of the guidewire and in the wall of the catheter (Supplementaral Figure 1). The sensor lumen contains a multicore optical fiber that runs through the full length of the device, from the optical connector to the distal tip of the device.

2. Docking base and docking top

The docking base is a unit clamped to the rail of the interventional operating table and provides a fixed reference point for attached devices. The unit has two components: a reusable base that is required to be covered by the sterile drape and a single-use docking top placed on top of the drape with sterile mechanical slots for the devices. There are three device slots in the docking top. The devices are clicked in place in the slots in the docking top, and the optical connector of the device is connected to the optical port of the docking base.

3. Trolley

The trolley contains the main hardware and software components of the system. It is equipped with two lasers, several electrical and optical components, and underlying computational software. The trolley analyses the reflected wavelength spectra from the optical fiber to compute the real-time shape of the device. The trolley is connected to the workstation via a local network connection.

4. Workstation

The workstation has the viewing software that provides the visualization the devices and the anatomical context in real time. The workstation is used to perform initial registration of the FORS-enabled devices.
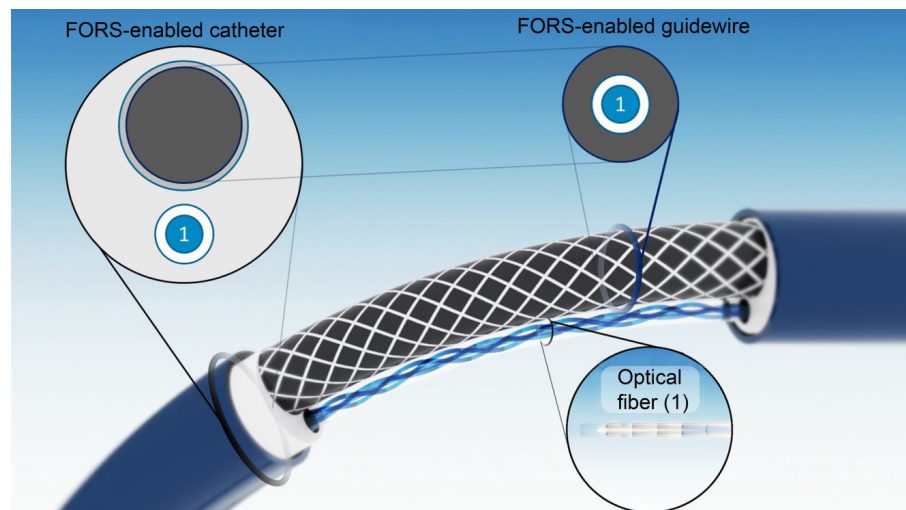
Supplemental Figure 1: *The integration of the optical fiber in FORS-enabled devices. The optical fiber is integrated in the core of the FORS-enabled guidewires. These FORS-enabled guidewires are conventional 0.035" width. The optical fiber is integrated in the wall of the FORS-enabled catheters, making them 0.5F wider than conventional catheters (6.5F).*

SUPPLEMENTAL FILE B: SUPPLEMENTAL TABLES

Supplemental Table 1: Results of the user experience questionnaire of the FORS system in the phantom model.

	Physician 1†	Physician 2*	Physician 3†	Physician 4†	Physician 5*	Physician 6†
Usefulness of FORS + anatomical roadmap in case of						
- CTA roadmap	Better than standard practice	Better than standard practice	Better than standard practice	Better than standard practice	Better than standard practice	Better than standard practice
- DSA roadmap	Better than standard practice	Better	Better than standard practice	Better than standard practice	Better than standard practice	Better than standard practice
Quality of the FORS-based device visualization and registration	Accurate	Accurate	Slightly off, but acceptable	Accurate	Slightly off, but acceptable	Accurate
Responsiveness of the FORS-based device visualization	Responsive enough for device manipulation	Responsive enough for device manipulation	Responsive enough for device manipulation	Responsive enough for device manipulation	Responsive enough for device manipulation	Responsive enough for device manipulation
Mechanical properties of FORS-enabled devices	At par with standard practice	Better than standard practice	At par with standard practice	At par with standard practice	At par with standard practice	At par with standard practice
Compatibility of FORS-enabled devices with ancillary devices	Adequate	Good	Good	Good	Adequate	Good

* Physician with ≤5 years of experience in the endovascular domain
† Physician with > 5 years of experience in the endovascular domain

Supplemental Table 2: Results of the user experience questionnaire of the FORS system in the porcine model.

	Physician 1†	Physician 2*	Physician 3†	Physician 4†	Physician 5*	Physician 6†
Usefulness of anatomical roadmap in case of						
- CTA roadmap	Better than standard practice	Better than standard practice	Better than standard practice	At par with standard practice	Better than standard practice	At par with standard practice
- DSA roadmap	Better than standard practice	Better than standard practice	Better than standard practice	Better than standard practice	Better than standard practice	Better than standard practice
Quality of the FORS-based device visualization and registration	Accurate	Accurate	Slightly off, but acceptable	Accurate	Slightly off, but acceptable	Slightly off, but acceptable
Responsiveness of the FORS-based device visualization	Responsive enough for device manipulation	Responsive enough for device manipulation	Responsive enough for device manipulation	Responsive enough for device manipulation	Responsive enough for device manipulation	Responsive enough for device manipulation
Mechanical properties of FORS-enabled devices	At par with standard practice	At par with standard practice	At par with standard practice	Worse than standard practice	At par with standard practice	At par with standard practice
Compatibility of FORS-enabled devices with ancillary devices	Adequate	Good	Good	Good	Adequate	Good
Ability to inject contrast agent through the FORS-enabled catheter	Good	Good	Good	Good	Good	Good

* Physician with ≤5 years of experience in the endovascular domain
† Physician with > 5 years of experience in the endovascular domain

CHAPTER | 8

First-in-Human Clinical Feasibility Study of Endovascular Navigation with Fiber Optic RealShape (FORS) Technology

ABSTRACT

Objective

Endovascular procedures are conventionally conducted using two dimensional fluoroscopy. A new technology platform, Fiber Optic RealShape (FORS), has recently been introduced allowing real-time, three-dimensional visualisation of endovascular devices using fiberoptic technology. It functions as an add on to conventional fluoroscopy and may facilitate endovascular procedures. This first in human study assessed the feasibility of FORS in clinical practice.

Methods

A prospective cohort feasibility study was performed between July and December 2018. Patients undergoing (regular or complex) endovascular aortic repair (EVAR) or endovascular peripheral lesion repair (EVPLR) were recruited. FORS guidance was used exclusively during navigational tasks such as target vessel catheterisation or crossing of stenotic lesions. Three types of FORS enabled devices were available: a flexible guidewire, a Cobra-2 catheter, and a Berenstein catheter. Devices were chosen at the physician's discretion and could comprise any combination of FORS and non-FORS devices. The primary study endpoint was technical success of the navigational tasks using FORS enabled devices. Secondary study endpoints were user experience and fluoroscopy time.

Results

The study enrolled 22 patients: 14 EVAR and eight EVPLR patients. Owing to a technical issue during start up, the FORS system could not be used in one EVAR. The remaining 21 procedures proceeded without device or technology related complications and involved 66 navigational tasks. In 60 tasks (90.9%), technical success was achieved using at least one FORS enabled device. Users rated FORS based image guidance "better than standard guidance" in 16 of 21 and "equal to standard guidance" in five of 21 procedures. Fluoroscopy time ranged from 0.0 to 52.2 min. Several tasks were completed without or with only minimal X-ray use.

Conclusion

Real time navigation using FORS technology is safe and feasible in abdominal and peripheral endovascular procedures. FORS has the potential to improve intra-operative image guidance. Comparative studies are needed to assess these benefits and potential radiation reduction.

INTRODUCTION

In recent decades, an enormous shift has occurred from open operations to fluoroscopically guided endovascular interventions. However, fluoroscopically guided navigation has several important limitations. While guidewires and catheters are being manipulated in a 3D space, these movements are presented to the physician in a 2D projection. This limits the ability to estimate the spatial relationship between the endovascular device and the vascular anatomy or to identify the shape and pointing direction of the device. These factors complicate conceptually basic tasks such as navigation through tortuous arteries and target vessel catheterisation. Further, fluoroscopy projections are shown as grayscale images. This reduces the ability to differentiate between visible structures on the image, especially if these have similar radiopaque characteristics.

Besides these qualitative limitations, exposure to X-ray radiation poses health risks for patients and also for medical staff, who are chronically exposed to radiation throughout their career.[1,2] The ever-growing number of endovascular procedures and their increasing complexity raises concerns about long-term risks. Therefore, the development of new endovascular guidance technologies, without these drawbacks, is of utmost importance.

Fiber Optic RealShape (FORS) technology offers 3D visualisation of specially designed endovascular devices comprising guidewires and catheters by means of light instead of X-ray. The research group recently reported the preclinical feasibility and safety of FORS technology in phantom and porcine models.[4] The potential of FORS technology was demonstrated by yielding positive results in technical success rates, user experience, accuracy, and safety. In the present first in human clinical study, the primary objective was to evaluate feasibility of endovascular navigation with FORS enabled catheters and guidewires in a clinical environment, thereby using FORS based guidance as an add on to standard X-ray guidance.

MATERIALS AND METHODS

Study design

This was a prospective, single arm feasibility study at a single centre. The University Medical Center Utrecht Medical Ethics Committee approved the study protocol (METC 18/422), and all patients signed an informed consent prior to enrolment.
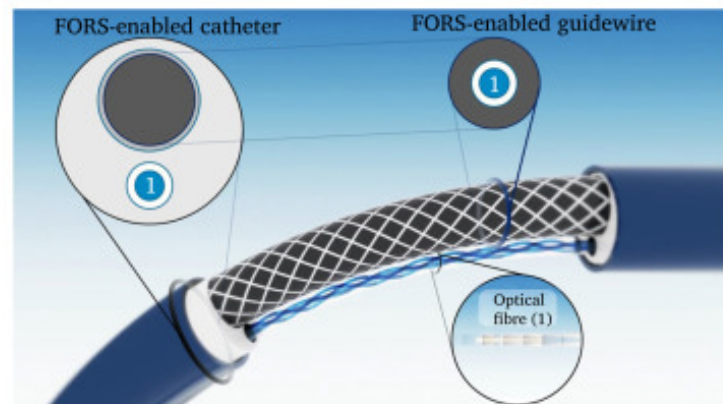
The Fiber Optic RealShape System

The FORS equipment sends laser light through a multicore optical fiber, the FORS fiber optic sensor, and then receives and analyses the returning light that runs through this optic sensor. Twists and bends in the optical fiber influence the wavelength spectrum of the light. By analysing the wavelength spectra of the returned light, it is possible to

reconstruct the 3D shape of the full length of the multicore optical fiber. Because these optical fibers are integrated in guidewires and catheters, FORS allows radiation free visualisation of the endovascular devices in real time and in 3D. The clinical set up of the FORS system is shown in *Figure 1* and *2*.

Figure 1: *Impression of the Fiber Optic RealShape (FORS) system. The FORS system with workstation (1), trolley (2), docking base (3), docking top that connects to the FORS-enabled devices (4). The FORS-enhanced devices are visualized in context of an anatomical roadmap on the screen (5). Copyright © (2020) Koninklijke Philips N.V. All rights reserved.*

Figure 2: *Fiber Optic RealShape (FORS) enhanced guidewire and catheter. These devices have a secluded sensor lumen with an integrated multicore optical fiber (1), through which laser light is transmitted. Copyright © (2020) Koninklijke Philips N.V. All rights reserved.*

For easy differentiation between the devices, the wire is shown in a bright yellow colour and catheters in distinctive blue, and for optimisation of visibility, the devices are shown 50% thicker than their actual size. The devices are tethered. Guidewires are only front loadable, while catheters are both front and back loadable. All FORS enabled devices are radiopaque like regular guidewires and angiography catheters and are also fully compatible with conventional guidewires and catheters.

Three endovascular devices equipped with FORS technology were used in this study (*Figure 3*):

- A 0.035 inch angled, hydrophilic angiographic guidewire with a flexible nitinol core and a floppy tip, and an in body working length of 120 cm.
- A 5.5F Cobra C2 angiographic catheter with an in body working length of 80 cm.
- A 5.5F Berenstein angiographic catheter with an in body working length of 80 cm.

FORS works in conjunction with a fluoroscopy system to create anatomical overlays of the arterial vessels from regular digital subtraction angiograms (DSA) or X-ray images. Also, pre-operative imaging data, like a CT scan, can be used to create a 3D overlay of the patient anatomy.
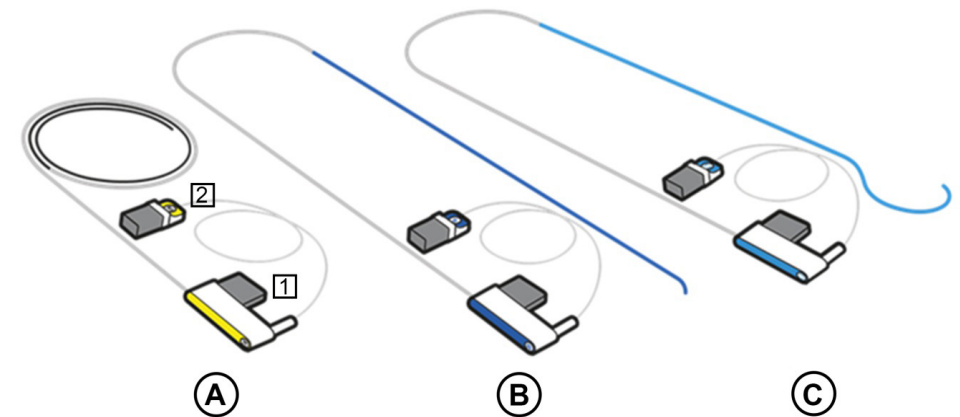
Figure 3: *The three available Fiber Optic RealShape (FORS) enabled devices. The floppy guidewire (A), Berenstein catheter (B), and Cobra-2 catheter (C). The docking fin (1) of the devices is connected to the docking top, and the optical connector (2) is connected to the docking base. Copyright © (2020) Koninklijke Philips N.V. All rights reserved.*

Patients

The target population of this study consisted of patients with abdominal aortic aneurysms (AAA) or iliac aneurysms (IA), or both, who were planned for endovascular repair (EVAR), and patients with peripheral arterial disease with haemodynamically significant stenotic lesions in the common iliac artery (CIA), superficial femoral artery (SFA) or popliteal artery (PA), or with a popliteal aneurysm planned for endovascular peripheral lesion repair (EVPLR). Inclusion and exclusion criteria are listed in *Table 1*.

Table 1. Inclusion and exclusion criteria

Inclusion criteria	Exclusion criteria
Age >18 years	Subjects unable to understand verbal and/or written informed consent
Signed informed consent	Emergency procedure
Scheduled for elective endovascular procedure for stenotic or aneurysmatic pathology	Subjects unwilling or unable to comply with the protocol
Anatomical conformation suitable for the investigational medical devices (5.5F 80-cm Cobra C2 catheter, and/or 5.5F 80-cm Berenstein catheter, and a 0.035-inch 120-cm guidewire	Intolerance to contrast media
	Current participation in a concurrent trial that may confound study results

Study Procedures

Procedures were performed by an experienced vascular surgeon (J.H. or C.H.) or an experienced interventional radiologist (E.V.) as the first operator. These clinicians were familiar with the FORS system as they have not only been involved in the development process of the FORS technology and devices but also used the FORS system in an animal study and in several procedures on phantoms.4 Before patients were enrolled into the study, the whole staff underwent hands on training to optimise and standardise the workflow with the FORS system.

Procedures were done in a hybrid operating room with a ceiling mounted C arm (Allura FD20 Flexmove with ClarityIQ; Philips Medical Systems Nederland B.V., Best, The Netherlands). After regular patient preparation and vascular access, the operator performed 2D–3D registration of X-ray to a pre-operative computed tomography angiogram (if available) to create the arterial anatomical overlay. Then, the operator acquired two X-ray images at > 30° different angles of the FORS enabled catheter and guidewire for registration of these devices. Subsequently, FORS enabled devices were ready to use. Endovascular tasks were started with FORS enabled guidewire and/or FORS enabled catheter, but during the task the operator could switch to any available catheter and guidewire, as in regular practice. However, the use of FORS enabled catheters and guidewires was encouraged.

The FORS system was intended to be used during the navigational part of the procedures only, whereas therapeutic tasks, such as stent graft deployment and balloon angioplasty, were performed with conventional X-ray guidance, as in standard practice. The intended endovascular tasks with the FORS enabled devices are summarised in *Table 2*, examples include catheterisation of the contralateral limb, catheterisation of a target vessel, or crossing of a stenotic lesion.

Study End Points

The primary study end point was the technical success of the intended endovascular tasks during aortic and peripheral endovascular procedures. A task was considered a technical success if the target vessel or contralateral stent graft limb were catheterised using a FORS enabled catheter and/or guidewire with the catheter and guidewire in a stable position. Technical success was confirmed by fluoroscopy or DSA, or both.

As secondary study end point, qualitative scores were collected from the first operator on performance parameters of FORS based image guidance. The scored parameters are listed in *Table 3*. An additional secondary study end point was fluoroscopy time.

Statistical Methods

There are no studies available which report on the navigation success rate when limiting the devices to a guidewire, a Berenstein and a Cobra 2 catheter. Reported success rates for comparable navigations without this limitation are between 90.5% and 100%.4,5 For this exploratory study, a reference rate of 92% was assumed. Sample size calculation with an 80% power, and a Wald 1-sided 95% confidence interval resulted in a sample size of at least 60 endovascular tasks. After reaching these, enrollment in the study was considered complete. Qualitative scores by the operators were pooled for the complete data set as well as for the EVAR and EVPLR groups individually.

For secondary end points, the mean and standard deviation were calculated for the overall cohort as well as for the patients in the EVAR and EVPLR groups. Statistical analysis was performed with SAS (Version 9.4, SAS institute Inc., Cary, NC, USA).

Table 2: Intended tasks with FORS-enabled devices

Intended tasks during EVAR with FORS-enabled devices
Catheterization of the aorta above the aneurysm
Catheterization of the contralateral limb of the stent graft
Catheterization of the target aortic side branches in case of fenestrated or branched EVAR
Catheterization of internal iliac artery in case of iliac branched EVAR
Intended tasks during EVPLR with FORS-enabled devices
Catheterization of the target vessel (iliac, femoral or popliteal artery)
Aortic crossover maneuver
Crossing of the stenotic lesion

Table 3: Qualitative scoring of performance of FORS parameters

Performance of FORS parameter	Answers	Scorings in EVAR patients	Scorings in EVPLR patients
1. The usefulness of the FORS-based image guidance during navigation	1-Better: More useful compared to standard practice	10/13	6/8
	2-At par: moderately useful, compared to standard practice	3/13	2/8
	3-Worse: not useful compared to standard practice	0/13	0/8
2. The quality of the visualization and registration of the FORS-based device image with x-ray	1-Accurate	4/13	7/8
	2-Slightly off but acceptable	8/13	1/8
	3-Not accurate and not acceptable	1/13	0/8
3. The responsiveness of the FORS-based device visualization	1-Responsive enough for device manipulation	13/13	8/8
	2-Not responsive enough for device manipulation	0/13	0/8
4. The ability to steer the FORS-based device during navigation (torquability, pushability, trackability)	1-Better than devices in current practice	0/13	0/8
	2- At par with devices in current practice	13/13	8/8
	3- Worse than devices in current practice	0/13	0/8
5. The compatibility of the FORS device when used in combination with ancillary devices	1-Good	13/13	8/8
	2-Moderate	0/13	0/8
	3-Poor	0/13	0/8
6. The ability to inject contrast agent manually through the FORS catheter compared with your current practice	1-Good	12/12	5/5
	2-Moderate	0/12	0/5
	3-Poor	0/12	0/5

RESULTS

The study enrolled 22 patients who met the inclusion/exclusion criteria. Procedures were performed between July 31, 2018, and December 11, 2018. In 1 patient (patient 11), the FORS system had a technical startup issue and could not be used. The patient was treated with only conventional devices and was therefore excluded from analysis.

The 21 patients, 5 women (24%) and 16 men (76%), were a mean age of 68 years (range, 48-89 years). Mean body mass index was 27.6 kg/m2 (range, 21-34 kg/m2). The planned intervention was EVAR in 13 patients and EVPLR in 8 patients. Baseline characteristics and comorbidities are specified in Supplemental Table 1 and 2, respectively. There were 67 endovascular tasks performed with at least 1 attempt with a FORS-enabled guidewire and/or a FORS-enabled catheter. Detailed information about the type of intervention is given in Supplemental Table 3.

One of these 67 tasks was retrospectively excluded from analysis, because one of the inclusion criteria was violated. Recanalization of the SFA in this patient was performed

from the contralateral groin, which required a working length of >80 cm.

From the remaining 66 tasks, 53 (80%) were performed during the EVAR procedures, and 13 (20%) were done during the EVPLR procedures. Seven tasks (10.6%) were performed from left brachial access, and the others from right or left femoral access. The specification of the tasks is reported in *Table 4*.

Table 4: Technical success rate with FORS-enabled devices

Procedure	Endovascular Task	N	TS	Prop	90% Confidence Limits Lower	90% Confidence Limits Upper
EVAR	ALL	53	49	0.92	0.865	0.984
	Catheterization of thoracic aorta from groin	21	21	1.00	1.000	1.000
	Catheterization of abdominal aortal from left arm	1	1	1.00	1.000	1.000
	Catheterization of celiac trunk	3	2	0.67	0.219	1.000
	Catheterization of superior mesentric artery	5	5	1.00	1.000	1.000
	Catheterization of Right Renal Artery	5	4	0.8	0.506	1.000
	Catheterization of Left Renal Artery	5	5	1.00	1.000	1.000
	Catheterization of fenestrated cuff (after partial deployment)	1	1	1.00	1.000	1.000
	Cross over aortic bifurcation	1	1	1.00	1.000	1.000
	Catheterization of contralateral limb stent graft	9	7	0.78	0.550	1.000
	Catheterization of internal iliac artery	2	2	1.00	1.000	1.000
EVPLR	ALL	13	11	0.85	0.682	1.000
	Cross over aortic bifurcation	2	1	0.50	0.000	1.000
	Catheterization of abdominal aorta from groin	2	2	1.00	1.000	1.000
	Recanalization Occluded (stent) in common iliac artery	1	1	1.00	1.000	1.000
	Crossing stenosis common iliac artery	3	3	1.00	1.000	1.000
	Recanalization occluded internal iliac artery	1	0	0.000	0.000	0.000
	Crossing stenosis superficial femoral artery	2	2	1.00	1.000	1.000
	Crossing stenosis popliteal artery	1	1	1.00	1.000	1.000
	Crossing popliteal aneurysm	1	1	1.00	1.000	1.000
TOTAL		66	60	0.91	0.851	0.967

TS = Technical success, Prop = proportion, EVAR = Endovascular Aorto-iliac Repair, EVPLR = Endovascular Peripheral Lesion Intervention

Primary End Point

Sixty of the 66 tasks (90.9%) were successfully performed with at least a FORS-enabled catheter or FORS-enabled guidewire. Forty-Four tasks (66.7%) were successfully completed with both a FORS-enabled catheter and FORS-enabled guidewire.

In 16 tasks (24.2%) successful catheterization was achieved with a FORS-enabled guidewire in combination with a regular non–FORS-enabled catheter. In 5 out of these 16 tasks, the targeted vessels were anatomically incompatible with the available shapes

of FORS-enabled catheters. Non–FORS SOS catheters (Soft-Vu, Angiodynamics, Inc. Queensbury, USA) were successfully used. In one of these tasks, a SOS catheter was used with FORS-enabled guidewire for embolization of the hypogastric artery. To avoid extra procedure steps, these devices were also used for the next task (catheterization of the thoracic aorta). In 5 other tasks that were performed with a FORS-enabled guidewire with a non-FORS catheter, a non-FORS pigtail catheter was needed in the aorta to perform angiography. In these tasks, the pigtail catheters were successfully navigated over the FORS wire. In the remaining 5 tasks (in two patients) technical issues were the reason for using a non-FORS-enabled catheter.

Five catheterization tasks (7.6%) were started with FORS-enabled devices but were switched to non-FORS catheters and non-FORS guidewires. Four of these tasks were successfully performed with SOS-0 and SOS-2 catheters. Because the operators knew in advance that these catheters would need to be changed over the wire when the targets were cannulated, they decided to combine the catheters with regular guidewires, that are back-loadable, in contrast to the FORS-enabled guidewires.

In the fifth task, a contralateral limb of a stent graft was cannulated with FORS-enabled devices; however, the FORS-enabled Berenstein catheter did not follow over the wire into the stent graft. Because the wire was not back-loadable, the wire had also to be removed from the contralateral limb. The devices were changed for a regular non–FORS-enabled guidewire (Radifocus, Terumo Medical, Tokyo, Japan) and comparably shaped regular catheter (Impress, Merit Medical Systems, South Jordan, USA). Catheterization of the contralateral limb was then successfully performed.

One task, recanalization of an occluded internal iliac artery (IIA), failed. The FORS-enabled guidewire and catheter passed the occlusion, but re-entry in the lumen of the distal IIA was not achieved, also not after changing to Non-FORS catheter and wire.

Supplemental Table 4 reports the final catheter and guidewire combinations that were used for the endovascular tasks, and Table 4 reports the rate of technical success with FORS-enabled devices for the different endovascular tasks.

Secondary End Points
Qualitative assessment of the performance of the FORS system
The detailed scorings of the qualitative assessment of the FORS system are provided in Table 3. Usefulness of the FORS-based image guidance during navigation was scored as "better than standard guidance" in 16 out of 21 procedures (76%) and was never scored as "worse than standard guidance". These scores were similar for aortoiliac and peripheral procedures.

Fluoroscopy time, dose area product and task duration
Fluoroscopy time, dose area product and task duration of all the different tasks is provided in Table 5. The series of tasks is relatively small, and the tasks are very heterogenous. Due

to this heterogeneity, it is not possible to draw solid conclusions regarding a potential reduction on x-ray use, despite the fact that several navigational tasks could be completed without or with only minimal x-ray use.

Complications
No device- or FORS-related complications were noted during the 21 procedures. During the hospital stay, a pulmonary infection occurred in 1 patient, that was treated with antibiotics. New-onset atrial fibrillation developed in a second patient, causing type II myocardial ischemia. A third patient showed temporary paraparesis of both limbs after fenestrated EVAR. None of these 3 complications were considered to be related to the FORS-enabled devices, and all 3 complications resolved during hospital stay.

DISCUSSION

This report describes the first clinical experiences from medical use of Fiber Optic RealShape technology, a new technology that shows FORS-enabled catheters and guidewires in color, in real time, in 3D, and using light instead of x-ray.

Sixty-six endovascular navigation tasks were attempted with FORS-enabled guidewire or catheter, or both. Sixty of these were performed successfully with FORS enabled devices, which appears promising, given that only 2 different catheters (Cobra C2 and Berenstein configuration) were available. In future releases of the system, more device lengths and catheter shapes are expected to be supported with FORS-technology. This will undoubtedly increase the usability of the FORS-system in a wider spectrum of anatomical variations.

FORS-enabled devices are radiopaque and fully compatible with regular 0.035-inch guidewires and catheters. When a FORS-enabled guidewire is used in combination with a regular catheter, the wire still provides excellent visibility with FORS, and the shape of the wire in most situations gives an impression of the position of the catheter (*Figure 4*).
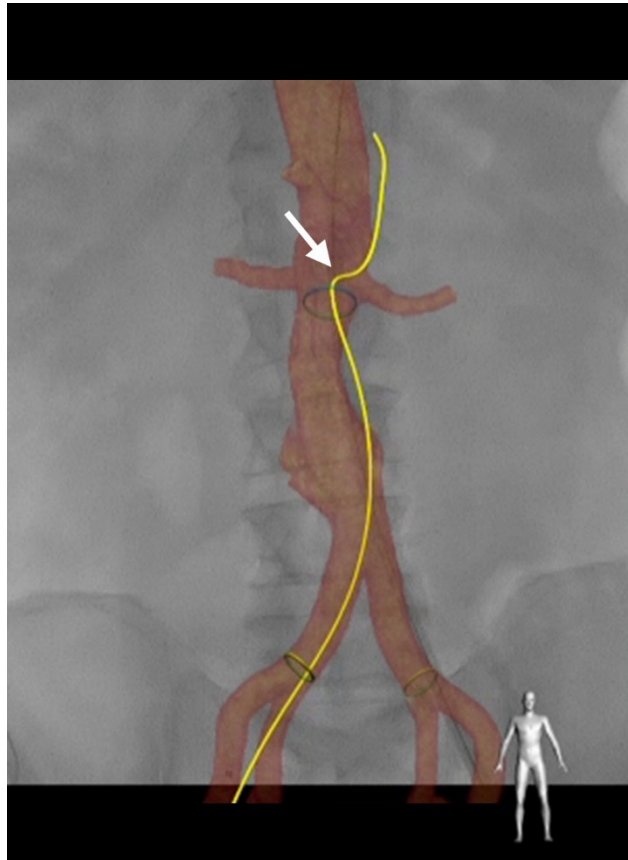
Figure 4: *Advancement of a conventional catheter over a Fiber Optic RealShape (FORS) enabled guidewire. A conventional pigtail catheter is advanced over the guidewire, which is visible due to the changes in guidewire shape. The white arrow indicates the position of the pigtail catheter.*

When the FORS-enabled catheter is combined with a regular non-FORS guidewire, the catheter is still visible in 3D. Depending on the stiffness of the wire, an impression of the position of the wire is visible, without using x-ray, as long as the wire is positioned in the catheter.

An important part of this feasibility study was the qualitive assessment of the performance of the FORS system. The technical characteristics of the FORS-enabled guidewire and catheters were rated as "at par" with regular devices. Also, the compatibility with ancillary devices and the responsiveness of the FORS-based visualization was scored positive in all cases.

The usefulness of the FORS-based image guidance during navigation was scored as "better than standard guidance" in 16 out of 21 procedures (76%) and "equal to standard guidance" in 5 procedures. "Standard guidance" for complex EVAR in our center means

the use of a 3D overlay of a peroperatively acquired cone-beam computed tomography angiography, which to our knowledge, is the best available x-ray based guidance so far. For EVPLR "standard guidance" consists of fluoroscopy with use of an overlay of 2D DSA.

The reason why the usefulness of FORS-based guidance was scored as "better," or "equal" compared to standard guidance, was not registered in the report forms. The operators were, however, positive on the ability to see the directions in which the devices pointed and moved in 3D. For comparison, an example of an x-ray image versus a FORS-based image is shown in *Figure 5*.
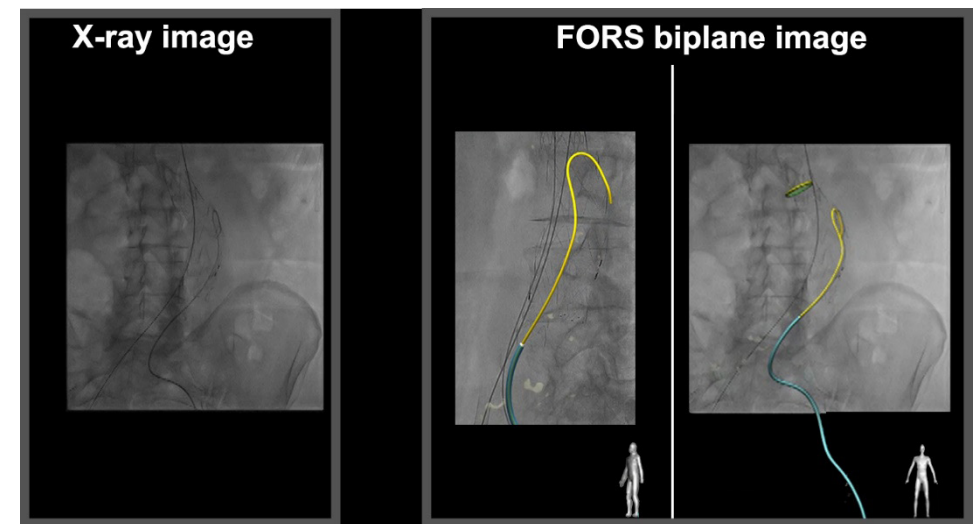
Figure 5: *Comparison of X-ray visualization and Fiber Optic RealShape (FORS) based biplane visualization of Cobra-2 catheter and guidewire. Shading, and distal tip marker emphasize the shape and facing direction of the devices.*

Furthermore, the fact that viewing angles with FORS are unrestricted, was experienced as a major advantage. *Figure 6* shows a patient with tortuous iliac arteries. In the anteroposterior view it appeared difficult to pass a severe kink. When the image was rotated to an extreme caudocranial view, the direction of the kink became clear, which facilitated navigation. This view would have been impossible with fluoroscopy because the C-arm would have needed to be rotated through the patient to achieve this.
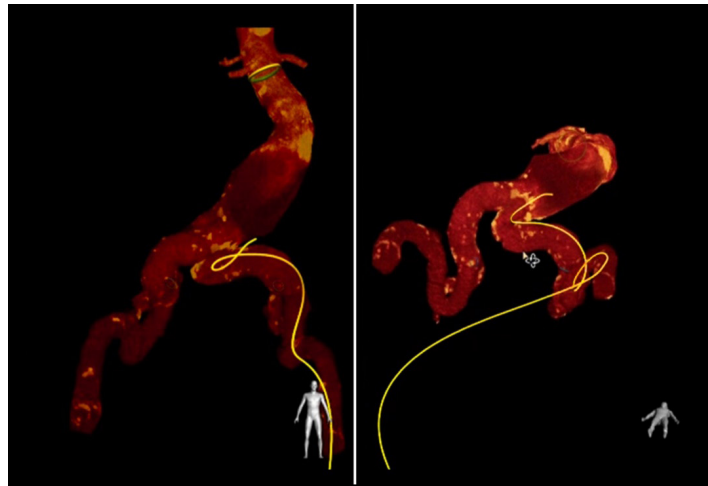
Figure 6: *Catheterization of a tortuous iliac artery using biplane viewing mode. The biplane visualization is composed of an anterior-posterior view (left) and caudal view (right) of the computed tomography angiography (CTA), and provides useful 3D information to assist device manipulation within a tortuous iliac segment.*

In addition, the operators found it beneficial to have a biplane view. For cannulation of a contralateral limb from a bifurcated stent graft, for instance, two x-ray images from different angles were acquired from the deployed stent graft. These x-ray images could be used as an overlay in the biplane mode, that, in combination with the 3D view of the guidewire and catheter, was experienced as helpful by the operators (*Figure 7*).
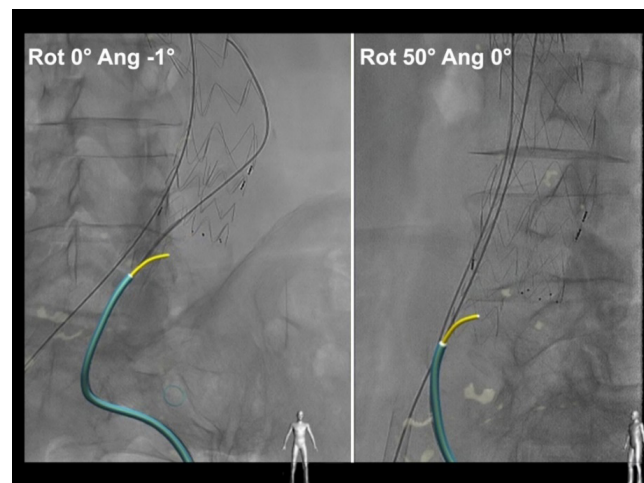
Figure 7: *Catheterization of a contralateral limb during endovascular aortic repair (EVAR), using biplane viewing mode. The biplane visualization is composed of an anterior-posterior X-ray projection (left) and a 50° LAO X-ray projection (right) of the EVAR stent, and provides 3D information to assist catheterization of the contralateral limb within the aneurysm sack.*

Besides improved visualization, FORS has also been developed to reduce x-ray doses. This first feasibility study, however, was not designed to prove radiation reduction with FORS. In this study we did see that several tasks could be performed without or with very limited use of x-ray, including: cross over of the aortic bifurcation, stenotic lesion crossing and cannulation of the contralateral limb. Randomized trials with less heterogenous pathology are needed to objectively quantify x-ray reduction using FORS technology. Similarly, procedure times, technical success and complication rates will have to be analyzed to assess the benefit of the adjunctive image guidance provided by FORS technology in more qualitative terms.

In literature, several other approaches have been proposed to enable x-ray reduction and/or 3D visualization of endovascular devices inside the body of which ultrasound-based systems, electromagnetic (EM) tracking systems and robotic catheter systems have shown particular potential.[5]

Duplex ultrasound or intravascular ultrasound (IVUS) guidance can reduce radiation exposure and contrast volume in endovascular procedures.[6–8] In fact, in patient with contrast allergy and straight-forward anatomy, duplex ultrasound was proven to be non-inferior to conventional fluoroscopic guidance in EVPLR.[9] While the use of US or IVUS imaging, has a positive impact on radiation and contrast use, it does not improve device navigation as these techniques lack 3D visualization and are characterized by a narrow field of view and high image noise.

EM tracking systems enable real-time tracking of endovascular devices in 3D space, using a combination of electromagnetic sensors embedded in the tip of the endovascular devices and an electromagnetic field generator.[10,11] Compared to FORS technology, these EM tracking systems have several drawbacks. Firstly, EM tracking quality is negatively affected by electromagnetic interference caused by nearby electronic equipment, such as the C-arm system. Secondly, the trackability of the current EM tracking systems is limited to the tip of the device, whereas FORS technology visualizes the entire devices. Full-length device visualization provides the physician additional cues on device tension, for instance, its likelihood to dislodge from its position. Thirdly, the integration of the EM sensors in guidewires and catheters, has been shown to influence their mechanical properties.[10,11] Whereas, in the current study, all operators rated the FORS-enabled guidewire and catheter as "at par" with the non–FORS-enabled devices that the operators normally used.

Robotic catheter systems are remotely operated steerable catheters with multiple degrees-of-freedom and a deformable catheter-tip. Robotic device control improves the stability and steerability of the device, resulting in fewer wall-hits and less histopathological damage compared to conventional catheter manipulation.[12] Device visualization is provided by either fluoroscopic imaging (in 2D), magnetic tracking (in 3D) and/or a visualization of the commanded catheter position (in 3D). Cochennec et al.[13] reported a 81% success rate of the cannulation of visceral and renal arteries during

FEVAR/BEVAR with a mean cannulation time of 4:20 minutes using fluoroscopic guidance. Bismuth et al.[14] reported 95% cannulation success rate during EVPLR with mean cannulation time of 21 minutes using a combination of fluoroscopic guidance and the visualization of the commanded catheter position. Both systems used in these single-arm feasibility studies are heavily dependent on fluoroscopic guidance, and lack full-length device visualization in 3D.

Limitations

Although the operators had experience with the system in preclinical studies, they went through a learning curve during clinical use. The optimal visualization settings (regarding viewing angle, magnification, monoplane or biplane mode, and optimal overlay) had to be identified for the different types of procedures. Also, workflow improvements, like the optimal positioning of the system, to work from both the groin and the arm, had to be learned during the study. In this first study, the technical success would probably have been higher when more than two differently shaped catheters had been available. Other limitations for clinical use are the limited working length of the catheters and guidewire available for this study and also the inability to backload the guidewires used in this study. These issues will be addressed in future releases of the system.

Final limitations during this study were technical issues with the FORS equipment. The technology could not be used in one patient, and using two FORS devices at the same time was impossible in one other patient, which probably affected study results.

CONCLUSION

Real-time 3D navigation using FORS technology is safe and feasible in endovascular procedures. Comparative studies are needed to prove and quantify the benefits and potential radiation reduction for all types of endovascular procedures.

ACKNOWLEDGEMENTS

REFERENCES

1   Cardis E, Vrijheid M, Blettner M, Gilbert E, Hakama M, Hill C, et al. Risk of cancer after low doses of ionising radiation - Retrospective cohort study in 15 countries. *Br Med J* 2005;**331**(7508):77–80. Doi: 10.1136/bmj.38499.599861.E0.

2   Leuraud K, Richardson DB, Cardis E, Daniels RD, Gillies M, O'Hagan JA, et al. Ionising radiation and risk of death from leukaemia and lymphoma in radiation-monitored workers (INWORKS): An international cohort study. *Lancet Haematol* 2015;**2**(7):e276–81. Doi: 10.1016/S2352-3026(15)00094-0.

3   National Research Council. Health Risks from Exposure to Low Levels of Ionizing Radiation: BEIR VII Phase 2. *Washington, DC Natl Acad Press* 2006:424. Doi: 10.17226/11340.

4   Jansen M, Khandige A, Kobeiter H, Vonken E-J, Hazenberg C, van Herwaarden J. Three Dimensional Visualisation of Endovascular Guidewires and Catheters Based on Laser Light instead of Fluoroscopy with Fiber Optic RealShape Technology: Preclinical Results. *Eur J Vasc Endovasc Surg* 2020;**0**(0). Doi: 10.1016/j.ejvs.2020.02.035.

5   De Ruiter QMB, Moll FL, Van Herwaarden JA. Current state in tracking and robotic navigation systems for application in endovascular aortic aneurysm repair. *J Vasc Surg* 2015;**61**(1):256–64. Doi: 10.1016/j.jvs.2014.08.069.

6   Makris GC, Chrysafi P, Little M, Patel R, Bratby M, Wigham A, et al. The role of intravascular ultrasound in lower limb revascularization in patients with peripheral arterial disease. *Int Angiol* 2017;**36**(6):505–16. Doi: 10.23736/S0392-9590.17.03866-4

7   Pearce BJ, Jordan WD. Using IVUS during EVAR and TEVAR: Improving Patient Outcomes. *Semin Vasc Surg* 2009;**22**(3):172–80. Doi: 10.1053/j.semvascsurg.2009.07.009.

8   Krasznai AG, Sigterman TA, Welten RJ, Heijboer R, Sikkink CJJM, Van De Akker LHJM, et al. Duplex-guided percutaneous transluminal angioplasty in iliac arterial occlusive disease. *Eur J Vasc Endovasc Surg* 2013;**46**(5):583–7. Doi: 10.1016/j.ejvs.2013.08.011.

9   Bolt LJJ, Krasznai AG, Sigterman TA, Sikkink CJJM, Schurink GWH, Bouwman LH. Duplex-guided versus Conventional Percutaneous Transluminal Angioplasty of Iliac TASC II A and B Lesion: A Randomized Controlled Trial. *Ann Vasc Surg* 2019;**55**:138–47. Doi: 10.1016/j.avsg.2018.07.047.

10 Tystad Lund K, Tangen GA, Manstad-Hulaas F. Electromagnetic navigation versus fluoroscopy in aortic endovascular procedures: a phantom study. *Int J Comput Assist Radiol Surg* 2017;**12**(1):51–7. Doi: 10.1007/s11548-016-1466-4.

11 Condino S, Calabrò EM, Alberti A, Parrini S, Cioni R, Berchiolli RN, et al. Simultaneous tracking of catheters and guidewires: Comparison to standard fluoroscopic guidance for arterial cannulation. *Eur J Vasc Endovasc Surg* 2014;**47**(1):53–60. Doi: 10.1016/j.ejvs.2013.10.001.

12 Rafii-Tari H, Riga C V., Payne CJ, Hamady MS, Cheshire NJW, Bicknell CD, et al. Reducing contact forces in the arch and supra-aortic vessels using the Magellan robot. *J Vasc Surg* 2016;**64**(5):1422–32. Doi: 10.1016/j.jvs.2015.06.215.

13 Cochennec F, Kobeiter H, Gohel M, Marzelle J, Desgranges P, Allaire E, et al. Feasibility and safety of renal and visceral target vessel cannulation using robotically steerable catheters during complex endovascular aortic procedures. *J Endovasc Ther* 2015;**22**(2):187–93. Doi: 10.1177/1526602815573228.

14 Bismuth J, Duran C, Stankovic M, Gersak B, Lumsden AB. A first-in-man study of the role of flexible robotics in overcoming navigation challenges in the iliofemoral arteries. *J Vasc Surg* 2013;**57**(2 SUPPL.):14S-19S. Doi: 10.1016/j.jvs.2012.08.124.

SUPPLEMENTAL TABLES

Supplemental Table 1: *Patient characteristics at baseline*

Variable	Procedure		All Patients
	Aneurysm Repair (N=13)	Peripheral Lesion Repair (N=8)	All Patients (N=21)
Sex, No.			
Female	2	3	5
Male	11	5	16
Age, y			
Mean (SD)	68.8 (10.1)	69.2 (5.8)	68.9 (8.5)
Min-Max	48-89	60-77	48-89
BMI, kg/m2			
Mean (SD)	27.7 (3.7)	27.5 (4.3)	27.6 (3.8)
Min-Max	23-34	21-33	21-34

Supplemental Table 2: *Comorbidities*

Parameter		Procedure				All Patients	
		Aneurysm Repair		Peripheral lesion treatment			
		N	%	N	%	N	%
CAD symptoms	MI	5	38.5	3	37.5	8	38.1
	UA	1	7.7	0	0	1	4.8
	No	7	53.8	5	62.5	12	57.1
COPD	Yes	1	7.7	2	25.0	3	14.3
	No	12	92.3	6	75	18	85.7
CVA	Yes	1	7.7	1	12.5	2	9.5
	No	12	92.3	7	87.5	19	90.5
Diabetes	Yes	1	7.7	3	37.5	4	19.0
	No	12	92.3	5	62.5	17	81.0
Hypercholesterolemia	Yes	4	30.8	0	0	4	19.0
	No	9	69.2	8	100	17	81.0
Hypertension	Yes	11	84.6	4	50.0	15	71.4
	No	2	15.4	4	50.0	6	28.6
Renal Insufficiency	Yes	5	38.5	2	25.0	7	33.3
	No	8	61.5	6	75.0	14	66.7
Smoking	Current	3	23.1	0	0	3	14.3
	Former	10	76.9	3	37.5	13	61.9
	Never			5	62.5	5	23.8
NYHA Class	I	5	38.5	0	0	5	23.8
	II	7	53.8	6	75.0	13	61.9
	III	1	7.7	2	25.0	3	14.3

CAD = coronary artery disease, MI = myocardial infarction, UA = unstable angina, COPD = chronic obstructive pulmonary disease, CVA = cerebrovascular accident

Supplemental Table 3: *Specification of study procedures*

Patient	Indication	Type of procedure
1	Iliac aneurysm	EVAR
2	PAOD	Recanalization Internal iliac Artery
3	Infrarenal Aortic Aneurysm	EVAR
4	PAOD	PTA SFA
5	Thoracoabdominal aneurysm	Fenestrated (3) and Branched (1) EVAR
6	PAOD	PTA SFA and PA
7	Juxtarenal Aortic Aneurysm	FEVAR (2 fenestrations)
8	Juxtarenal Aortic Aneurysm	FEVAR (4 fenestrations)
9	PAOD	PTA CIA
10	Infrarenal Aortic Aneurysm	EVAR
12	Infrarenal Aortic Aneurysm	EVAR
13	Infrarenal Aortoiliac Aneurysm	EVAR + IBD
14	PAOD	PTA CIA
15	PAOD (Iliac in-stent stenosis)	PTA iliac stent
16	PAOD	Recanalization occluded iliac stent
17	Popliteal aneurysm	EVPR
18	Infrarenal Aortic Aneurysm	EVAR
19	Thoracoabdominal Aneurysm	BEVAR (3 Branches)
20	Thoracoabdominal Aneurysm	BEVAR (3 Branches)
21	Infrarenal Aortoiliac Aneurysm	EVAR with embolization IIA
22	Juxtarenal Aortic Aneurysm	FEVAR (4 fenestrations)

EVAR = endovascular aortic repair, PAOD = peripheral arterial occlusive disease, IBD = iliac branched device, PTA = percutaneous transluminal angioplasty, SFA = superficial femoral artery, PA = popliteal artery, CIA = common iliac artery, EPR = endovascular popliteal artery repair, FEVAR = fenestrated endovascular aortic repair, BREVAR = branched endovascular aortic repair. IIA = internal iliac artery

Supplemental Table 4: *Final catheter and guidewire combinations*

Completed Task	Guidewire	Catheter	N Tasks	%
Yes	FORS-enabled	FORS-enabled Berenstein	34	51.5
	FORS-enabled	FORS-enabled Cobra 2	10	15.2
	FORS-enabled	Regular	16	24.2
	Regular	Regular	5	7.6
No			1	1.5
Total			66	100

CHAPTER | 9

Summary, General Discussion
and Future Directions

SUMMARY

Endovascular techniques have gone from an emerging technology to a market share leader in the treatment of common vascular diseases. Compared to traditional open surgical treatment, the endovascular approach shows improved peri-operative morbidity, recovery time and short- to midterm outcomes in the majority of the patient population. Making the endovascular approach particularly suitable for older and fragile patients. While the proportion between endovascular and open surgical treatment has stabilized around 60%, population-based registry studies in the EU and US show continued growth in absolute procedure rates due to an aging population and a shift towards early intervention.

Market evaluations in 2021 estimated the endovascular device market at a net worth of €5.1 billion, with projected year-over-year growth of 5% until 2026.[1] This growth has led to increased investment in the research and development of innovative endovascular technologies, with a significant portion of these efforts being focused on imaging. Endovascular imaging plays a critical role in planning and execution of endovascular procedures, and advancements in this field can improve patient outcomes, reduce procedure times, and increase efficiency.

To ensure the continued advancement of the endovascular field, it is crucial to prioritize the development of more advanced imaging technologies beyond the current cornerstone of fluoroscopy. While fluoroscopy has been widely used and established for the past two decades, it falls short in meeting all the needs of modern complex endovascular treatment. Two significant limitations of fluoroscopy are: the negative side effects of radiation and the limitations of fluoroscopy in terms of image guidance.

The negative side effects of radiation

Medical imaging and interventional procedures that involve radiation are widely used in modern medicine. While the benefits of radiation-based imaging outweigh the risks, repeated exposure can accumulate and pose a risk. Especially in progressive diseases that require repeated monitoring scans and interventions, such as vascular aneurysms or peripheral artery disease.

Despite efforts to minimize radiation exposure, complex procedures remain a challenge, leading to long procedure times and high radiation exposure[2,3]. Further reducing the radiation exposure levels is important for the patient, but perhaps even more so for the medical staff in the operating room. Although exposure levels of staff members are significantly lower than those of patients, physicians do accumulate a significant amount of radiation throughout their lifelong careers in endovascular surgery. In fact, the yearly occupational dose of interventional radiologists and vascular surgeons is amongst the highest observed in employees in medicine. Especially when considering that nowadays physicians are introduced to endovascular techniques early

on in their careers, leading to substantial overall accumulative lifetime doses. Exposure at younger age further increases the chance that radiation-induced damage with long latency phase can break out into cancer at an older age [4], especially for those that are more radiosensitive.

Therefore, it is crucial to develop more advanced imaging technologies beyond fluoroscopy to reduce the radiation burden of endovascular procedures and decrease the risk of negative side effects for both patients and medical staff.

The limitations of fluoroscopy in terms of image guidance

Fluoroscopy's limitations in providing adequate image guidance during complex procedures are well documented. This 2D projection-based imaging method can result in overlapping structures and misleading images when viewed from a single angle. To overcome these limitations, there is a growing need for physicians to have access to real-time 3D imaging of the entire vascular system and the endovascular devices, providing more accurate morphological assessment, sizing, and spatial guidance. Additionally, visualization of the devices in 3D can improve device steerability, providing crucial cues on device tension, curvature, and the direction of the distal tip.

Aim

This thesis aims to provide insights in the evolving tools for 1) radiation reduction and 2) improvement of intraoperative image guidance, during endovascular treatment of aneurysmatic aorta disease and peripheral artery disease. In doing so, this thesis has a specific focus on a newly released technology for intraoperative image guidance developed by Philips Medical: Fiber Optic RealShape. A technology that holds premise to both reduce radiation effects and improve intraoperative image guidance.

Part I: Radiation and Education

The essentials of radiation physics of standard 2D fluoroscopy are discussed in **Chapter 2**. This chapter provides physicians with clinically relevant strategies to keep radiation exposure of themselves, their operating team and their patients as low as reasonably achievable, while maintaining image quality and workflow ergonomics. Some important strategies include the optimization of operating room setup and imaging protocols, frame rate reduction, active field size collimation, minimization of C-arm rotation and optimization of operator shielding. Perhaps most importantly, this chapter stimulates physicians to recognize and anticipate radiation-demanding tasks and settings during endovascular interventions, which allows physicians to take precautions on moments when they are most needed.

Additional to these best practice guidelines, we have investigated a recent development that can help shield physicians from scatter radiation: disposable radiation-absorbing drapes, as described in **Chapter 3**. These sterile drapes are placed on top of

the patient's body and cast a low radiation 'shadow' in which physicians can position themselves throughout the procedure. This non-randomized study, involving 49 patients, demonstrates the efficacy of the radiation absorbing drape in the endovascular treatment of peripheral artery disease. The drapes account for a 66-68% reduction of the relative chest exposure of the primary and secondary physician. The drape has shown no added benefit nor drawback for sterile nurses during peripheral interventions, as their exposure levels are already low in general. Radiation absorbing drapes thereby form a useful addition to the existing strategies to lower occupational radiation exposure, such as collimation and ceiling-mounted leaded glass-shields.

Chapter 4 proposes a new preclinical cadaver model for research and training of endovascular image guided interventions in the aorta and lower extremity. This model, developed in the UMC Utrecht, uses the torsos and lower extremities of fresh frozen human body donors. The cadaver model thereby offers a safe environment with high clinical fidelity to conduct guidewire and catheter manipulation, contrast injection and endovascular treatment with stents or atherectomy devices. This model is suitable to gain clinical experience and assess new endovascular techniques. Additionally, this model is suitable for the optimization of intraoperative imaging protocols, rotational scans and radiation studies, because of its clinically similar tissue and radiation properties.

Part II: Intraoperative Image guidance

Throughout the last decade, new imaging tools and techniques have appeared that provide multiplanar or three-dimensional visualization of the vascular anatomy and/or endovascular devices. The current state of imaging and navigation in aortic interventions have been reviewed by de Hertault et al.[5] and de Ruiter et al.[6], respectively. Recent developments include robotic, electromagnetic and ultrasound-assisted approaches to localize and control endovascular devices, and the use of cone beam computed tomography (CBCT), image fusion (IF) and intravascular ultrasound (IVUS) to enhance the intraoperative visualization of the abdominal aorta and its side branches.

In **Chapter 5** we seek to provide a similar overview of the current state of imaging and navigation, in the domain of peripheral endovascular interventions. In addition to standard 2D fluoroscopy, we determined nine alternative imaging modalities in this systematic review. Most of these imaging modalities were used as an add-on to fluoroscopy, rather than a replacement. Currently, seven of these imaging modalities are commercially available: CTA, cone beam computed tomography (CBCT), Image Fusion, ultrasound (US), intravascular ultrasound (IVUS) and optical coherence tomography (OCT). We can divide these into two broad categories:

- *Imaging tools that offer real-time insights in the structural composition of the vessel wall and atherosclerotic lesion, such as US, IVUS and OCT.* Being able to differentiate the layers of the vascular wall can aid intraluminal

guidance and re-entry during subintimal crossing. But more importantly, structural information can become pivotal in selecting appropriate treatment strategies for each individual, based on composition and morphology of the atherosclerotic lesion.

- *Imaging techniques that offer 3D insights in vascular anatomy and device location to aid device guidance, such as intraoperative CTA, CBCT and Image Fusion.* These techniques provide a broader overview of the vascular tree, to help navigate devices towards their intended destination. Of these imaging tools, Image Fusion is the most widely adopted in the field of aortic and peripheral endovascular interventions.

In **Chapter 6** we will dive deeper into the benefits and limitations of Image Fusion. Image Fusion combines conventional real-time fluoroscopy with preoperative imaging data, such as CTA. After vessel segmentation and rigid image registration, the three-dimensional vascular anatomy is projected on top of conventional fluoroscopy to form an image fusion roadmap. Insertion of endovascular devices, such as stiff guidewires and stent grafts, cause stretching and elongation of the arteries. This intraoperative displacement of the arteries may deteriorate the utility of the image fusion roadmap.

In this chapter we assess the intraoperative displacement of the arteries during fenestrated and branched endovascular aneurysmatic repair (FEVAR and BEVAR) caused by the insertion of a stiff guidewire and stent deployment system. The focus of this study lies on the displacement of the ostia of the renal and visceral arteries (e.g. coeliac trunk, superior mesenteric artery and left and right renal artery), as the cannulation of these target vessels forms a major component of FEVAR and BEVAR procedure. This study comprises 77 target vessels in 20 patients, in which an average displacement of 7.8 mm was measured compared to the position on preoperative CTA. This extend of misalignment is undesirable in FEVAR and BEVAR procedures, as target vessel cannulation requires high precision; for example, the cannulation of a stenotic renal artery with a luminal diameter of 4mm. Besides, our research shows that the target vessels all move in different directions, which makes it impossible to realign all relevant target vessels at once using re-registration. It is therefore not possible to fully rely on the guidance of the 3D roadmap without continuously having to check its validity and adjust the roadmap's position multiple times throughout the procedure.

Chapter 7 and 8 focus on improvement of the endovascular device navigation using a new-to-world technology in the medical field: Fiber Optic RealShape (FORS). FORS technology has been developed to improve endovascular device navigation and minimize the use of radiation. FORS enables real-time 3D visualization of guidewires and catheters and functions on the principle of measuring strain in optical fibers. These optical fibers are integrated in endovascular guidewires and catheters and transmit laser light. Part of the light is reflected backwards. The wavelength spectrum of this reflected

light depends upon the three-dimensional shape of the optical fibers. By analysing the reflected light, the system can compute the 3D geometry and position of the device.

Priorly, electromagnetic and ultrasound-based systems have already proven capable of tracking of the tip of an endovascular device in 3D. However, FORS is the first technology that allows full-length 3D visualization of an endovascular device, thereby enhancing insight in device tension and overall shape. The FORS system functions in conjunction with a static fluoroscopy system, to register devices and anatomical imaging. The visualization of the FORS-enhanced devices is projected on top of the anatomical imaging. All FORS devices are radiopaque and compatible with conventional guidewires and catheters.

The preclinical study in **Chapter 7** provides proof of concept of the FORS system and its application in the aorta and peripheral arteries. This feasibility study was executed in 3 phantom and 3 porcine models, and involved four user-scenarios with different combinations of anatomical roadmaps (CTA or X-ray) and FORS and non-FORS devices. Six independent physicians (vascular surgeons and interventional radiologists) executed each 24 cannulation tasks. Throughout these experiments the usability and safety of the FORS system was assessed.

The study results show a 99% success rate of the cannulation tasks, without occurrence of any safety issues and with adequate accuracy of the device visualization. User experience was positive. Users unanimously agreed that FORS guidewire and catheters visualization was superior compared to device visualization with conventional X-ray, without compromising mechanical device properties, such as torquability, trackability or pushability.

The subsequent clinical study in **Chapter 8** reports the first experiences of FORS in clinical practice. In total 21 patients with aneurysmatic disease or obstructive peripheral artery disease were included in this feasibility study. The FORS system was used exclusively during navigational tasks of these interventions, while therapeutic tasks were performed according to standard practice using conventional fluoroscopic guidance and conventional treatment devices. Examples of navigational tasks included a.o. the cannulation of a target vessel or cannulation of a stenotic lesion.

In total 66 navigational tasks were performed, of which 44 were succeeded with a FORS-enabled guidewire and catheter and 16 with a combination of a FORS-enabled device and a conventional device. The remaining 5 tasks required conventional guidewires and catheters, due to incompatibility of the catheter shapes with the anatomical geometry. User experience was positive, and the median dose area product (DAP) was 7.14 Gycm², with 3:14 minutes of fluoroscopy time during total task durations of 13:17 minutes. Of these 66 tasks, 9 tasks were executed without any X-ray radiation, and 44 tasks with <60s of fluoroscopy time (mean DAP; 0.79 Gycm², mean task duration; 5:30 min). Thereby holding promise for procedural radiation reduction. Nonetheless, fluoroscopy will remain foundational for therapy execution and verification, at least in

the foreseeable future. Registries and follow-up studies are needed to assess the effect of FORS on technical success, procedure time, radiation dose and contrast volume in clinical practice.

GENERAL DISCUSSION AND FUTURE PERSPECTIVES

Throughout this thesis the importance of endovascular imaging is highlighted for the proper planning and execution of endovascular procedures. Having established the crucial role of endovascular imaging, it is now imperative to consider the future directions and potential advancements in this field.

The future of endovascular imaging and navigation will be shaped by a dynamic interplay between the demands and desires of clinicians and the technological innovations of device manufacturers. In recent years, we have seen promising developments in imaging tools that offer more sophisticated and reliable techniques for guiding endovascular procedures. In the following sections, we will explore some of these cutting-edge advancements and their potential implications for the future of endovascular imaging and navigation.

Visualization of Devices
Multiple chapters of this thesis involve an emerging tool for device visualization in endovascular surgery: Fiber Optic RealShape (FORS). FORS technology breaks through traditional limitations of endovascular imaging by enabling real-time 3D visualization of guidewires and catheters inside the body. This helps clarify the orientation of the proximal tip of the device and provides clues on device tension and torque. All factors which can aid device navigation through the vasculature.

Similar to GPS navigation, device visualization only makes sense if relevant context of the surrounding environment is provided. The surrounding vascular anatomy is provided by means of co-registration of pre-operative (CTA, MRA) or intra-operative (angiography) imaging techniques to show the contours of the vessels. This enables physicians to plan and advance their route towards the anatomical target in 3D space.

Although FORS technology represents a big leap forward from conventional fluoroscopic guidance, there are still several hurdles to take with this novel technology. The FORS platform is currently exclusively available as a limited market release to allow for technology refinement prior to full commercialization. The possibilities and limitations of the FORS platform will solidify as the technology matures and hands-on experience grows. So far, the technology seems to be best fitted for complex endovascular procedures to justify the additional upfront costs.

The FORS-enabled devices are optically connected to the FORS-platform via a docking top and base. Because the devices are tethered, there is no ability to back-load

the guidewires, which limits physicians to switch from one catheter-shape to another. This forms a serious limitation as the shape of the catheter plays a fundamental role to reach the desired target, and multiple catheter shapes may be needed to reach the endpoint.

The need for switching between catheter shapes could be reduced by using steerable sheath whose distal shape can be adapted while in-situ. The distal tip of the sheath can be deflected via a rigid pull-wire mechanism that is controlled from the proximal handle. Within this context, Panuccio et al.[7] was the first to describe the use of steerable sheaths in combination with FORS-enabled guidewires and catheters. Although not part of primary objectives, the authors observed a decrease in torque control of the FORS-enabled catheters compared to conventional catheters when operated through a steerable sheath. The authors decided to change strategy by combining the FORS-enabled guidewires with conventional catheters rather than FORS-enabled catheters, even if this meant the loss of catheter visualization.

To overcome issues with catheter design and torquability, the recently released second generation of the FORS platform has been opened up to conventional catheters from all manufacturers by means of a catheter-agnostic 3D Hub. The 3D Hub is connected to the back of a conventional catheter using a standard Luer-lock system and enables physicians to combine the FORS-enabled guidewire with conventional catheters of choice. Meaning that the catheter design of the FORS platform does no longer have to compete with those from established manufacturers with decades of experience.[8]

While moving away from FORS-enabled catheters, the FORS-enabled guidewires will play an even more important role in procedures. Currently, the FORS-enabled guidewire is available in a single hydrophilic wire configuration, designed to be used across aortic and peripheral procedures (above the knee). To stimulate broad adoption, the portfolio of guidewires will need to be expanded to a multitude of guidewires with different mechanic properties optimized for specific procedures and tasks.

Overall, we can state that FORS technology is still rapidly evolving, with the expansion towards conventional catheters via the 3D Hub as its most important advancements.

The mechanistic benefits of Fiber Optic Shape sensing are not limited to vascular devices and can be applied to a broader range of applications within the vessels, lungs and heart. Bronchoscope navigation in the lungs could be a particularly interesting field for shape sensing technology, as the complexity of navigation through bronchi and bronchioles rises quickly when reaching the outer edges of the lung. The company Intuitive, known for its robotic surgery platforms such as the DaVinci robot, already adopted fiber optic realshape technology in their Ion™ Endoluminal platform. Ion™ consists of a robotic arm and a thin flexible bronchoscope with embedded fiber optic shape sensor to provide precise real-time location and shape information throughout the navigation and biopsy process. Initial results show a strong safety profile, and an encouraging diagnostic yield for smaller and larger nodule biopsy.[9]   As fiber optic

shape sensing continues to evolve, it is likely that we will see even more applications for this technology in a variety of medical applications beyond endovascular and bronchoscopic use.

Although every application of shape sensing presents unique challenges, tracking the advancements in different medical fields can facilitate cross-field knowledge exchange and ultimately enhance the technology for all medical applications.

Manipulation of Devices
While FORS-guidance can greatly improve real-time navigation, it's important to acknowledge that successful target vessel cannulation relies on more than just accurate navigation. Manipulation of the devices can remain tedious and time-consuming, even when the route towards the target is clearly understood. Especially when dealing with stenotic segments that lead to high torque of the device, or large aneurysmal spaces that lead to instability of the device. Steerable sheaths could offer a solution. But their effectiveness can be limited by the number of tortuous vessel segments encountered, because the rigid pull-wire mechanism cannot fully transfer its steering effect from the handle to the tip when the device is already bend through multiple curves.

Another alternative could be robotic assistance, which can combine the benefits of 3D device visualization with robotically precise 3D device steering. Examples of robotic systems in related fields of medicine include the CorPath GRX system from Corindus (coronary interventions) and the Genesis system from Stereotaxis (electrophysiology). While these systems use different operating principles, both make use of the mechanistic benefits of robotic stability, millimetre precision and automated movements to improve endovascular device manipulation. Whereas CorPath initiates device motion from the proximal handle like a conventional device, Stereotaxis technology directly steers the distal tip. This direct tip control remains even when the device is already bend through multiple curves – a feature that can be transformative in difficult cannulations of target vessels.

In addition to improving navigation and precision, robotic systems offer a range of benefits including reduced occupational hazards, and the ability to perform interventions from a distance. This ensures that the physician is protected from radiation exposure, and can work comfortably from the control room without the need to wear lead or scrubs.

The combination of 3D device imaging and robotic assistance can hold great promise for complex endovascular procedures in the future, as it enables 3D movement with high precision. By leveraging these advanced technologies, we may be able to push boundaries of what is possible in the field of endovascular intervention.
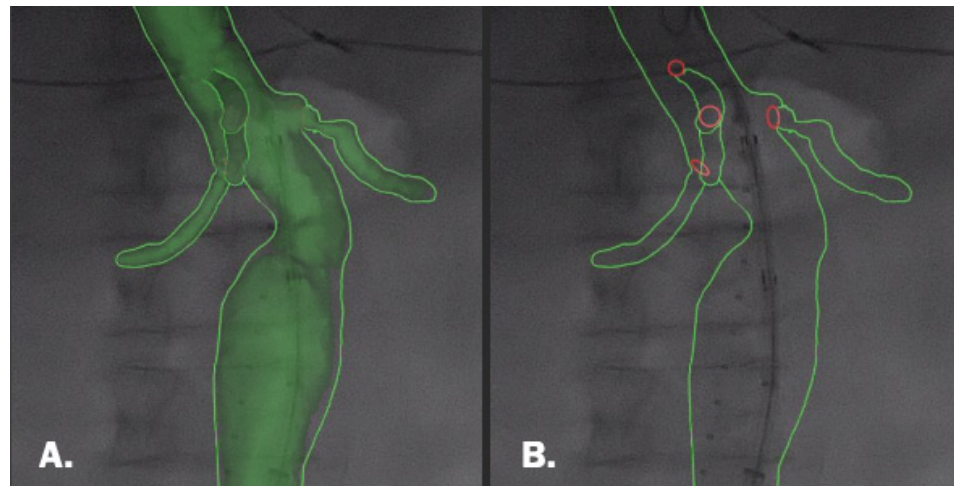
Visualization of Anatomy
The concept of device visualization is intertwined with the visualization of the vascular anatomy. A 2D fluoroscopic image may suffice to gain understanding of the vasculature

in simple procedures, but a more sophisticated approach will be needed when procedural complexity increases. This thesis reported a variety of imaging techniques to visualize vascular anatomy during endovascular procedures, of which 'image fusion' has been the main focus.

Image fusion is the technique of overlaying preoperative CTA or MRA data on live fluoroscopy to aid the 3D understanding of device position in relation to the anatomy. The exact image that is overlayed can range from a full segmentation of the vasculature to simplified graphics of the vessels of interest (*Figure 1*). Image fusion helps to guide endovascular devices towards their anatomical targets, and can reduce overall dose. This dose reduction is especially important for complex endovascular procedures where image fusion helps to avoid multiple angiography runs and steep angulations of the C-arm, both which are key manoeuvres responsible for exponentially increasing radiation exposure.

The popularity of image fusion applications has increased over the last decade when static fluoroscopy systems became standard utility in modern operating suits. These systems were capable of performing image fusion and C-arm cone-beam computed tomography (CBCT) to create intraprocedural 3D images. However, one of the drawbacks of current image fusion applications, is that they extract a rigid geometrical model of the vasculature from the preoperative CTA or MRA. This rigid model forms a static 3D image, that does not correct for any of the morphological changes in vessel geometry – which are bound to occur throughout a typical endovascular intervention. Take for example the stretching and elongation of vessels after stiff guidewire advancement.

To address this issue, various manufacturers are working on the development of deformable (dynamic) image registration applications. These applications generate deformable models of the vascular geometry, in which the distance between certain subsections can be modified or stretched to allow dynamic corrections that match with real-time anatomy. These applications are built on artificial intelligence methods including neural networks and deep learning algorithms. It is likely that these deformable image registration techniques will be broadly adopted in the upcoming years. In fact, Cydar Medical (Cydar Limited; Barrington, UK) has already released an application with dynamic morphology correction, based on deep learning algorithms, shown in *Figure 2*.

Note, that deformable image registration needs real-time geometrical data of the vasculature to perform dynamic morphological corrections of the underlying 3D models. The most simplistic way to generate this data is to extract vessel contours of angiography images. An alternative method is to use shape extraction of the endovascular devices, rather than the vessel contours themselves. After all, the devices can be assumed to lie within the vasculature – and this information is available without performing angiography.
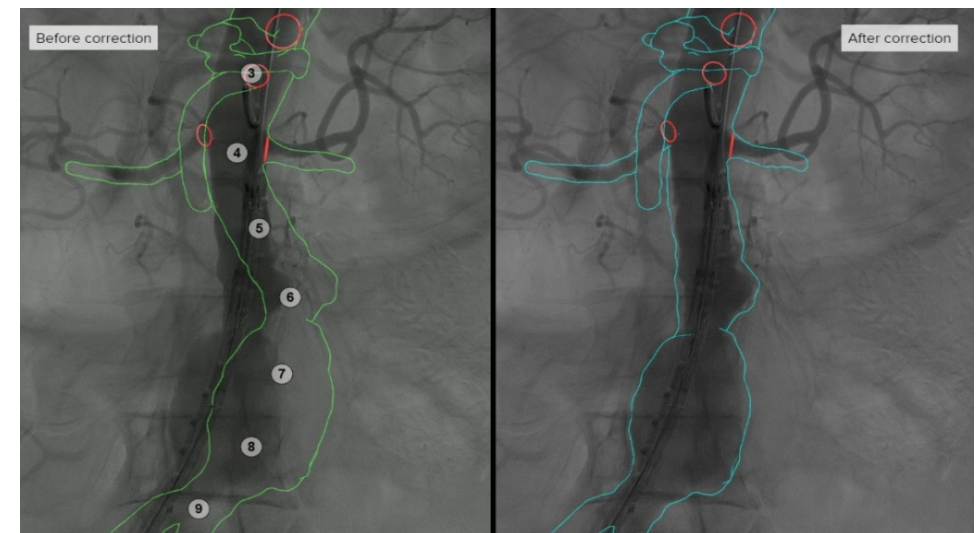
***Figure 2: Dynamic image registration of a CTA-overlay projected on top of fluoroscopy.** The software from Cydar Medical shows the projected outlines of the vascular model before (left) and after (right) dynamic morphology correction. The green outline on the left shows rigid image registration. Whereas the blue outline on the right is based deformable image registration, in which the 3D vascular model is modified by Cydar's deep learning algorithm to match with the real-time imaging. Note the improved match of angiography and vascular model after dynamic morphology correction. All image rights reserved by Cydar Ltd.*

***Figure 1: Image fusion overlay of CTA projected on top of real-time fluoroscopy.** A) Image fusion overlay displayed as full segmentation of the vasculature B) Image fusion overlay displayed as simplified outline of the vasculature (green) with ring markers at the ostium of the target vessels (red). All image rights reserved by Cydar Ltd.*

Several strategies have been investigated to extract the geometry of endovascular devices from fluoroscopy images. Gindre et al.[10] and Kaladji et al.[11] succeeded in creating finite element models (FEM) that could estimate the 3D shape of the endovascular devices. The use of these models in clinical practice have been limited by long computation times. Breininger et al.[12] succeeded in the simultaneous 3D reconstruction of multiple stiff guidewires in the iliac arteries and aorta based on device extraction of fluoroscopic images. But again, the clinical feasibility of this approach was limited due to a low refresh rate and the need for additional fluoroscopy angles that would add procedure time and radiation dose. To approach a clinically acceptable workflow in the future, these algorithms will need to become more sophisticated.

The introduction of shape sensing technology such as FORS, creates new opportunities to extract the geometrical shape from endovascular devices. Firstly, the FORS-platform readily provides full-length computations of the 3D geometry of endovascular devices. The 3D geometry of the devices comes in as a convenient real-time data stream with high refresh rate, without having to use angiography or even fluoroscopy. And perhaps most important, the FORS-platform can co-registers the 3D geometrical device position to a 3D vascular model constructed from CTA or MRA data. The combination of these features forms an ideal foundation to perform dynamic morphology corrections of the 3D vascular model based on the real-time position of the devices. The only thing lacking, is an underlying software algorithm to create and adapt deformable 3D vascular models, as the current FORS platform is only capable of constructing rigid 3D vascular models.

With ongoing advancements in deformable image registration and machine learning, the field of image-guided navigation holds many exciting possibilities for the future. Machine learning algorithms are becoming increasingly sophisticated and able to fuse different types of images more effectively. As a result, we can expect that even very challenging image sources, such as ultrasound or OCT, can be integrated more seamlessly with other imaging modalities, like fluoroscopy, CTA or MRA. This means that image-guidance navigation workflows can become more powerful and accurate, enabling clinicians to identify patterns more effectively and help to improve their clinical decision making.

To fully realize the potential of these advancements, a digital infrastructure will be required that can efficiently and consistently combine the input of multiple imaging sources. Such infrastructure can help to standardize the workflow, reduce imaging artifacts, and stimulate collaborations among clinicians. With these efforts we can look forward to a future where image-guided navigation is more accurate, informative, and collaborative than ever before.

CONCLUSION

In conclusion, the development of advanced imaging and device navigation technologies such as FORS has the potential to revolutionize the field of endovascular image guidance. By improving anatomical understanding and device guidance while reducing the need for ionizing radiation, these technologies offer significant benefits for both patients and healthcare providers.

As 3D imaging and device navigation technologies become more widely adopted, we anticipate that they will simplify endovascular tasks, speed up procedure times, and aid in clinical decision making. By continuing to invest in technological advancements, we can ensure that these tools become widely available and accessible to physicians, enabling them to deliver the highest quality care to their patients.

Overall, the future of endovascular treatment looks bright, and the continued development and adoption of advanced imaging and device navigation technologies will be key to unlocking its full potential.

REFERENCES

1. GLOBE NEWSWIRE. Medi-Tech Insights: Global Endovascular Devices Market. (2022).

2. Hong, M. S., Beck, A. W. & Nelson, P. R. Emerging national trends in the management and outcomes of lower extremity peripheral arterial disease. *Ann Vasc Surg* **25**, 44–54 (2011).

3. Goldsweig, A. M. *et al.* Patient Radiation Dosage During Lower Extremity Endovascular Intervention. *JACC Cardiovasc Interv* **12**, 473–480 (2019).

4. World Health Organization 2016. *Communicating Radiation Risks in Paediatric Imaging.* (2016).

5. Hertault, A. *et al.* Recent developments in intraoperative imaging and navigation during aortic interventions. *Journal of Cardiovascular Surgery* **58**, 883–888 (2017).

6. de Ruiter, Q. M. B., Moll, F. L. & van Herwaarden, J. A. Current state in tracking and robotic navigation systems for application in endovascular aortic aneurysm repair. *J Vasc Surg* **61**, 256–264 (2015).

7. Panuccio, G. *et al.* Endovascular Navigation with Fiber Optic RealShape (FORS) Technology. *J Vasc Surg* 1–8 (2022) doi:10.1016/j.jvs.2022.08.002.

8. Bydlon, T. M., Torjesen, A., Fokkenrood, S., Di Tullio, A. & Flexman, M. L. 3D Visualisation of Navigation Catheters for Endovascular Procedures Using a 3D Hub and Fiber Optic RealShape Technology: Phantom Study Results. *EJVES Vasc Forum* **59**, 24–30 (2023).

9. Reisenauer, J. *et al.* Ion: Technology and Techniques for Shape-sensing Robotic-assisted Bronchoscopy. *Annals of Thoracic Surgery* **113**, 308–315 (2022).

10. Gindre, J. *et al.* Patient-Specific Finite-Element Simulation of the Insertion of Guidewire During an EVAR Procedure: Guidewire Position Prediction Validation on 28 Cases. *IEEE Trans Biomed Eng* **64**, 1057–1066 (2017).

11. Kaladji, A. *et al.* Prediction of deformations during endovascular aortic aneurysm repair using finite element simulation. *Computerized Medical Imaging and Graphics* **37**, 142–149 (2013).

12. K. Breininger *et al.* Simultaneous reconstruction of multiple stiff wires from a single X-ray projection for endovascular aortic repair. *Int J Comput Assist Radiol Surg* **14**, 1891–1899 (2019).

CHAPTER 10

Nederlandse samenvatting

Endovasculaire technieken zijn tegenwoordig niet meer weg te denken als behandeling van veelvoorkomende vasculaire aandoeningen. Endovasculaire technieken zijn populairder geworden dan traditionele open chirurgie, vooral omdat ze veiliger en sneller herstel mogelijk maken, met name bij oudere en kwetsbare patiënten. Ongeveer 60% van de vasculaire behandelingen worden tegenwoordig uitgevoerd met behulp van endovasculaire technieken. Bovendien groeit het aantal endovasculaire ingrepen vanwege een vergrijzende bevolking en een verschuiving naar vroegtijdige behandeling van vasculaire aandoeningen.

In 2021 werd de waarde van de endovasculaire markt geschat op €5,1 miljard, met een verwachte groei van 5% per jaar tot 2026.[1] Deze groei heeft geleid tot een toename van investeringen in onderzoek en ontwikkeling van innovatieve endovasculaire technologieën, waarvan een aanzienlijk deel gericht is op beeldvorming. Endovasculaire beeldvorming speelt een cruciale rol bij de planning en uitvoering van endovasculaire procedures, en vooruitgang op dit gebied kan de resultaten voor patiënten verbeteren, proceduretijden verkorten en de efficiëntie verhogen. Om de vooruitgang van endovasculaire technieken te waarborgen, is het dan ook van cruciaal belang om de ontwikkeling van geavanceerde beeldvormingstechnologieën te prioriteren.

Momenteel wordt fluoroscopie gebruikt als voornaamste beeldvormingstechnologie in endovasculaire procedures. Fluoroscopie is een röntgenfilm waarbij gedurende langere tijd wordt doorstraalt met röntgenstraling om zo bewegende structuren en instrumenten in beeld te brengen. Fluoroscopie wordt al zeker twee decennia lang gebruikt, en qua techniek is er relatief weinig veranderd. Dit terwijl moderne endovasculaire behandelingen een stuk complexer zijn geworden in de loop der tijd. Kort samengevat zijn er twee belangrijke beperkingen van fluoroscopie die we hieronder zullen bespreken. Ten eerste wordt er röntgenstraling gebruikt, wat nadelige gevolgen heeft voor de patiënt en het personeel en ten tweede is de beperkte mogelijkheid tot 3D interpretatie.

Röntgenstraling
Röntgenstraling wordt veel gebruikt in verschillende beeldvormende technieken in de moderne geneeskunde. Hoewel de voordelen van deze beeldvorming opwegen tegen de risico's, kan bij herhaalde blootstelling aan straling een risico opbouwen.
Ondanks inspanningen om stralingsblootstelling te minimaliseren, zijn er regelmatig Forse uitschieters wat betreft proceduretijden en stralingsblootstelling, vooral in complexe procedures.[2,3]

Het verder verlagen van de stralingsblootstelling is belangrijk voor de patiënt, maar ook voor het medisch personeel in de operatiekamer. Hoewel de blootstellingsniveaus van het medisch personeel aanzienlijk lager zijn dan die van patiënten, verzamelen artsen gedurende hun carrière een aanzienlijke hoeveelheid straling. Interventieradiologen en vaatchirurgen zitten zelfs in het top-segment wat betreft jaarlijkse cumulatieve stralingsdosis. De totale cumulatieve dosis wordt waarschijnlijk alleen nog maar hoger, aangezien artsen tegenwoordig al vroeg in hun carrière worden blootgesteld aan endovasculaire technieken. Blootstelling op jonge leeftijd vergroot verder de kans dat stralingsgerelateerde schade met een lange latentiefase kan leiden tot kanker op oudere leeftijd[4], vooral bij degenen die gevoeliger zijn voor straling. Daarom is het cruciaal om meer geavanceerde beeldvormingstechnologieën te ontwikkelen om de stralingsbelasting van endovasculaire procedures te verminderen en het risico op negatieve bijwerkingen voor zowel patiënten als medisch personeel te verlagen.

Beperkte 3D interpretatie
Fluoroscopie is een 2D projectiegebaseerde beeldvormingsmethode, wat inhoudt dat verschillende structuren in hetzelfde vlak over elkaar heen worden geprojecteerd. Dit kan leiden tot overlap van structuren en misleidende beelden, wanneer deze vanuit slechts een enkele hoek worden bekeken. Er is dan ook een groeiende behoefte aan realtime 3D-beeldvorming van de bloedvaten en de endovasculaire devices, waardoor de afwijking nauwkeuriger kan worden gediagnostiseerd en er betere navigatie van de endovasculaire devices kan worden geboden.

Doelstelling
Dit proefschrift heeft tot doel inzicht te bieden in de evoluerende tools voor 1) stralingsvermindering en 2) verbetering van intraoperatieve navigatie tijdens de endovasculaire behandeling van aneurysmatische aortaziekte en perifere arterieel vaatlijden. Hierbij ligt de specifieke focus op een nieuw ontwikkelde technologie voor intraoperatieve navigatie, ontwikkeld door Philips Medical: Fiber Optic RealShape. Een technologie die belofte inhoudt voor zowel het verminderen van straling als het verbeteren van intraoperatieve navigatie.

Deel I: Stralingsvermindering en Educatie
Hoofdstuk 2 bespreekt de essentie van stralingsfysica bij standaard 2D-fluoroscopie. Dit hoofdstuk biedt artsen klinisch relevante strategieën om stralingsblootstelling voor henzelf, hun operatieteam en hun patiënten zo laag mogelijk te houden, terwijl ze de beeldkwaliteit en ergonomie van de workflow behouden. Enkele belangrijke strategieën zijn het optimaliseren van de operatiekameropstelling, het verminderen van de framesnelheid, actieve collimatie, minimalisatie van rotatie van de C-arm en optimalisatie van stralings beschermende middelen. Dit hoofdstuk stimuleert artsen om situaties in de endovasculaire ingreep te herkennen waar veel straling bij vrijkomt, zodat ze voorzorgsmaatregelen kunnen nemen op de momenten dat dit het meest nodig is.

Naast deze richtlijnen voor 'best practices' hebben we gekeken naar recent ontwikkelde maatregelen tegen strooistraling, namelijk de stralingsabsorberende doek, zoals beschreven in **Hoofdstuk 3**. Deze steriele doeken worden op het lichaam van de patiënt gelegd en werpen een zwakke stralings 'schaduw' waarin artsen zich gedurende

de procedure kunnen positioneren. Deze non-randomized studie, met 49 patiënten, toont de doeltreffendheid van de stralingsabsorberende doek aan bij de endovasculaire behandeling van perifere arteriële aandoeningen. De doek zorgt voor een vermindering van 66-68% van de relatieve blootstelling aan straling op de borst van de primaire en secundaire arts. De doek heeft geen extra voordeel of nadeel laten zien voor steriele verpleegkundigen tijdens perifere ingrepen, aangezien hun blootstellingsniveaus over het algemeen al laag zijn. Stralingsabsorberende doeken vormen dus een nuttige aanvulling op de bestaande strategieën om de blootstelling aan beroepsstraling te verminderen, zoals afstemming en aan het plafond gemonteerde loodglas-afschermingen.

In **Hoofdstuk 4** wordt een nieuw preklinisch kadavermodel voorgesteld voor onderzoek en training van endovasculaire navigatie in de aorta en de onderste extremiteit. Dit model, ontwikkeld aan het UMC Utrecht, maakt gebruik van de torso's en onderste extremiteiten van ingevroren menselijke lichaamsdonoren. Het kadavermodel biedt daardoor een veilige omgeving met een hoge klinische nauwkeurigheid om guidewire- en kathetermanipulatie, contrastinjectie en endovasculaire behandeling met stents of atherectomie-apparaten uit te voeren. Dit model is geschikt om klinische ervaring op te doen en nieuwe endovasculaire technieken te beoordelen. Bovendien is dit model geschikt voor de optimalisatie van intraoperatieve beeldvormingsprotocollen, rotatiescans en stralingsstudies, vanwege de klinisch vergelijkbare weefsels en stralingseigenschappen.

Deel II: Intraoperatieve Navigatie

Gedurende het afgelopen decennium zijn nieuwe beeldvormingstools en -technieken verschenen die multidimensionale visualisatie van de vasculaire anatomie en/of endovasculaire devices bieden. De huidige stand van beeldvorming en navigatie bij aorta-interventies is beoordeeld door de Hertault et al.[5] en de Ruiter et al.[6], respectievelijk. Recente ontwikkelingen omvatten robotica, elektromagnetische en ultrasone ondersteunde benaderingen om endovasculaire apparaten te lokaliseren en te bedienen, evenals het gebruik van cone-beam computed tomography (CBCT), beeldfusie (IF) en intravasculaire ultrasone (IVUS) om de intraoperatieve visualisatie van de abdominale aorta en zijn zijtakken te verbeteren.

In **Hoofdstuk 5** proberen we een soortgelijk overzicht te bieden van de huidige stand van beeldvorming en navigatie in het domein van perifere endovasculaire ingrepen. Naast standaard 2D-fluoroscopie hebben we in deze systematische review negen alternatieve beeldvormingsmodaliteiten geïdentificeerd. De meeste van deze modaliteiten werden als aanvulling op fluoroscopie gebruikt, eerder dan als vervanging ervan. Momenteel zijn zeven van deze beeldvormingsmodaliteiten commercieel verkrijgbaar: CTA, cone-beam computed tomography (CBCT), image fusion (IF), ultrasoon (US), intravasculaire ultrasoon (IVUS) en optische coherentie tomografie (OCT). Deze kunnen in twee brede categorieën worden ingedeeld:

- *Navigatietools die realtime inzicht bieden in de structuur van de vaatwand en atherosclerotische laesie, zoals US, IVUS en OCT.* Het vermogen om de lagen van de vaatwand te differentiëren, kan intraluminale begeleiding en herintroductie tijdens subintimale doorgang vergemakkelijken. Maar nog belangrijker is dat structurele informatie cruciaal kan zijn bij het selecteren van geschikte behandelingstrategieën voor elke individuele patiënt, op basis van samenstelling en morfologie van de atherosclerotische laesie.
- *Beeldvormingstechnieken die 3D-inzicht bieden in de vasculaire anatomie en de locatie van apparaten om de apparaatgeleiding te ondersteunen, zoals intraoperatieve CTA, CBCT en IF*. Deze technieken bieden een breder overzicht van de vasculaire boom om apparaten naar hun beoogde bestemming te navigeren. Van deze beeldvormingstools is Beeldfusie het meest wijdverbreid in het veld van aorta- en perifere endovasculaire interventies.

In **Hoofdstuk 6** gaan we dieper in op de voordelen en beperkingen van image fusion. Image fusion combineert conventionele realtime fluoroscopie met preoperatieve beeldgegevens, zoals CTA. Na vaatsegmentatie en rigide beeldregistratie wordt de driedimensionale vasculaire anatomie geprojecteerd bovenop de conventionele fluoroscopie om een image fusion-routekaart te vormen. Invoeging van endovasculaire devices, zoals stijve guidewires en stentgrafts, veroorzaakt oprekking en verlenging van de slagaders. Deze intraoperatieve verplaatsing van de slagaders kan de bruikbaarheid van de image fusion-routekaart verminderen.

In dit hoofdstuk beoordelen we de intraoperatieve verplaatsing van de slagaders tijdens endovasculaire aneurysmareparatie (FEVAR en BEVAR) veroorzaakt door de invoeging van een stijve geleidingsdraad en stentsysteem. De focus van deze studie ligt op de verplaatsing van de ostia van de nier- en viscerale slagaders (bijv. de coeliakie truck, de superieure mesenteriale slagader en de linker- en rechter nierslagader), aangezien de katheterisatie van deze doelvaten een belangrijk onderdeel vormt van de FEVAR- en BEVAR-procedure. Deze studie omvat 77 doelvaten bij 20 patiënten, waarbij een gemiddelde verplaatsing van 7,8 mm werd gemeten in vergelijking met de positie op de preoperatieve CTA. Deze mate van misalignement is ongewenst bij FEVAR- en BEVAR-ingrepen, omdat nauwkeurige katheterisatie van het doelvat vereist is; bijvoorbeeld bij de katheterisatie van een vernauwde nierslagader met een luminaal diameter van 4 mm. Bovendien laat ons onderzoek zien dat de doelvaten allemaal in verschillende richtingen bewegen, waardoor het onmogelijk is om alle relevante doelvaten tegelijkertijd opnieuw uit te lijnen door herregistratie. Het is daarom niet mogelijk om volledig te vertrouwen op de begeleiding van de 3D-routekaart zonder deze voortdurend te controleren op geldigheid en de positie van de routekaart meerdere keren tijdens de procedure aan te passen.

Hoofdstuk 7 en **8** richten zich op de verbetering van de navigatie van endovasculaire devices met behulp van een nieuwe technologie in de medische wereld: Fiber Optic RealShape (FORS). FORS-technologie is ontwikkeld om de navigatie van endovasculaire devices te verbeteren en het gebruik van straling te minimaliseren. FORS maakt realtime 3D-visualisatie van guidewires en katheters mogelijk en werkt op basis van optische fibers. Deze optische fibers zijn geïntegreerd in endovasculaire guidewires en katheters en zenden laserlicht uit. Een deel van het licht wordt gereflecteerd. Het golflengtespectrum van dit gereflecteerde licht hangt af van de driedimensionale vorm van de optische fibers. Door het gereflecteerde licht te analyseren, kan het systeem de 3D-geometrie en positie van het device berekenen.

Voorheen hebben elektromagnetische en echografie-gebaseerde systemen al bewezen in staat te zijn om de punt van een endovasculair apparaat in 3D te volgen. Echter, FORS is de eerste technologie die volledige 3D visualisatie van een endovasculair apparaat mogelijk maakt, waardoor inzicht in de spanning en algehele vorm van het apparaat wordt verbeterd. Het FORS-systeem werkt samen met een statisch fluoroscopie-systeem om apparaten en anatomische beeldvorming te registreren. De visualisatie van de met FORS verbeterde apparaten wordt geprojecteerd bovenop de anatomische beeldvorming. Alle FORS-apparaten zijn radiopaque en compatibel met conventionele guidewires en katheters.

De preklinische studie in **Hoofdstuk 7** levert het conceptuele bewijs voor het FORS-systeem en de toepassing ervan in de aorta en perifere slagaders. Deze haalbaarheidsstudie werd uitgevoerd in 3 fantoom- en 3 varkensmodellen, en omvatte vier gebruikersscenario's met verschillende combinaties van anatomische routekaarten (CTA of röntgen) en FORS- en niet-FORS-devices. Zes onafhankelijke artsen (vaatchirurgen en interventieradiologen) voerden elk 24 canulatietaken uit. Gedurende deze experimenten werd de bruikbaarheid en veiligheid van het FORS-systeem beoordeeld. De resultaten van de studie tonen een slagingspercentage van 99% voor de canulatie taken, zonder enige veiligheidsproblemen en met voldoende nauwkeurigheid van de device visualisatie. De gebruikerservaring was positief. Gebruikers waren het er unaniem over eens dat de visualisatie van FORS guidewires en katheters superieur was in vergelijking met device visualisatie met conventionele röntgenstraling, zonder dat dit ten koste ging van mechanische eigenschappen van het apparaat, zoals draaibaarheid, volgzaamheid of duwkracht.

De daaropvolgende klinische studie in **Hoofdstuk 8** rapporteert de eerste ervaringen van FORS in de klinische praktijk. In totaal werden 21 patiënten met aneurysmatische aandoeningen of obstructieve perifere arteriële aandoeningen opgenomen in deze haalbaarheidsstudie. Het FORS-systeem werd uitsluitend gebruikt tijdens navigatietaken van deze ingrepen, terwijl therapeutische taken werden uitgevoerd volgens de standaardpraktijk met conventionele fluoroscopische begeleiding en conventionele devices. Voorbeelden van navigatietaken omvatten onder andere het canuleren van een

doelvat of het canuleren van een stenotische laesie. In totaal werden 66 navigatietaken uitgevoerd, waarvan er 44 slaagden met een FORS-guidewire en FORS-katheter, en 16 met een combinatie van een FORS-device en een conventioneel device. De overige 5 taken vereisten conventionele guidewires en katheters, vanwege de onbruikbaarheid van de FORS-kathetervormen in de desbetreffende anatomische geometrie. De gebruikerservaring was positief, en het mediane dosis-oppervlakte product (DAP) was 7,14 Gycm², met 3:14 minuten fluoroscopietijd tijdens totale taakduur van 13:17 minuten. Van deze 66 taken werden 9 taken uitgevoerd zonder enige röntgenstraling, en 44 taken met minder dan 60 seconden fluoroscopietijd (gemiddeld DAP: 0,79 Gycm², gemiddelde taakduur: 5:30 minuten). Dit biedt hoop voor het verminderen van procedurele stralingsbelasting. Desalniettemin zal fluoroscopie voorlopig essentieel blijven voor de uitvoering en verificatie van therapieën. Registries en vervolgstudies zijn nodig om het effect van FORS op technisch succes, proceduretijd, stralingsdosis en contrastvolume in de klinische praktijk te beoordelen.

REFERENTIES

1.   GLOBE NEWSWIRE. Medi-Tech Insights: Global Endovascular Devices Market. (2022).
2.   Hong, M. S., Beck, A. W. & Nelson, P. R. Emerging national trends in the management and outcomes of lower extremity peripheral arterial disease. *Ann Vasc Surg* **25**, 44–54 (2011).
3.   Goldsweig, A. M. *et al.* Patient Radiation Dosage During Lower Extremity Endovascular Intervention. *JACC Cardiovasc Interv* **12**, 473–480 (2019).
4.   World Health Organization 2016. *Communicating Radiation Risks in Paediatric Imaging.* (2016).
5.   Hertault, A. *et al.* Recent developments in intraoperative imaging and navigation during aortic interventions. *Journal of Cardiovascular Surgery* **58**, 883–888 (2017).
6.   de Ruiter, Q. M. B., Moll, F. L. & van Herwaarden, J. A. Current state in tracking and robotic navigation systems for application in endovascular aortic aneurysm repair. *J Vasc Surg* **61**, 256–264 (2015).

APPENDICES

&
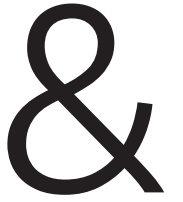
CO-AUTHORS

Rick H.J. Bergmans, MSc
Master Technical Medicine
University of Twente
Enschede, the Netherlands

Trijntje Bloemert-Tuin, MSc
Department of Vascular Surgery
University Medical Center Utrecht
Utrecht, The Netherlands

Prof. Gert J. de Borst, MD, PhD
Department of Vascular Surgery
University Medical Center Utrecht
Utrecht, The Netherlands

Roland W. M. Bullens, MSc, PhD
Image Guided Therapy
Philips Medical Systems
Best, Netherlands

Prof. Ronald L.A.W. Bleys, MD, PhD
Department of Anatomy
University Medical Center Utrecht
Utrecht, The Netherlands

Robbert W. van Hamersvelt, MD, PhD
Department of Radiology
University Medical Center Utrecht
Utrecht, The Netherlands

Constantijn E.V.B. Hazenberg, MD, PhD
Department of Vascular Surgery
University Medical Center Utrecht
Utrecht, The Netherlands

Prof. Joost A. van Herwaarden MD, PhD
Department of Vascular Surgery
University Medical Center Utrecht
Utrecht, The Netherlands

Anuradha Khandige, B Eng
Image Guided Therapy
Philips Medical Systems
Best, Netherlands

Hicham Kobeiter, MD, PhD
Department of Radiology
University Hospital CHU Henri Mondor
Crétei, France

Arjan Koster, MSc
Master Technical Medicine
University of Twente
Enschede, the Netherlands

Prof. Frans L. Moll, MD, PhD
Department of Vascular Surgery
University Medical Center Utrecht
Utrecht, The Netherlands

Quirina M.B. de Ruiter, MSc, PhD
Department of Vascular Surgery
University Medical Center Utrecht
Utrecht, The Netherlands

Prof. Cornelis H. Slump, MSc, PhD
Department of Robotics and
Mechatronics,
University of Twente
Enschede, the Netherlands

Stefan P.M. Smorenburg, MSc
Master Technical Medicine
University of Twente
Enschede, the Netherlands

Merel van der Stelt, MSc
Master Technical Medicine
University of Twente
Enschede, the Netherlands

Evert-Jan P. Vonken, MD, PhD
Department of Radiology
University Medical Center Utrecht
Utrecht, The Netherlands

LIST OF PUBLICATIONS

This thesis

M.M. Jansen, C.E.V.B. Hazenberg, J.A. van Herwaarden. "Reducing radiation exposure in endovascular procedures - Intraoperative management". *Biomaterials and Digital Technologies for Future Individualized Patient Management in Vascular Surgery*. 2019; 103-112. ISBN: 978-2-9544771-3-8

M.M. Jansen, C.E.V.B. Hazenberg, Q.M.B. de Ruiter, R.W. van Hamersvelt, R. L.A.W. Bleys, J.A. van Herwaarden, "Feasibility of fresh frozen human cadavers as a research and training model for endovascular image guided interventions". *PLOS ONE,* 2020: 15(11): e0242596. DOI: 10.1371/journal.pone.0242596

M.M. Jansen, A. Khandige, H. Kobeiter, E.J.P. Vonken, C.E.V.B. Hazenberg, J.A. van Herwaarden. "Three-dimensional visualization of endovascular devices based on laser light instead of fluoroscopy with Fiber Optic RealShape (FORS) technology: Preclinical results.". *Eur J Vasc Endovasc Surg.* 2020 (): S1078-5884(20)30235-5. DOI: 10.1016/j.ejvs.2020.02.035

J.A. van Herwaarden, M.M. Jansen, E.P.A. Vonken, T. Bloemert-Tuin, R.W. M. Bullens, G. J. de Borst, C.E.V.B. Hazenberg, "First-in-Human Clinical Feasibility Study of Endovascular Navigation with Fiber Optic RealShape (FORS) Technology". *Eur J Vasc Endovasc Surg* 2020. DOI: 10.1016/j.ejvs.2020.10.016

M. M. Jansen, M. van der Stelt, S.P.M. Smorenburg, C.H. Slump, J.A. van Herwaarden, C.E.V.B. Hazenberg. "Target vessel displacement during fenestrated and branched endovascular aortic repair and its implications for the role of traditional CTA roadmaps". *QIMS.* 2021; 11(9): 3945-3955. DOI: 10.21037/qims-20-1077

M.M. Jansen, A. Koster, J.A. van Herwaarden, C.E.V.B. Hazenberg, "Reduction of occupational radiation exposure of operators during peripheral endovascular procedures by means of radiation absorbing drapes". In: *Annals of Vascular Surgery*. 2022: 84(8); 336-343. DOI: 10.1016/j.avsg.2022.01.030

Other

Q.M.B. de Ruiter, M.M. Jansen, F.L. Moll et al. "Procedure and step-based analysis of the occupational radiation dose during endovascular aneurysm repair in the hybrid operating room". J Vasc Surg, 2018; 67(6):1881-1890. DOI: 10.1016/j.jvs.2017.09.043

W.H. Nijhof, M.M. Jansen, G.J. Jager et al. "Feasibility of a low concentration test bolus in CT angiography". *Clin Radiol.* 2016; 71(12): 1313.e1-1313.e4. DOI: 10.1016/j.crad.2016.08.008

S. Ailoaei, P. Wright, S. Griffiths, M.M. Jansen, S. Ernst. "Telerobotic interventions from a distance: an intial experience in 3D phantom mapping". *Eur Heart Journal.* 2021; 2(4). DOI: 10.1093/ehjdh/ztab104.3087

DANKWOORD

Zes jaar geleden rolde ik vanuit mijn afstudeerstage Technische Geneeskunde in dit onderzoekstraject. Een PhD op de afdeling Vaatchirurgie van het UMCU met een nog wat onduidelijke focus. De jaren die volgden zaten vol variatie, maar weefden zich rondom die rode draad; het verbeteren van intra-operatieve imaging tijdens endovasculaire procedures. Ik ben trots en opgelucht dat alles nu samenkomt in dit werk, dat nu voor jullie ligt, hier in dit proefschrift.

De jaren in het UMC Utrecht hebben mijn klinische blik verruimd, mijn academische kennis vergroot en mijn netwerk verbreed. Ik heb zo veel fantastische mensen mogen ontmoeten en het gevoel van saamhorigheid en teamspirit op de operatiekamer leren kennen. Ook nu, na mijn PhD blijft die operatiekamer onderdeel van mijn werkende leven. Het geruis van OK-kleding en piepende crocs op een schone vloer – heerlijk.

De laatste delen van dit proefschrift zijn geschreven tijdens de highs en lows van het post-PhD tijd. Een tijd waarin ik enorm veel moeite had om dit proefschrift definitief af te ronden, te midden van het geraas van het dagelijks leven vol nieuwe uitdagingen en avonturen. Het feit dat dit dankwoord tot stand is gebracht vanuit 3 verschillende koffiekamers van ziekenhuizen in de Benelux illustreert dat gegeven. Het is onvermijdelijk dat ik met der tijd mensen ben vergeten te benoemen, maar ik ben er van overtuigd dat jullie weten wie jullie zijn.

Allereerst mijn gewaardeerde promotor, Joost van Herwaarden. Bedankt voor je onuitputtelijke enthousiasme, je vertrouwen en je deskundige en kritische blik. Je hielp me steeds weer de juiste focus aan te brengen wanneer de samenhang wazig werd. Hoewel ik veel van je heb geleerd op het gebied van de wetenschap, blijven de gedeelde uren op de operatiekamer toch echt mijn favoriet. Dank voor het delen van je al je kennis en ervaring tijdens de boeiende vaatchirurgie procedures.

Stijn Hazenberg, mijn copromotor, bedankt voor de twee-wekelijkse updates die me hielpen het overzicht (enigszins) te bewaren en vervolgstappen te definiëren. Jou positiviteit was een goede bron van motivatie, en de uitstapjes naar het dierenlab waren een welkome afwisseling van de dagelijkse sleur.

Quirina de Ruiter, na een eerste dag meesnuffelen op de operatiekamer was ik meteen diep geïntrigeerd. Je oprechte enthousiasme voor het FORS project werkte aanstekelijk en ik ben dankbaar voor de tijd en moeite die je hebt gestoken in een soepele overdracht.

Vaatchirurgen, fellows, onderzoekers, collega's, dames van het secretariaat vaatchirurgie, de hele crew van Philips FORS, Natasja (!!!) en Trijntje (!!!), dank voor al jullie veelzijdige input; de belangrijke inhoudelijke zaken, de kletspraatjes, de lessen in statistiek, het aanbrengen van context en nuance, de cappuccino's tussen twee procedures door, de vele ochtenden Insanity, en het gezelschap op de vele congressen. Maar vooral, dank dat jullie me samen altijd het gevoel hebben gegeven dat ik welkom was.

Colleagues from the electrophysiology field, Tommi (!!!), Stefano (!!!), my sincere gratitude, not only for the wealth of knowledge you've shared, but also for teaching me to let go and accept what I can't change.

Stefan, heel veel dank voor je stok achter de deur. Ook al was ik lastig mens af en toe.

Mijn lieve, lieve vrienden, dank voor alle support, afleiding en geduld. Met zoveel leuke en uiteenlopende vrienden om me heen besef ik me dat ik een heel gelukkig mens ben. Ik voel zoveel warmte en dankbaarheid voor al die fijne momenten waarop ik met jullie heb mogen dansen, eten, festivallen, mijmeren, beachvolleyballen, surfen, kroeghangen, bellen lekkere koffie halen, wildkamperen, uitrazen, grenzen verleggen, kerstdiners koken, zonsondergangen kijken bij Jumpteam, oesters plukken, nieuwe plekken ontdekken, mijlpalen vieren. Dankzij jullie waren er altijd nieuwe prikkels om te onderzoeken en verder te ontwikkelen. En er was altijd ruimte om mezelf te zijn.

Mijn familie, mam (!!!), pap (!!!), Thomas (!!!), oma (!!!) jullie hebben altijd oprechte interesse getoond, in zo ongeveer alles wat ik doe. Ik weet dat jullie altijd trots op me zullen zijn – en dat is een waardevol goed. Met liefde reisde ik van West naar Oost voor een kop thee, een verjaardag, kerstdiner, een kopje soep, of een bioscoop bezoek, en dat blijf ik maar al te graag doen.

Floriaan, dankzij jouw aanwezigheid voelde ik de veiligheid en de vrijheid om te ontdekken - mijn hart in nieuwe avonturen te storten. Onze levens zijn soms rommelig, en passen niet altijd perfect, maar ik ben zo dankbaar voor alle warmte die ik heb gevonden in jouw armen.

CURRICULUM VITAE

Marloes Jansen was born on the 20th of August, 1991 in Deventer, the Netherlands. She obtained her Master's degree in Technical Medicine at the University of Twente, with a special focus on Medical Imaging and Interventions. This Master was completed with a research internship at the Vascular Surgery department of the UMC Utrecht on enhanced imaging methods during endovascular treatment of peripheral artery disease. The work carried out in the Vascular Surgery department of the UMC Utrecht continued into a PhD program, focused on imaging and navigation during endovascular treatment of aortic and peripheral artery disease.

From 2020 to 2023 Marloes worked at Stereotaxis as a Key Account Manager Benelux and UK. Stereotaxis is a pioneer in robotics within electrophysiology. In 2023 Marloes transitioned into a role as freelance Field Clinical Specialist for Ablacon, a start-up company aiming to personalize ablation strategy for atrium fibrillation based on novel mapping technology.